



UNIVERSIDADE DE ÉVORA

ESCOLA DE CIÊNCIAS E TECNOLOGIA

DEPARTAMENTO DE GEOCIÊNCIAS

Exploratory spatial analysis of topographic surface metrics for the prediction of water table occurrence

F. Raquel R.F. de Sousa

Orientação: António Chambel

Co-orientação: Nuno Neves

Mestrado em Ciências da Terra, da Atmosfera e do Espaço

Área de especialização: Processos Geológicos

Dissertação

Évora, 2014

UNIVERSIDADE DE ÉVORA
ESCOLA DE CIÊNCIAS E TECNOLOGIA
DEPARTAMENTO DE GEOCIÊNCIAS

**Exploratory spatial analysis of topographic surface metrics
for the prediction of water table occurrence**

F. Raquel R.F. de Sousa

Orientação: António Chambel
Co-orientação: Nuno Neves

Mestrado em Ciências da Terra, da Atmosfera e do Espaço

Área de especialização: Processos Geológicos

Dissertação

Évora, 2014

Agradecimentos

Em breves palavras aproveito a oportunidade para perpetuar os meus sinceros agradecimentos a todos aqueles que estiveram presentes durante o trabalho que fui desenvolvendo e que culminou na presente tese de mestrado. Em especial ao Professor Nuno Neves e ao Professor António Chambel pela sua disponibilidade, dedicação, apoio, profissionalismo e orientação durante um trabalho caracterizado desde o início pela imprevisibilidade, que sendo uma constante foi ao e ao mesmo tempo a chave para o sucesso do estudo que se foi revelando consoante ia avançando.

Agradeço ainda a todos aqueles que se disponibilizaram tanto na partilha de dados como no apoio pedagógico no âmbito das suas áreas de especialidade, entre os quais nomeio a Rita Nicolau do Igeo, o professor Carlos Ribeiro da Universidade de Évora, a Judite Fernandes e a Carla Midões do Lneg, o Professor Rui Dias e toda a equipa do Pólo de Estremoz da Universidade de Évora e do Centro Ciência Viva de Estremoz e por último mas não menos importante o Sérgio Godinho da Universidade de Évora.

E por fim um agradecimento muito especial a todos aqueles que estão sempre presentes mesmo quando ausentes.

A todos vós!

Bem hajam!

F. Raquel R.F. de Sousa

Exploratory spatial analysis of topographic surface metrics for the prediction of water table occurrence

Abstract

Starting from the premise that water table in aquifers follows topographic surface as well as underground flow direction tends to be consistent with the surface streams flow directions, the present work presents the essays of the research to define a model that predicts, through a piecewise multiple regression, groundwater level in the Estremoz-Cano Aquifer System and in the surrounding igneous and metamorphic rocks of the OMZ as a function of topography, namely a set of terrain metrics like curvature and structural curvature to be related with the static water level (SWL) measured on dug wells of farms and cottages.

The spatial analysis of the topographic surface draining water to the sampled aquifer systems is based on a DEM at different resolutions to acquire and infer information about the surface shape and processes, namely the hydrologic characteristics of the basins and its relation with infiltration process and the prediction of water table.

Key-words: Water table, topography, curvature, piecewise multiple regression, GIS.

Análise exploratória da métrica da superfície topográfica para previsão do nível freático da água subterrânea

Resumo

O presente trabalho parte da premissa de que não só o nível freático acompanha a linha topográfica do terreno, mas também a direcção de escorrência das bacias subterrâneas tende a coincidir com a direcção predominante de escorrência das bacias hidrográficas à superfície, principalmente em aquíferos fraturados.

O presente trabalho apresenta o estudo realizado na investigação de um modelo que explique o nível freático no sistema aquífero Estremoz-Cano e na área circundante a este, nas rochas ígneas e metamórficas da ZOM, em função da curvatura e das características métricas do terreno. Na base dos modelos desenvolvidos estiveram os dados de elevação do terreno a diferentes resoluções, a curvatura e a convexidade deste, assim como as características hidrológicas e a influência destas nos processos de infiltração.

Palavras-Chave: Nível freático, topografia, curvatura, regressão linear do tipo Piecewise, SIG.

Index

Thanks
Abstract
Resumo

Chapter 1 – Introduction.....	1
1.1. Work setting.....	1
1.2. Objectives.....	3
1.3. General methodology.....	4
Chapter 2 - Geographic setting.....	5
2.1 Location.....	5
Chapter 3 – Physical Geographic setting.....	6
3.1 Geomorphology	6
3.1.1 The peneplain of Alto Alentejo.....	7
3.1.2 Reliefs in the peneplain of Alto Alentejo.....	8
Mountain range Serra d’Ossa	7
Estremoz Anticline – Calcareous Massif of Estremoz.....	8
3.2 Climate.....	8
3.2.1 Precipitation	9
3.3 Soils	10
3.3.1 General characterization and soil occupation	11
Chapter 4 – Geologic setting	14
4.1 – Geology.....	14
4.1.1 Hesperic Massif.....	14
4.2 – Lithostratigraphy.....	16
4.2.1 Blastomylonitic Belt.....	17
4.2.2 Alter do Chão – Elvas Sector.....	17
4.2.3 Estremoz-Barrancos Sector.....	18
4.2.3.1 Estremoz Anticline (Sub-domain in Estremoz Barrancos Sector).....	18
4.2.4 Montemor – Ficalho Sector.....	20
4.2.5 Cenozoic Formations.....	20
4.2.6 Magmatic Rocks.....	21
4.2.6.1 Pre-Variscan magmatic rocks.....	20
Basic and ultra-basic massif of Alter do Chão, Elvas and Campo Maior.....	20
Sienitic Complex of Alter do Chão, Elvas and Campo Maior.....	20

Granitic Orthogneisses	20
4.2.6.2 Variscan magmatic rocks.....	22
Plutonic Complex of Monforte – Santa Eulália	
Pavia massif.....	22
Santa Sofia Diorites and Gabbros.....	22
Mora – Évoramonte two micas granite.....	22
São Miguel de Machede e Redondo Massifs.....	22
.Tonalites.....	23
Vale de Maceira and Veiros Massif.....	23
4.2.6.3 Vein rocks.....	23
Granite porphyritic.....	23
Great vein of Alentejo.....	23
4.3 – Tectonic.....	24
4.3.1 Blastomylonitic Belt.....	24
4.3.2 Alter do Chão – Elvas Domain.....	25
4.3.3 Estremoz-Barrancos Domain.....	25
4.3.4 Évora – Beja Domain.....	26
Chapter 5 – Hydrologic and Hydrogeological setting.....	27
5.1 Hydrology	27
5.2 Hydrogeological setting.....	29
5.2.1 Hesperic massif – Low productivity Sector of the OMZ.....	30
5.2.2 Estremoz-Cano Aquifer system.....	32
Cano Sector	32
Estremoz sector.....	33
5.2.3 Elvas –Vila Boim Aquifer system.....	34
5.2.4 Aquifer system Alter do Chão – Monforte.....	34
5.2.5 Igneous rocks of Nisa, Portalegre and Santa Eulália.....	35
5.2.6 Aquifer system Pavia – Mora.....	35
Chapter 6 - Exploratory Models for water table occurrence prediction.....	37
6.1 Theoretical framework	37
6.2 Definition of the Study Area.....	39
Spatial Analysis.....	40
Topo to Raster.....	40
Fill Tool.....	41
Flow Direction.....	43
Flow Accumulation	44
Watershed.....	45
6.3 Statistical Analysis Introduction.....	47
6.3.1 Inferring and validating the best model.....	48

P - Level (p) – Significance level.....	49
R – Correlation coefficient.....	49
R ² – Determination coefficient.....	49
Multicollinearity	49
6.3.1.1 Models verified	50
Multiple Linear Regression.....	50
Piecewise Linear Regression	51
6.4 Exploratory Models for water table occurrence prediction	51
6.4.1 Normalized Mean Curvature Index (NMC).....	51
6.4.1.1 Curvature Tool from ArcGis ®	53
6.4.1.2 Neighborhood Tool - Focal Statistics.....	54
6.4.1.3 The Normalized Mean Curvature Index.....	56
6.4.1.4 Local tool – Cell Statistics	58
6.4.1.5 Statistical Analysis	59
6.4.2 Convexity Index.....	62
6.4.2.1 Convex calculation.....	62
6.4.2.2 Statistical Analysis	68
6.4.3 Structural Index.....	71
6.4. 3.1 Structural Convexity Index 1	71
Flow length Tool.....	73
6.4.3.1.1 Statistical Analysis.....	76
6.4. 3.2 Structural Convexity Index 2.....	80
6.4.3.2.1 Statistical Analysis	82
Chapter 7 –Conclusion.....	87

Bibliography

Attachments

- Dug Wells Data
- Convex - Dependent and Independent Variables Values -
- NMC - Dependent and Independent Variables Values-
- StructConvex1_25 - Dependent and Independent Variables Values -
- StructConvex1_50 - Dependent and Independent Variables Values -
- StructConvex1_100 - Dependent and Independent Variables Values -
- StructConvex1_200 - Dependent and Independent Variables Values -
- StructConvex2_25 - Dependent and Independent Variables Values -
- StructConvex2_50 - Dependent and Independent Variables Values -
- StructConvex2_100 - Dependent and Independent Variables Values -
- StructConvex2_200 - Dependent and Independent Variables Values -

Figures Index:

Figure 1: Watershed profile and identification of both topographic and phreatic lines.....	2
Figure 2: Water resources in Portalegre and Évora Districts (Data source: http://www.pordata.pt and http://insaar.inag.pt).....	3
Figure 3: Districts and municipalities covered by the study area.....	5
Figure 4: Digital elevation model and surface slope of the topographic surface in the study area; microbasins within the study area.....	6
Figure 5: Average total annual precipitation in Portugal mainland specially in the study area (Adapted from Nicolau 2002).....	9
Figure 6: Type of soil within the study area (Adapted from SROA).....	11
Figure 7: Soil occupation in the study area, description according to level 1 of COS2007 (Adapted from COS2007, IGM 2007).....	13
Figure 8- Paleogeographic and tectonic unities in the Iberian Peninsula. (Adapted from Ribeiro et al, 1990).....	14
Figure 9: Geological domains of the Peninsular SW, with special attention to the ZOM.(Adapted from Apalagegui <i>et al</i> , 1990 in Lopes, 2003.).....	15
Figure 10: Geological setting of the study area (Mapped at the scale of 1:50000)	16
Figure 11: The main basins and micro-basins (A to H) of the study area. Main watersheds adapted from APA (Environment Atlas from the Portuguese Agency of the Environment).....	27
Figure 12: The four main hydrogeological units in Portugal mainland (Adapted from SNIRH 1995) and the Aquifer Systems within the study area (Adapted from ERHSA 2001) as well as the wells where the SWL was measured.....	30
Figure 13: Water flow directions in the Aquifer of System Estremoz-Cano; A – Area covered by the study area (Adapted from ERHSA 2001).....	33

Figure 14: Water flow directions in the Aquifer of System Elvas – Vila Boim; A – Area Covered by the study area (Adapted from ERHSA, 2001).....	34
Figure 15: Example of a dug well where SWL was measured resorting To a piezometric probe as illustrated in the image.....	38
Figure 16: Digital elevation model of the study area for different raster resolutions	41
Figure 17: Digital elevation Model after filling the sinks by using the Fill Tool of The Hydrology Toolset.....	42
Figure 18: Color and number coding of the direction flow scheme use in Flow Direction	43
Figure 19: Flow direction within the study area for different raster resolutions.....	44
Figure 20: Flow accumulation within the study area for different raster resolutions.....	45
Figure 21: Definition of the study area by resorting to the Watershed Tool of the Hydrology Toolset.....	46
Figure 22: Flowchart of the statistical analysis and the best model definition.....	48
Figure 23: Flowchart illustrating the computation of NMC.....	52
Figure 24: ArcGis surface curvature scheme (Source: ArcGis 10 Help).....	53
Figure 25: Curvature within the study area calculated with the Curvature Tool of the Spatial Analyst Extension on ArcGis 10 [®]	54
Figure 26: Mean Curvature within the study area calculated after the Curvature Raster with the Neiborhood Tool of the Spatial Analyst Extention of ArcGis 10 [®]	55
Figure 27: Scheme of the circle neighborhood applied with the neighborhood tool.....	56
Figure 28: NMC Index calculated after the curvature from ArcGis 10 [®] for different resolutions.....	57
Figure 29: Cells Statistics of NMC Index calculated with the Local Tool of the Spatial Analyst Extension of ArcGis 10 [®]	58

Figure 30: Flowchart with the scheme of the calculation of <i>Convex</i>	62
Figure 31: Mean Digital Elevation Model; mean elevation for a tree cells Circle neighborhood.....	64
Figure 32: Height calculated from the difference between the elevation and the mean elevation; variable considered in the calculation of <i>convex</i>	65
Figure 33: Convexity Index (<i>Convex</i>) in the study area.....	67
Figure 34: Flowchart illustrating all the steps in the computing of <i>StructConvex_1</i>	72
Figure 35: Flow Length within the study area, showing the downstream distance along a flow path for each cell to the pour points of each water flows.....	73
Figure 36: Transported Convexity computed with the Flow length Tool considering as an input weight the <i>Convex</i> calculated before.....	74
Figure 37: Mean Transported Convexity calculated by dividing the Transported Convexity by the Flow Length for the watersheds in the study area.....	75
Figure 38: Structural Convexity Index (<i>StructConvex1</i>) for the study area.....	76
Figure 39: Flowchart illustrating all the steps in the computing of <i>StructConvex_2</i>	81
Figure 40: Structural Convexity Index (<i>StructConvex2</i>) for the study area.....	82
Figure 41: SWL calculated with Model 2.....	88

Tables Index

Table 1: Area occupied by the different types of soil within the study area, according to the classification of the SRAP (Service of Recognition and Agricultural Planning).....	12
Table 2: Occupied area by each class considered in COS'2007 (IGP, 2007).....	13
Table3: Drainage density of the micro basins within the study area.....	28
Table 4: Efficient infiltration in the aquifer systems of the study area.....	36
Table 5: Higher and lower mean curvature calculated for each curvature Raster at different resolutions.....	53
Table 6: Values for which the surface is upwardly convex, flat or upwardly concave in the NMC Index.....	57
Table 7: Correlation Analysis for all the independent variables calculated for the computing of NMC.....	59
Table 8: Correlation and determination coefficient among the dependent variable(SWL) and the independent variables selected for a Piecewise Linear regression and a Multiple Linear Regression – NMC.....	60
Table 9: Bivariate correlations matrix for the independent variables considered in the calculus of NMC.....	61
Table 10: Proposal of the 3 models that best explain SWL based on the independent variables considered in the computation of Curvature Index – NMC.....	61
Table 11: Results for Model 1- Piecewise Linear Regression for the independent variables NMC_25 and DEM_50.....	62
Table 12: Horizontal distance applied in the calculus of <i>convex</i> , depending on the cell size for each of the resolution considered.....	66
Table 13: Correlation Analysis for all the independent variables calculated for the computing of the <i>Convex</i>	68
Table 14: Correlation and determination coefficients for each independent variable calculated during the calculus of <i>Convex</i> for both models Piecewise and multiple linear regressions	69
Table 15: Bivariate correlations matrix for the independent variables for	

the calculus of <i>Convex</i>	69
Table 16: Proposal of the 3 models that best explain SWL based on the independent variables considered in the computation of <i>Convex</i>	70
Table 17: Results for Model 2- Piecewise Linear Regression for the independent variables <i>convex_50</i> and <i>DEM_25</i> -.....	70
Table 18: Correlation Analysis for all the independent variables calculated during the computing of <i>StructConvex1</i>	77
Table 19: Correlation and determination coefficients for each independent variable calculated for the determination of <i>StructConvex1</i> for both models Piecewise and multiple linear regressions	78
Table 20 to 23: Bivariate correlations matrix for the candidate independent variables calculated for the determination of <i>StructConvex1</i>	78 - 79
Table 24: Proposal of the 2 models that best explain SWL based on the Independent variables considered in the computation of <i>StructConvex1</i>	79
Table 25: Results for Model 3- Piecewise Linear Regression for the independent variables <i>convex_50</i> and <i>StructConvex1_50</i>	80
Table 26: Correlation Analysis for all the independent variables Calculated for the computing of the <i>StructConvex2</i>	83
Table 27: Correlation and determination coefficients for each independent variable calculated for the determination of <i>StructConvex2</i> for both models Piecewise and multiple linear regressions.....	84
Table 28 to 31: Bivariate correlations matrix for the candidate independent variables calculated for the determination of <i>StructConvex2</i>	84 - 85
Table 32: Proposal of the 3 models that best explain SWL based on the Independent variables considered in the computation of <i>StructConvex2</i>	85
Table 33: Results for Model 4- Piecewise Linear Regression for the independent variables <i>convex_50</i> and <i>StructConve2_50</i>	86
Table 34: Best models inquired all through the statistical analysis	87
Tables 35 and 36: Estimation results for Model 2 for both aquifer systems where SWL was measured (A4- Estremoz Cano Aquifer System; OMZ – Igneous and metamorphic rocks of OMZ.).....	89

Chapter 1 – Introduction

1.1 Work setting

We all grew up thinking of earth resources as eternal and endless, specially water in its timeless and nearly perfect cycle. Of the total amount of water in our planet only 2.5% is freshwater (UNEP 2002). From the total amount of freshwater nearly 68.9% is kept in ice and glaciers and 30.8 % correspond to raw groundwater, in general of naturally great quality (UNEP 2002). Despite that only 0.3% of the total freshwater is in rivers and lakes which corresponds to 0.007% of the total water on earth, they are yet the principal resources we use in our daily lives (USGS). Groundwater represents over 90% of the world's readily available freshwater resource (Boswinkel 2000). Since our main freshwater resources lay under our feet, it is critical to characterize and evaluate the hazard and potential risk and especially monitor freshwater supplies. In December 2000 the "Directive 2000/60/EC of the European Parliament and of the Council" established a framework for the Community action in the field of water policy", the so known Water Framework Directive (WFD 2000) whose main objective is to define a legal framework to protect and restore clean water across Europe: inland surface waters, transitional waters, coastal waters and groundwater. On what concerns groundwater, some of the main objectives are:

- ✓ To ensure the reduction of global pollution of groundwater;
- ✓ To avoid or limit the discharge of pollutants on groundwater;
- ✓ To protect, improve and reconstitute groundwater and ensure the balance between catchment and recharge of aquifer's water;
- ✓ Routinely screen the state of water (chemically and quantitatively);
- ✓ To prevent and control groundwater pollution;
- ✓ To evaluate the risk of contamination of groundwater;

Raw groundwater normally and naturally has great quality and supplies are stable, which makes aquifers excellent sources of safe water supply for our society needs, both in rural and urban areas, as well as viable in what concerns its exploration costs. Aquifers are the best resource for the public access to potable water, turning it essential to characterize, monitor, quantify and protect. More and more modeling groundwater systems are becoming a priority to ensure an efficient management of water resources, namely in the definition of a proficient knowledge of the spatial distribution of groundwater and consequently availability for exploration.

The water amount that reaches the phreatic level resulting on aquifer recharge is the outcome of water balance, a consequence of the climate, type of cover, terrain characteristics, type of soils and the hydrogeological aquifer characteristics.

The volume stored underground (S_g) is calculated by the following equation (Lencastre and Franco 1984):

$$S_g = I - (G + R_g + E_g + T_g)$$

I – Infiltration

G – Groundwater flow

R_g – Upwelling of the groundwater flow outcropping in the surface

E_g – Evaporation

T_g – Transpiration feed by water from the soil

In the terrains of a watershed two lines are defined: the topographic or superficial line and the phreatic and underground line (Lencastre and Franco 1984) (Figure 1).

This way the water from precipitation that infiltrates, flowing underground, crosses the topographic line corresponding simultaneously to an output for the watershed (Lencastre and Franco 1984) and to an input to groundwater.

The position of the phreatic line is not only influenced by the geological structure and the hydrogeological characteristics inherent to the aquifer's nature, but also by topography. In fact topography can be used to quantify surface drainage and infiltration processes (Beven and Kirkby 1979, O'Loughlin 1986, Moore et al. 1988 a,b in Hutchinson and Dowling 1991).

The level of the phreatic line varies during the year with the natural variations of water table position between the dry and the wet season; therefore the higher is the phreatic line the closer both phreatic and topographic lines are, this is expected to happen mainly during the wet season (Lencastre and Franco 1984).

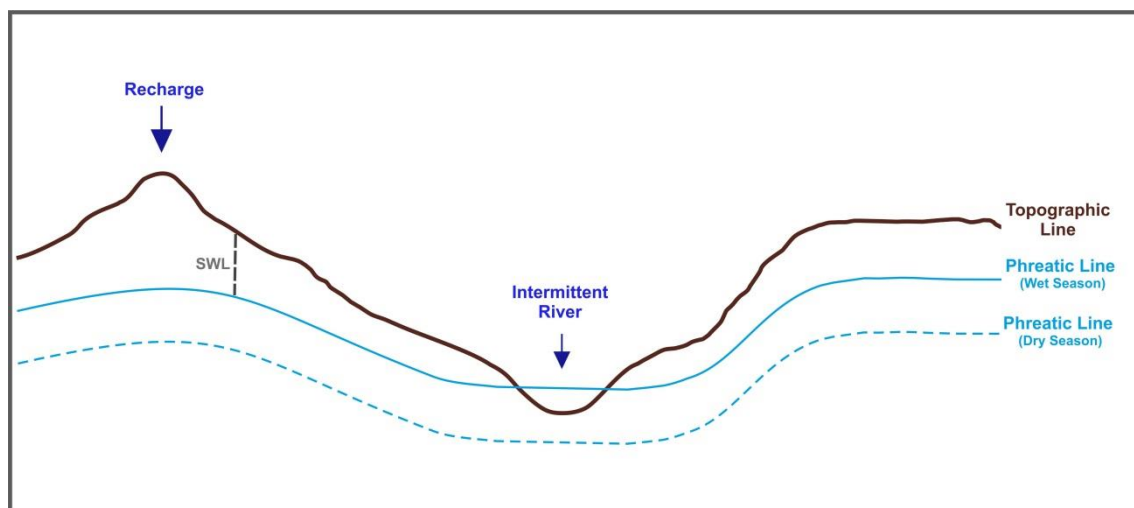


Figure 1: Watershed profile and identification of both topographic and phreatic lines.

Alentejo, the Portuguese region where the study area is located, is characterized by the low availability of surface water resources and periodic droughts. In this context groundwater is the main water supply resource in some counties, as in the ones within the study area of the present work (Figure 2).

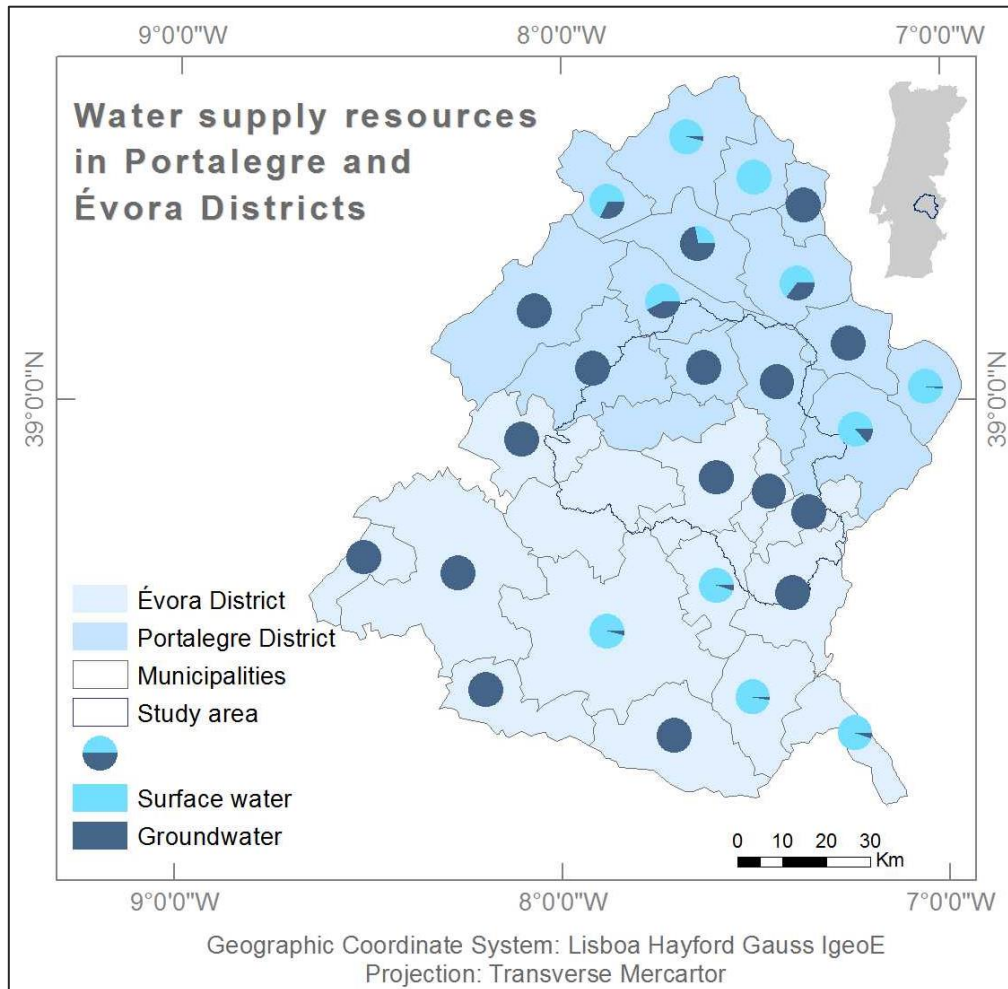


Figure 2: Water resources in Portalegre and Évora Districts
(Data source: <http://www.pordata.pt> and <http://insaar.inag.pt>).

1.2 Objectives

Starting from the premise that in aquifers not only the phreatic surface tends to follow the topographic surface, especially in fractured aquifers, but also groundwater flow direction tends to be consistent with the surface flow direction (Custodio & Llamas 1983, Driscoll 1986), the main objective of the present work is to gauge a model to predict groundwater level in the Estremoz-Cano aquifer system and in the surrounding hard rocks of the Ossa Morena Zone (OMZ) as a function of topography and the terrain's metrics, mainly curvature, based on the static water level (SWL) measured on dug wells of farms and cottages.

1.3 General methodology

✓ **Data Acquisition: Static Water Level (SWL)**

The models introduced in the present dissertation were developed based in the SWL measured with a piezometric probe in dug wells of farms and cottages, in the districts of Portalegre and Évora.

✓ **Digital Elevation Model (DEM) construction**

A digital elevation model was created from elevation points and contour lines resorting to the interpolation method Topo to Raster in Arcgis®.

✓ **Hydrological analysis**

The study here stated, aiming the creation of a predicted model for groundwater occurrence, has a strong dependency on the flow direction and magnitude of surface water, therefore the hydrological analysis was crucial for its success. It started from the definition of the water flow direction in the topographic surface followed by the creation of a flow accumulation raster in which the main streams were identified and finally by the delimitation of the micro basins draining water to the aquifers where the SWL was measured coinciding with the definition of the study area.

✓ **Analysis of the topographic surface metrics**

With the objective of studding a linear regression translating the distance between the phreatic line and the topographic line, in other words a model that explains SWL and groundwater occurrence, several indices reflecting topographic metrics were calculated:

- Normalized Mean Curvature (**NMC**)
- Convexity Index– Local Convexity (**Convex**)
- Structural Convexity Indexes (**StructConvex_1 and StructConvex_2**)

By extracting the topographic indices values corresponding to the location of wells where SWL was measured a statistical analysis to ascertain a possible correlation was then performed.

✓ **Statistical analysis**

The SWL data and the topographic indices were object of study in a statistical analysis that revealed the topographic indices with the higher correlation with SWL and the model that best explain groundwater occurrence. Three parameters were analyzed: the significance level; the correlation coefficient and the determination coefficient.

Chapter 2 - Geographic setting

2.1 Location

The region where the study area is located, Alentejo, is divided in two main regions Baixo Alentejo (“South Alentejo”), which coincides with the entire District of Beja, and Alto Alentejo (“North Alentejo”), which includes both the Districts of Évora and Portalegre. The study area covers part of Portalegre and Évora districts and encloses part or in some case the total area of the parishes of Avis, Alter do Chão, Fronteira, Monforte, Alter do Chão, Mora, Sousel, Elvas, Arraiolos, Estremoz, Borba, Vila Viçosa, Redondo and Alandroal (Figure 3).

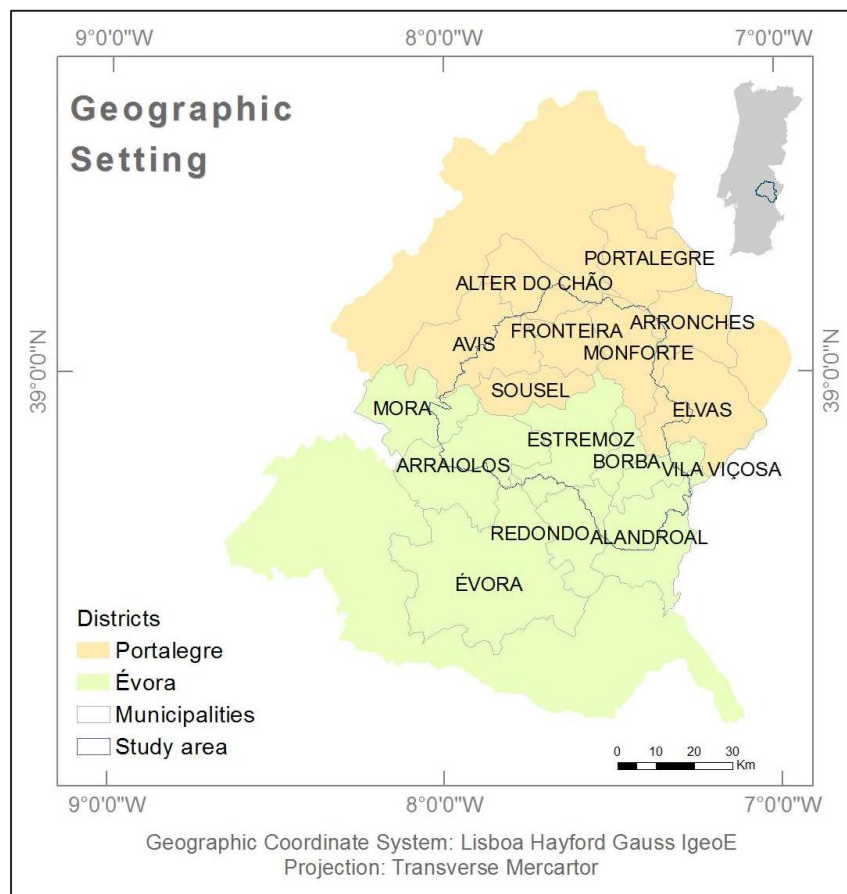


Figure 3: Districts and municipalities covered by the study area.

Chapter 3 – Physical Geographic setting

3.1 Geomorphology

The form of real topographic surface at any point in time is the result of the action of processes on the forms that existed in previous times, and models of physical landscape development must therefore postulate some initial form on which modeled processes can operate (Goodchild and Mark 1987). Both slope and elevation are the result of the erosive processes over the past millions of years together with the tectonic evolution on the Iberian Peninsula. Slope depends on the elevation change over distance which influences runoff velocity and thus the time water takes to concentrate in riverbeds of the drainage network. This influences the greater or lesser opportunity for water to infiltrate and the erosion susceptibility of soils on the watershed (Lencastre and Franco 1984). On gradually sloping terrains water has more time to infiltrate and to reach the water table, whereas on steeper slopes runoff is faster and infiltration is less efficient. The models proposed in the present thesis aim to predict water table, starting from the topographic surface and its elevation, slope and curvature. The study area corresponds to a rather flat terrain where small hills are observed and towards SE elevation increases and there is a lenticular elongated relief corresponding to the anticline of Estremoz.

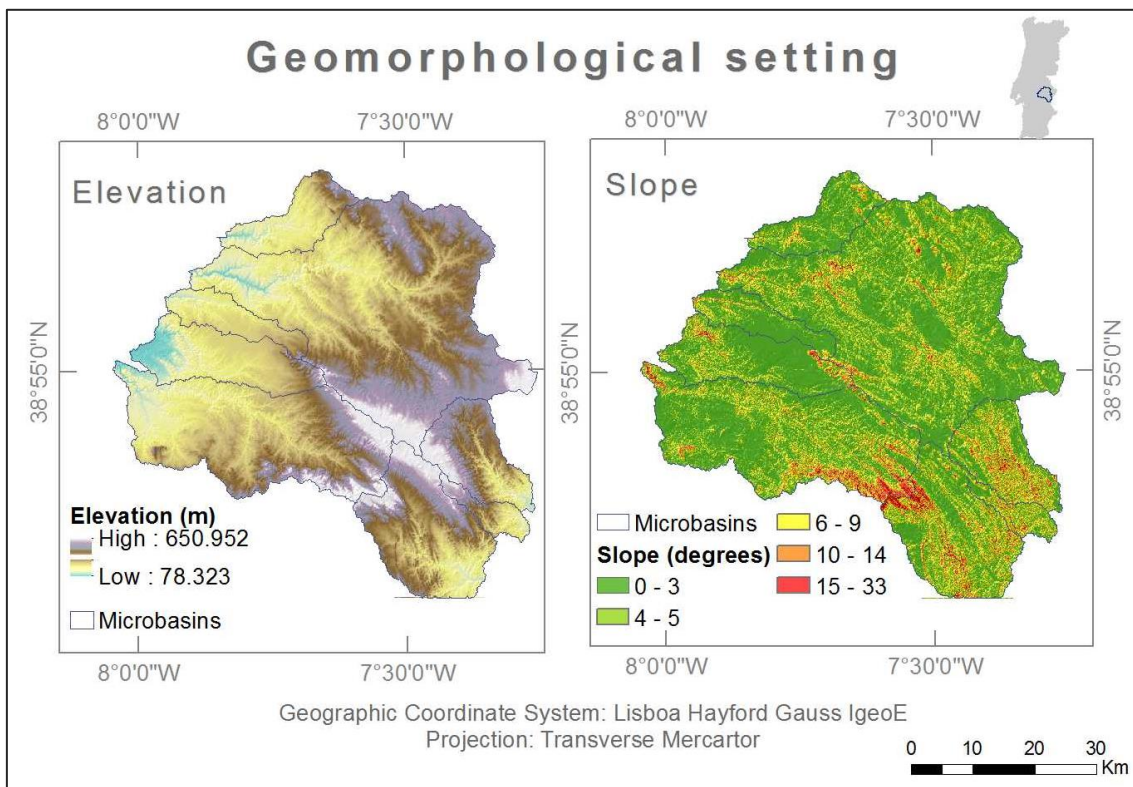


Figure 4: Digital elevation model and surface slope of the topographic surface in the study area; micro basins within the study area.

The area is rather flat and most part of the terrain is just slightly tilted. Towards SE and coincidentally with the higher elevations the terrain is steeper and slope varies from 6 to 33 degrees (Figure 4). Based on the work of Feio (1993), the following description is intended to briefly describe the topographic shapes not only of the study area but also the important reliefs in the surrounding area.

The distinction between the two administrative sub-regions: Alto Alentejo and Baixo Alentejo is marked in the terrain by two important geomorphologic structures the Vidigueira escarpment and Portel Mountain W-E oriented.

In Alto Alentejo the so-called peneplain of Alentejo is less evident for the terrain is more fractured and the plain is interrupted by some hills along topography.

3.1.1 The peneplain of Alto Alentejo

South of the city of Évora, until a distance of about 10 km, the peneplain is well conserved at elevations ranging from 240 to 250 m while towards N the peneplain is higher, reaching elevations up to 320 m. Towards east, NE of Évora between the cities of Estremoz and Redondo, rises the mountain of Serra D'Ossa. Near the city of Estremoz, along the crystalline limestone and dolstone massif of Estremoz the peneplain reaches an altitude of 440 m. The area E of Estremoz is dominated by a wide elongated NW-SE depression at 300 to 320 m asl (above sea level), called the depression of Terrugem-Ciladas. This depression is limited towards NE by the Vila Boim-Vila Fernando-Elvas Plateau, raised along a tectonic accident up to 420 to 450 m asl.

Further E, NE of Estremoz in the direction of Veiros and Monforte the peneplain is up to 300 m asl. Near Alter do Chão the elevation is irregular, ranging from 240 to 270 m asl due to the presence of standout land reliefs associated to harder lithologies such as orthogneisses, quartzites, conglomerates and basic volcanic rocks that overhang comparing to less resistant rocks of the OMZ such as shales and granites.

3.1.2 Reliefs in the peneplain of Alto Alentejo

Mountain range of Serra d'Ossa

With an approximate NW-SE orientation, this mountain range tops at about 653 m asl and is divided in two sections, one further NE composed by siliceous shales and the second further SE, designed by Pia-do-Lobo-Évoramonte, formed also by metamorphic rocks. The two sectors are separated by a fracture valley. The NE alignment corresponds to the Barrancos formation and is approximately 2 km width while the

Pia-do-Lobo-Évoramonte sector is characterized by a vigorous scarp tilting about 19%, leading to a decrease in elevation from 570 to 345 m asl.

Estremoz Anticline – Limestone Massif of Estremoz

The anticline of Estremoz extends along 37 km in the WNW-ESE direction. With a maximum width of about 6 km in the area of the city of Estremoz. In the dependence of the limestone formations, mainly the dolomitic limestones, the structure is about 440 m asl.

3.2 Climate

The weather conditions, mainly rainfall and evaporation, are a determining factor in the evaluation of water balance and aquifer recharge. Climate characterizes weather conditions based on climate elements such as temperature, atmospheric pressure, precipitation, wind, humidity, among others, in a certain area, considering an analyzing the average values for a long period of time. The normal length of time used for statistical climate characterization is 30 years, defined by the WMO (World Meteorological Organization). A spatial analysis of the normal climatic parameters from 1960 to 1990 shows that the average annual temperature in Portugal varies from 7°C in center-interior higher lands to 18°C in the south coast. The average annual precipitation has its higher values in the north between Minho and Douro's coast and the smaller values in the south interior of Baixo Alentejo (Portuguese Sea and Atmosphere Institute, I. P. (IPMA, IP)). According to the Koppen-Geiger classification (1936) the climate in Portugal mainland is either weather seasoned with wet winter and dry warm summer in the southern inner Portugal or seasoned with wet winter and dry or temperate summer in the north and on the coast of Portugal mainland (IPMA). The average values of the air temperature and precipitation from 1971 to 2000 in the Iberian Peninsula can be found in the Iberian Climatic Atlas (ICA 2011). The annual average temperature in Évora and Portalegre districts is 17.5 °C; the annual average minimum temperature goes from 10 to 12.5°C and the annual average maximum temperature is about 22.5 °C. In the half south part of the Iberian Peninsula the maximum temperature is superior to 25° C in more than 110 days (ICA 2011).

3.2.1 – Precipitation

The characterization of the precipitation in climate studies considers not only the average annual precipitation but also the temporal distribution throughout the four seasons. In the Iberian Peninsula, the rainiest month is December and the driest month is

July. Between 1971 and 2000 the average total annual precipitation in the districts of Évora and Portalegre ranged from 500 to 700 mm (ICA 2011).

In the study carried out by Nicolau (2002) in her PhD thesis on the modeling and mapping of the spatial precipitation distribution in mainland Portugal, the annual precipitation estimated for the period between 1959/60-1990/91 in the studied area of the present thesis ranges in most of the area from 300 to 700 mm except in the SE of the area corresponding to the SE half of the Aquifer system of Estremoz-Cano where precipitation annual mean ranges nearly from 670 to 870 mm (Figure 5).

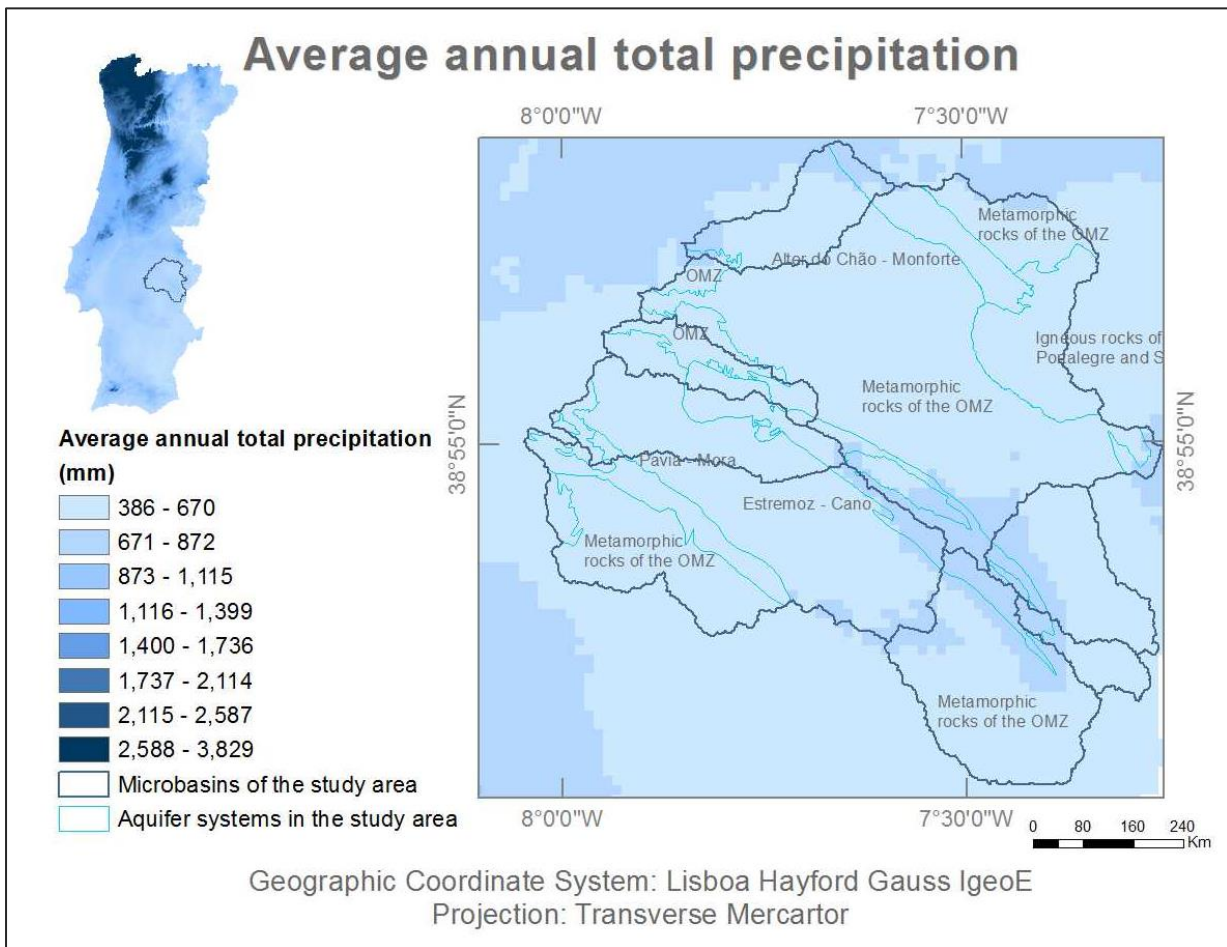


Figure 5: Average total annual precipitation in Portugal mainland specifically in the study area (Adapted from Nicolau 2002).

3.3 Soils

The aquifers recharge is in part dependent on the hydrodynamic and hydraulic characteristic of the vadose zone and above all of the type of soil and its textural characteristics and its occupation. As water reaches the earth surface through precipitation it penetrates along the soil and the vadose zone influenced by gravity along with soil capillary potential. Infiltration is mostly influenced by the type of soil and its texture, the cover, the soil use, the soil humidity, the vadose zone thickness, the compression level and the precipitation duration. As the soil infiltration capacity is reached water starts to flow superficially. Water movement along the soil occurs as unsaturated flow caused by infiltration, percolation, redistribution and evaporation (Santos 1999).

The vadose zones corresponds to the geological profile between the surface and the water table and includes in its profile the soil, the intermediate vadose zone and the capillary fringe where water flow is unsaturated, a consequence of infiltration, percolation, redistribution and evaporation processes.

3.3.1 General characterization and soil occupation

The characterization of the type of soil on each region, together with the soil use, is fundamental on the territory, political, economic and social planning and on the evaluation of the environmental impact not only on the soil itself but also on the aquifers under these soils. The definition of the areas, the extension, use of soil and the definition of the potential of each area for different anthropogenic activities allows the planning of the territory and also the evaluation of important information such as the soil erosion and waterproofing. The information of the Soils of Portugal used in the present work is a polygon feature data based on the topographic maps at the scale 1:25000, in which the different soils are defined according to the classification of the SROA (Service of Recognition and Agricultural Planning) (Figure 6).

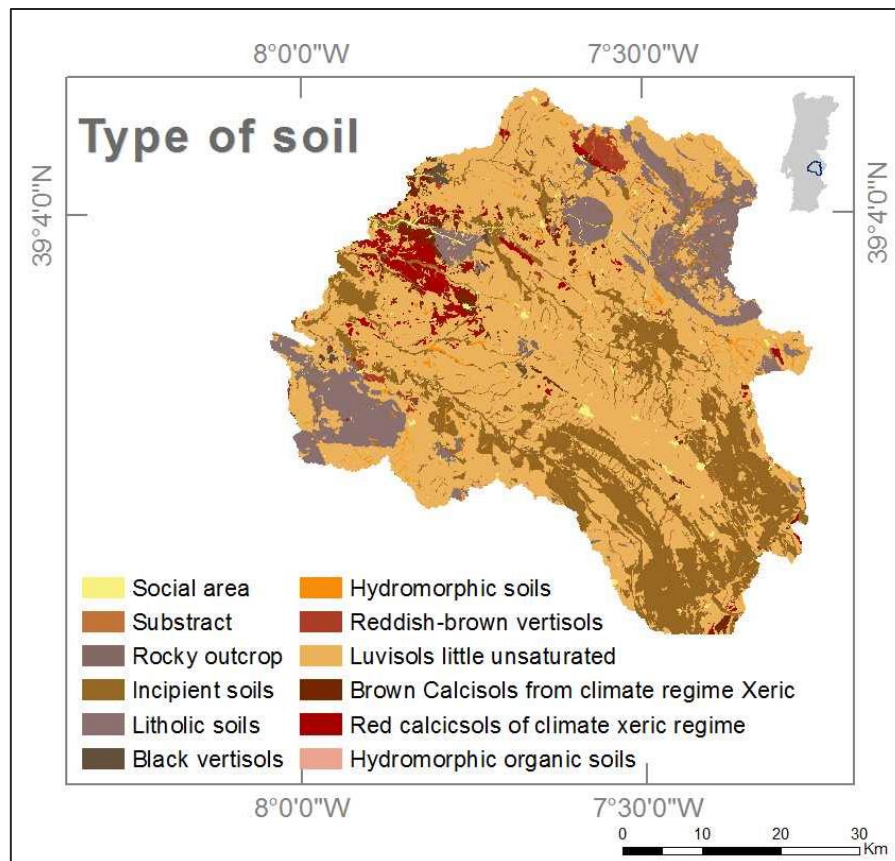


Figure 6: Type of soil within the study area (Adapted from SROA).

Karst regions in the OMZ are characterized by thin soil. Within the study area, over 50% of the total area is covered by evolved brownish and reddish to yellow unsaturated luvisols, characteristic of Mediterranean climate regions, followed by nearly 20% of incipient soils and 11% of litholic soils, both slightly evolved (Table 1). While incipient and very thin soils are absent in differentiated horizons and rocks outcrop directly in many areas, litholic soils formed from on non-carbonated rocks. In these areas, the soils are very thin, chemically poor and also poor in organic compounds.

Table 1: Area occupied by the different types of soil within the study area, according to the classification of the SRAP (Service of Recognition and Agricultural Planning).

Type of Soil	Area (km²)
Luvisols little unsaturated	1517
Incipient soil	582
Litholic soils	316
Luvisol little unsaturated	128
Red calcisols of climate xeric regime	73
Brown Calcisols from climate regime Xeric	52
Substract	43
Hydromorphic soils	33
Social area	30
Reddish-brown vertisols	24
Black vertisols	14
Rocky outcrop	4
Hydromorphic organic soils	0

Infiltration and runoff is influence by the type of cover; the presence of arboreal vegetation favors infiltration and reduces runoff velocity and therefore erosion and flow occurrence (Lencastre and Franco 1984). In 2007, the Portuguese Institute of Geography (IGP) updated the Soil Occupation map from 1990 (COS'90) and produced the Soil Occupation map for 2007 (COS'2007) with several modifications in relation to the previous one (COS'90) and with the objective of setting it in the European and world wild policies of geographic data. The COS'2007 was done at the scale of 1:25000 with the Minimum Cartographic Unity of 1 ha and based on the visual interpretation of areal digital images. The nomenclature of the COS'2007 is hierarchical and considers 5 levels and 193 classes (Figure7).

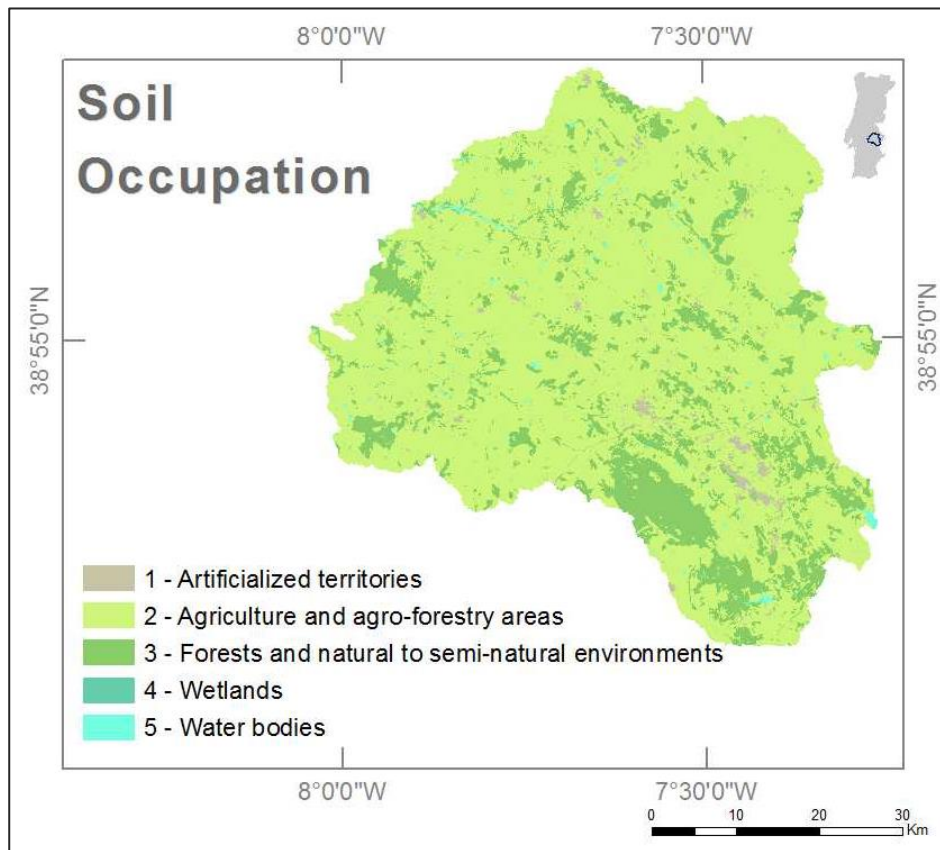


Figure 7: Soil occupation in the study area, description according to level 1 of COS2007
(Adapted from COS2007, IGM 2007)

Nearly 80% of the soil within the study area is used for agriculture and agro-forestry activities and about 18% corresponds to forests and natural to semi-natural environments (Table 2).

Table 2: Occupied area by each class considered in level 1 of COS'2007 (IGP, 2007).

Classe	Nomenclature	Area (km ²)	%
1	Artificialized territories	45.00	1.60
2	Agriculture and agro-forestry areas	2240.00	79.52
3	Forests and natural to semi-natural environments	506.00	17.96
4	Wetlands	0.00	0.00
5	Water bodies	26.00	0.92
	Total	2817.00	100.00

Chapter 4 - Geologic setting

4.1 Geology

The Iberian Peninsula is divided into morphotectonic unities that express the Wilson Cycles which acted on the Iberian Peninsula territory since the Paleozoic. According to Ribeiro et al. (1979) in the Iberian Peninsula 4 morphostructural unities can be identified:

- Cenozoic basins
- Meso-Cenozoic basins with Alpine tectonic inversion
- Alpine Chains
- Variscan basement (Hesperic Massif)

4.1.1 Hesperic Massif

The studied area is located in the Variscan Basement, in a tectonic stratigraphic sub-unity called Ossa Morena Zone (OMZ) (Figure 8). Thereby, the tectonic-stratigraphic analysis of the Hesperic Massive allowed the differentiation of the following sub-unities in which the OMZ is included: Cantabric Zone (CZ), Astúrico Occidental Leonesa Zone (AOLZ), Center Iberia Zone (CIZ), Galaico Transmontana Zone (GTZ), Ossa Morena Zone (OMZ), South Portugesa Zone (SPZ) (Figure 8).

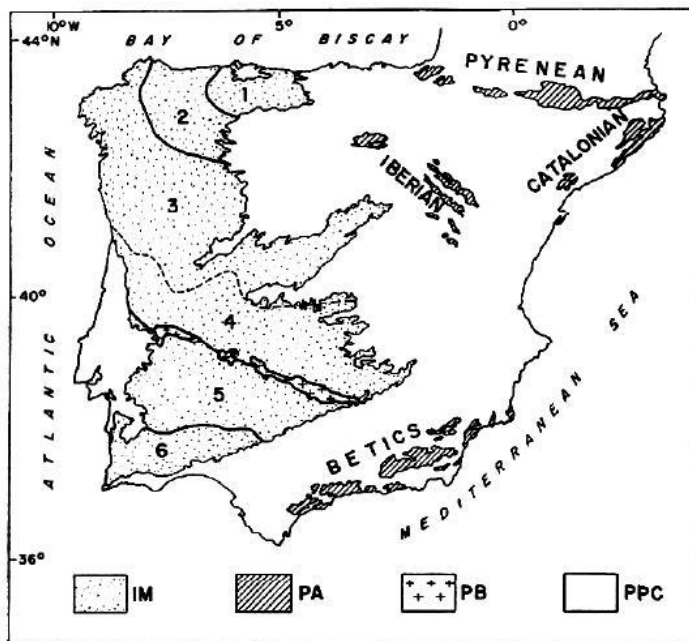


Figure 8- Paleogeographic and tectonic unities in the Iberian Peninsula. IM – Iberian Massif; PA – Pre-Cambrian and paleozoic outcrops in the Alpine chains; PB – Pedroches batholith; PPC – Post-paleozoic coverage, 1 – CZ; 2 – ZAL; 3 and 4 – CIZ; 5 – OMZ; 6 – SPZ. (Adapted from Ribeiro et al. 1990).

To the south, the OMZ contacts with the SPZ and to the north with the CIZ. The three paleogeographic zones differ on their lithological and stratigraphic characteristics and on their metamorphic degree. The stratigraphy of OMZ has been presented in zones and subzones (Carvalho et al. 1971 in Araújo et al. 2006) or in tectonic-stratigraphic domains (Chacón et al. 1974, Delgado et al. 1977, Apalategui et Al., 1990 in Araújo et al. 2006 (Figure 9)). Recently, the separation of the main structure in sectors was introduced, which allows a better comprehension of several depocenters, whether the geographic limits coincide with a tectonic accident or not (Oliveira et al. 1991 in Araújo et al. 2006).

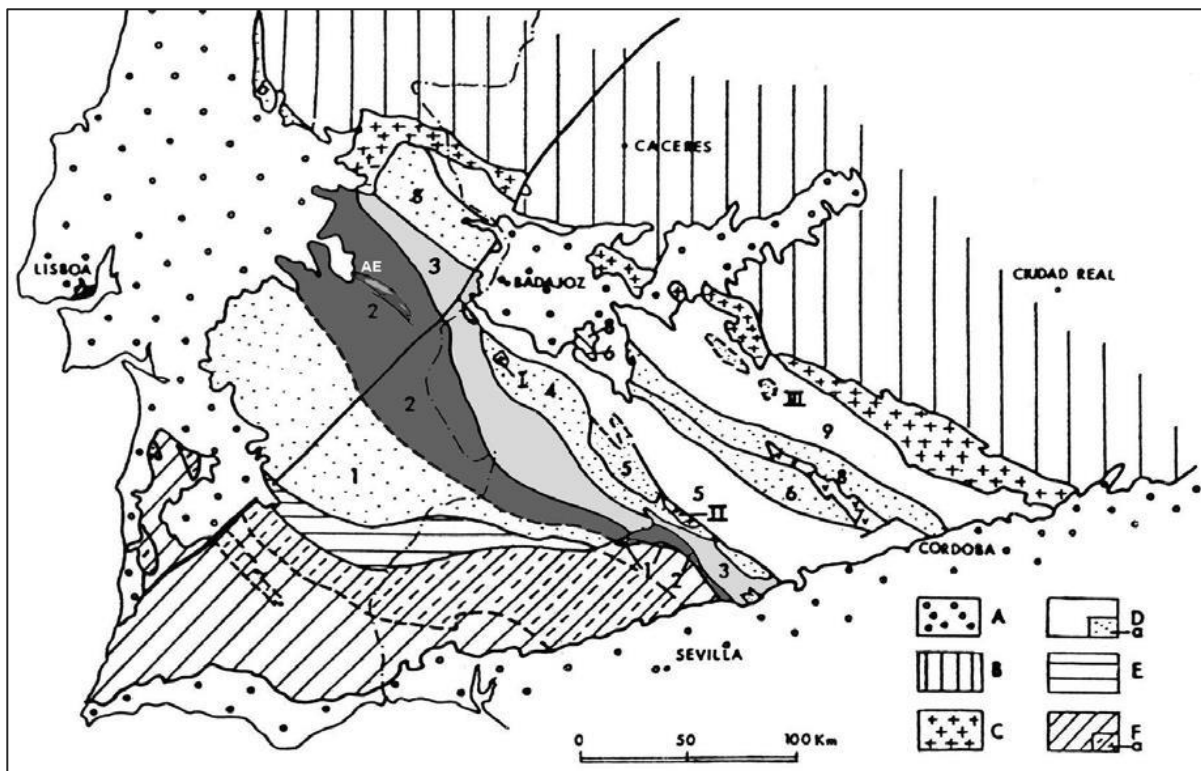


Figure 9: Geological domains of the Peninsular SW, with special attention to the OMZ.

(Adapted from Apalategui et al., 1990 in Lopes, 2003) A – Post-Paleozoic; B – CIZ; C – Pedroches-Alpalhão-Nisa batholith; D – OMZ; F – SPZ; 1 – Beja – Aracena Domain; 2 – Estremoz – Barrancos – Hjnojales Domain; 3 – Elvas- Cumbres Mayores Domain; 4 - Arroyo Molinos Domain; 5 – Zafra – Monesterio Domain; 6 – Serra Albarrana Domain; 7 – Villa Viçosa – La Coronada Domain; 8 – Tomar – Badajoz – Córdoba Shear Zone; 9 - Obejo- Valsequillo-Puebla de la Reina Domain; AE Anticline of Estremoz.

OMZ is formed by a great variety of igneous and metamorphic rocks such as granites, granodiorites, quartz-diorites, tonalitic rocks, diorites, gabbros, charnokites, andesites and shales, greywackes, gneisses, amphibolites, metamorphised volcanic rocks, and metamorphic limestones (Chambel et al. 2007).

Its terrains present high metamorphic grade and it are divided in the following tectonic-stratigraphic sectors:

- Blastomilonítica Belt;
- Alter do Chão-Elvas;
- Estremoz-Barrancos;
- Montemor-Ficalho;

4.2 – Lithostratigraphy

In the study area outcrop formations from the four tectonic-stratigraphic sectors being formed essentially by metamorphic rocks, such as shales and metamorphic limestones, a great variety of volcanic and plutonic igneous rocks from the Paleozoic and sedimentary deposits from the Cenozoic as hereafter is describe (Figure 10).

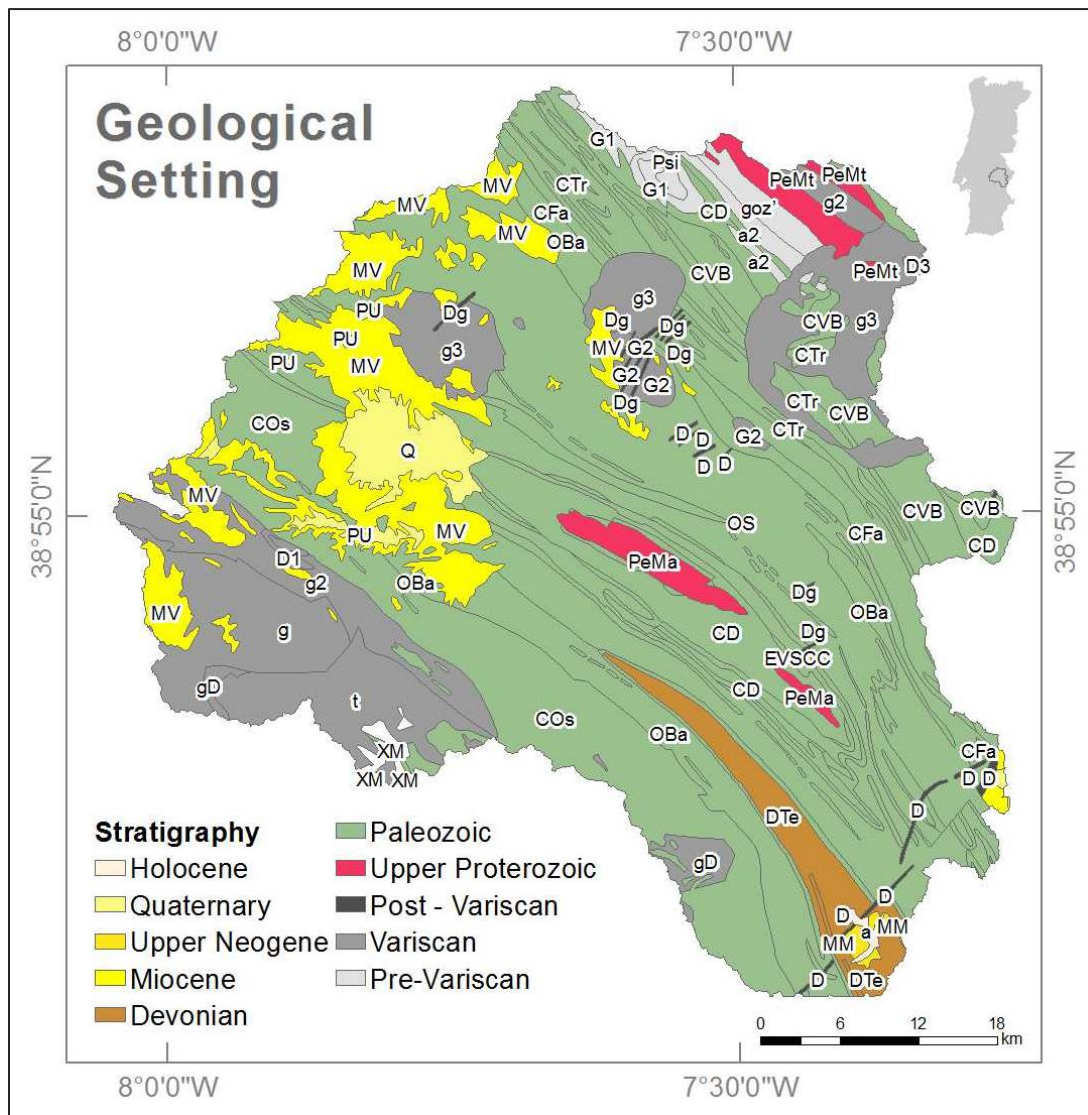


Figure 10: Geological setting of the study area (Mapped at the scale of 1:50000).

4.2.1 Blastomylonitic Belt

Mosteiros Formation (PeMt)

Upper Proterozoic

This formation is divided into two members identified in the NE flank of the anticline structure. The lower member is formed by a lenticular level of metarkoses followed by greenish shales, and the upper member by a sequence of shales, greywackes and dark-grey psammities intercalated by black metacherts and some levels of limestones and amphibolites (Gonçalves and Oliveira 1986 in ERHSA 2001).

4.2.2 Alter do Chão-Elvas Sector

Dolomitic limestones and marbles (CD)

Lower cambric

With about 500 m thickness and without any fossil evidences, this formation is poorly known in Portugal. Mainly dolomitic, it is constituted by limestones and conglomerates, with acid volcanic rocks in the base.

Vila Boim Formation (CVB)

Lower Cambrian

Concordant with the carbonated formation lays the Vila Boim Formation. With more than 600 m thickness, it is formed by alternated layers of sandstones and psammities. Some acid volcanic rocks such as continental basalts are also intercalated in this formation (Gonçalves and Assunção 1970, Mata 1986 in ERHSA 2001).

The Vila Boim Formation ends in the so known Quartzitic Bar, a micaceous quartzitic layer that sideways and towards NW changes to conglomerates with rolled quartz pebbles (Oliveira 1984 in ERHSA 2001).

Terrugem Vulcano Sedimentary Complex (C_{T1})

Middle Cambrian

With about 2000 m thickness above the Quartzitic belt is represented by a terrigenous sequence with shales, psammities, metagreywackes and some carbonates. Its sequence is also intercalated by rhyolites and tuffites, and alkaline basalts followed by extrusive peralkaline rocks.

Fatuquedo Formation (CFa)

Middle Cambrian

The Fatuquedo Formation is characterized by the presence of quartzites impregnated with oxides of iron and manganese that sideways and towards north change to

polygenic conglomerates with quartz, quartzites, basic and acid volcanites and granitic rocks pebbles. Upon the ferruginous quartzitic horizon lays dark-grey shales.

4.2.3 Estremoz-Barrancos Sector

Ossa Formation (COs)

Middle Cambrian (?)

Dated from the middle Cambrian, but also reaching the upper Cambrian (Piçarra et al. 1992 in ERHSA 2001) this is the oldest formation in this sector. Mainly formed by shales and psammites, greywackes become more abundant towards NW. The base is characterized by an extended belt of basic volcanic rocks.

Barrancos Formation (OBa)

Middle Cambrian

This formation is constituted by purple to violet thin micaceous shales with intercalations of greenish to gray shales and rare occurrence of finely laminated psammites.

Terena Formation (DTe)

Devonian

In the nucleus of a syncline structure extending from Estremoz until Aracena (Spain), outcrops the Terena formation, a turbidity sequence formed by shales and greywackes interbedded with some conglomeratic levels.

4.2.3.1 Estremoz Anticline (Sub-domain in Estremoz-Barrancos Sector)

The Estremoz-Barrancos sector is bounded at SW by the Montemor-Ficalho sector and at NE by the Alter do Chão-Elvas sector. The geologic unity of the anticline of Estremoz was already established in 1899 in the Geological Map of Portugal at the scale of 1:500000. With about 42 km length and 8 km width, it is a structure nearly symmetric; an antiform anticline that stands along the direction NW–SE.

Mares Formation (PeMa)

Upper Proterozoic

Created in the Neo-Proterozoic, the anticline core is 700 to 540 million years old. The Mares Formation surfaces in two cores in the axial zone of the anticline. This formation is formed by black shales, greywackes and highly metamorphosed cherts.

Over this formation lays a vulcanoclastic member, considered by many as the mark of a discordance of the lower Cambrian over the Proterozoic basement (Araújo et al. 2006).

Dolomitic Formation (CD)

Lower Cambrian

In discordance over the vulcanoclastic member lays the Dolomitic Formation formed by a conglomerate base, acid and basic volcanites, and dolomitic and calcitic limestone. This formation has dolomitic limestone with several interspersed siliceous levels more developed in the top, which can be interpreted as a middle–upper Cambrian gap, when the carification and silicification of the dolomites happened (Oliveira 1984 in Araújo et al. 2006).

There are doubts about the age of the Dolomitic Formation however it is considered from the lower Cambrian (Carvalhosa et al. 1987). In the top of this formation occurs a sulfur mineralized silicate horizon, which is said to be an important hiatus, consequence of a sub-aerial exposition during the middle-upper Cambrian and local silicification and karstification (Carvalhosa et al. 1987).

Estremoz Vulcano-Sedimentary-Carbonated Complex (CVSCE)

Upper Cambrian - Ordovician (?)

Apparently concordant over the Dolomitic Formation rests the Estremoz Vulcano-Sedimentary-Carbonated Complex (CVSCE) which consists of different marble varieties, calc-schist rocks, intercalated with acid and basic metavolcanic and intrusive magmatic rocks (Araújo et al. 2006). The marbles are explored as an ornamental rock and present several karstification marks, with caves that can reach decametric dimensions, filled with shale (Araújo et al. 2006). On the top of this complex, the volcanites are more common and are mainly basic. The basic volcanites present a chemical composition that goes from alkaline basalts to trackyandesites (Mata and Munhá 1985 in Araújo, et al. 2006). The felsic rocks are classified as peralkalines (Coelho and Gonçalves 1970 in Araújo et al. 2006) and occur next to the SE termination of the antiform.

The age of the complex is still uncertain, although it is considered from the Ordovician (Oliveira et al. 1984 Carvalhosa et al. 1987 in Lopes 2003); however other authors admit that it can be Silurian (Sarmiento et al. 2000). This complex dates probably from the Upper Ordovician, between 455 and 435 million years old (Lopes, L. 2007). Involving the CVSCE are quartzites, limestones and black shales with graptolites from the lower Silurian (Piçarra 2000 in Araújo, A. et al. 2006). This sequence is followed by a sequence of black shales and psammites. The transition, in the upper Silurian, of

black shales to alternated shales and psammities points to a tectono-sedimentary evolution since the lower Devonian (Araújo et al. 2006).

4.2.4 Montemor – Ficalho Sector

Moura-Santo Aleixo Vulcano Sedimentary Complex (Moura Shales) (XM)

Ordovician - Silurian (?)

This complex is mainly formed by phyllite sericite-chloritic shales with abundant exudation of quartz. In the base occurs a thin level of black shales. In some higher geometric positions intercalations of black shales, basic and acid metavolcanic rocks and also limestone shales and marbles can occur, corresponding to tectonic repetition of the Estremoz Volcano-Sedimentary-Carbonated Complex.

4.2.5 Cenozoic Formations

In Alentejo Cenozoic terrains are found in different tectonic-sedimentary domains, whose evolution was confined by paleogeography and structural factors (ERHSA 2001).

Vale do Guiso Formation (MV)

Miocene

The base of this formation is characterized by carbonated cement coarse deposits followed by reddish to rosy levels formed by coarse or thin sediments, such as arkosic sand and clay and also greenish to red pelites. In the top of the formation, carbonated cement sandstones change sideward to carbonated formations with a reduced clastic fraction. This sequence evidences a progressive organization of the drainage network from a torrential to fluvial regime. In some locals where this formation was identified, ravine surfaces and pale-channels with poorly rolled pebbles are observed, which that tend to get thinner to the top of the layer (ERHSA 2001).

Moura, Mourão, Quintas and Campo Maior Deposits (MM)

Upper Neogene

Mainly formed by clays, sands, marls and limestones, these deposits are less than 30 m thick and are usually associated to areas next to tectonic accidents.

Alluvium (a)

Holocene

This layer is essentially formed by clayey sands and different pebble's dimension.

Quaternary Terraces (Q)

Quaternary

These unities correspond to coarse heterogeneous highly ferrous detritic deposits that in many areas of Alentejo cover plain extensions over the Variscan basement.

In the NW periclinal termination of the Estremoz anticline above the Paleozoic formations are the Cano limestones, formed by limestone and calcareous gaps. They surface in depressed zones and have a big expression in the region of Cano, forming a very regular surface (Cupeto 1991). The calcareous gaps are formed by ferruginous limestone gaps that can go from very coarse sandstone, crystalline dolomitic limestone and crystalline to semi-crystalline limestone.

4.2.6 Magmatic Rocks

4.2.6.1 Pre-Variscan magmatic rocks

Basic and ultra-basic massif of Alter do Chão, Elvas and Campo Maior (G|Psi)

This massif is formed by ultrabasites such as peridotites, dunites and pyroxenites (Psi) and basites such as gabbro, andolivinic and anorthositic gabbro (G). The outcrop extends for a large area along the NW-SE direction, and intrudes the Cambrian carbonated series originating a considerable metamorphic edge.

Syenitic Complex of Alter do Chão, Elvas and Campo Maior (a₂)

The granites and syenitic orthogneisses form elongated massifs, showing clear signs of tectonic deformation. Here and there they show a blastomylonitic structure especially common in the Precambrian intercalations.

Granitic Orthogneisses (goz)

These rocks occur in different areas of the OMZ, where the most important outcrops are in the contact with Beja Massif near Viana do Alentejo and Alvito, in Escoural and Alcáçovas. According to Carvalhosa (1977) (ERHSA 2001) these gneisses are pre-tectonic and are related to the Variscan deformation. The orthogneisses granites are composed of quartz, microcline, albite and oligoclase, and less represented biotite, muscovite, amphibole, sphene, apatite and zircon.

4.2.6.2 Variscan magmatic rocks

Plutonic Complex of Monforte – Santa Eulália (D3 | g3)

With a circular geometry, this igneous annular complex intrudes the NE-SW hercinic structures. From the border towards the center different types of granites can be distinguished. The border of this complex is characterized by rose-colored granites, with medium to coarse texture, followed by grey nearly monzonitic granites that tend to change to a thinner texture in the inner rocks. Dispersed within the rose granites occur some mafic to intermediate igneous rocks: mainly gabbro, diorites and granodiorites.

Pavia massif (g)

The igneous massif varies in its mineralogical and chemical composition so that the granites lean towards more alkaline facies into the center. In the border of the massif the two micas granite predominantly biotitic is present, with medium to fine grain gradually changing to porphyritic granite in the center. The massif is also characterized by the presence of aplite-pegmatite veins.

Santa Sofia Diorites and Gabbros (D₁)

It is common to find diorites associated to gabbros in particular in the outcrops SW of Santa Sofia. The diorites have fine grain even though sometimes they can go from coarse grain to pegmatitic with well-developed amphiboles or porphyritic texture with plagioclase phenocrysts. According to their mineralogy, different lithotypes can take place.

Mora – Évoramonte two micas granite (g₂)

Also present near Seda parish between Évoramonte and Mora, they occur along the NW–SE band, where three types of gneissic granites are identified: fine grain amphibolitic granites; fine to mean grain two micas granite; and coarse grain two micas granites frequently associated to pegmatites.

São Miguel de Machede and Redondo Massifs (gD)

The granodiorite–quartz diorite intrusive rocks of Redondo and S. Miguel de Machede massifs are represented in two different outcrops: the first in Redondo and the second near Évoramonte, where it is intercepted by the Pavia Massif. In what concerns the rocks facies, they are essentially granodiorities, having sometimes tonalites associated to granodiorites.

Tonalites (t)

Distributed along a wide area between Arraiolos, Montemor-o-Novo and Évora, these intermediate-felsic rocks represent a significant part of the intrusive massifs. They are typically intermediate, non-porphyrific changing to diorite when quartz is less abundant.

Vale de Maceira and Veiros Massif (G2)

Intruding the Silurian formations, the basic rocks in this massif constitute more or less NW-SE oriented elongated domes. In the Veiros Massif, rocks have fine grain with a microgranular to microporphyroblastic texture abundant in mafic minerals, mainly pyroxene. Also present in less quantities are olivine and biotite, and also plagioclase and alkali feldspar. In Vale de Maceira gabbros are essentially hypersthene with abundant hypersthene, and olivine is absent. Biotite, plagioclase and hornblende, despite being less abundant, are also present.

4.2.6.3 Vein rocks

Porphyritic (Granite p)

The acid porphyries that occur along the veins steering NNE-SSW to NE-SW have well visible phenocrysts in a fine matrix, usually microcrystalline. The matrix is mainly composed by feldspar, quartz and micas (biotite and chlorite), while the phenocrysts can go from quartz, orthoclase, to oligoclase and albite.

Great vein of Alentejo (D)

From the SW extreme of Portugal in Vila do Bispo till Campo Maior, extending to Spain, NE-SW oriented, this vein crosses all Alentejo. It is formed by basic rocks such as dolerites and doleritic gabbros with ophitic texture, where clinopyroxene and calcic plagioclase are predominant. This great vein reflects the post-variscan magmatic activity.

4.3 Tectonic

Studies on the geodynamics and evolution of the Iberian geology consider the OMZ an ancient continental fragment contacting with other two: in the north it contacts with Centro Iberia Zone (CIZ) and in the south with the South Portuguese Zone (SPZ). The limit with the CIZ is mechanic, represented by the Shear Zone Tomar-Badajoz-Córdoba.

OMZ was deformed and metamorphosed during the collision of two continents, and the construction of a mountain chain. The existing continents grew together in the so-called *Pangaea*. The compressive regime installed then was responsible for the edification of several mountain chains. The Variscan Orogeny affected the whole Iberian Peninsula and Estremoz was no exception. The Estremoz anticline was affected by the Variscan Orogeny and two deformation phases are distinguished in a continuously ductile non-coaxial regime, with the formation of folds.

The fact that the sequence of the Dolomitic Formation appears in the four sectors suggests sedimentation on a depositional bay in expansion together with its subsidence, in a time characterized by the expansion of the oceans in an oceanic crust distension regime that lasted till the Silurian age. The silica nature and the presence of organic matter that gives the black color to shales indicate a calm anoxic sedimentary environment, not too deep. During the distention, normal faults were formed originating the gravitational slip of the non-consolidated sediments. The faults created correspond today to alignments on fractured rocks with approximate W-E directions.

OMZ is characterized by a flower structure geometry with center structures that tend to be sub-vertical and boundary sections with opposite vergence. In the limit with the CIZ in the NE section vergence is towards NE, in the SW border vergence is towards SW (Araújo 1995). The vergence to SW from the main Varisc deformation phase dominates along the whole SW share of the OMZ; but in the S sector it is affected by the obduction mechanism of the Ophiolitic South Portuguese Terrain (Araújo 1995). The center of the flower structure is characterized by an important intracontinental left shear.

4.3.1 Blastomylonitic Belt

The SW vergence of the SW border of the OMZ is observed in the S part of the Blastomylonitic Belt as well as the vergence towards NE in the N division extending to the Shear Zone Tomar-Badajoz-Cordoba. The Blastomylonitic Belt is characterized by a strong variscan deformation present over the whole belt, which some authors

attribute to a crustal weakness zone, consequence of a previous inherited orogenic suture dated from Cadomian (Abalos and Eguiluz 1991, Abalos et al. 1991, Quesada et al. 1991, Abalos and Eguiluz 1992, Abalos 1992, Quesada 1992, Ribeiro 1993, in Araújo 1995). In the nucleus of the belt a strong Variscan left shear zone deformation can be observed.

4.3.2 Alter do Chão – Elvas Domain

Towards N the contact between the Alter do Chão – Elvas Sector and the Blastomitic Belt is done by the Alter do Chão nape with vergence to SW. The south limit corresponds to the thrust belt of Juromenha, responsible by the tectonic overlay of the Alter do Chão–Elvas units over the SW units of the Estremoz-Barrancos domain (Gonçalves 1971, Ribeiro et al. 1979, Ribeiro 1981, Chacón et al. 1983, in Araújo 1995). Currently, the existence of the Juromenha thrust belt is questionable by recent studies based on lithostratigraphic data, which seems to show that the transition from the middle Cambrian Alter do Chão–Elvas formation to the lower Ordovician formation is done through an unconformity.

4.3.3 Estremoz-Barrancos Domain

The Estremoz-Barrancos Sector is limited at N by the Juromenha thrust belt and at S by the Santo Aleixo da Restauração thrust belt (Araújo 1986, 1987, 1989, in ERHSA 2001). The deformation and metamorphism are similar to the Alter do Chão Sector, and individualization of the Estremoz Anticline is essentially based on paleogeographic criteria (Araújo 1989, Oliveira et al. 1991 in ERHSA 2001).

The rocks of the anticline were compressed along the NE – SW direction. IN the first deformation phase e the axial direction was next to N-S; the second deformation phase is more common and has originate axial directions NW-SE, the same as the anticline structure. The second phase is responsible for the orientation of the anticline and presents a more fragile character. The anticline presents a tangential deformation parallel to the structures that had created the anticline segmentation, with the formation of sub-vertical discontinuities with orientation NNW–SSE to NW–SE and left lateral component (Lopes 2003). In the final stages of the Variscan Orogeny a fragile behavior is observed, represented by sub-vertical faults WSW-ESE oriented, NNE-SSW shear and diacase directions fracturing the rocks, which correspond to traction fractures of the second phase of deformation.

Finally, the anticline was intercepted by sub-vertical WSW-ENE to NE-SW oriented veins, installed along faults with the same directions. During the Mesozoic, the

Variscan Orogeny was eroded and the resulted sediments were transported and deposited in the Meso-Cenozoic sedimentary Basins. Today, the karstification and the relief are the last episodes of the geological evolution of the anticline of Estremoz.

4.3.4 Évora-Beja Domain

According to Oliveira et al. (1991), this domain embraces both the Montemor-Ficalho and the Beja Massifs. The presence of several variscan intrusive massifs, essentially acid in the Évora Massif and basic in the Beja Complex (Gonçalves and Antunes 1992 in ERHSA 2001), is characteristic of this domain. The intrusive rocks were only affected by the last deformation phase, while the enclosing rocks from the Proterozoic and the Cambrian present the complete Variscan deformation. The uncertainty about the ages of the sedimentary and volcano sedimentary sequences in this domain is mainly due to the tectonic nature of the contacts between the different units. The sequences present tectonic deformation, characteristic of lower structural stage. Towards SW, a precocious deformation associated to the intrusion of the Beja-Acebuches Ophiolitic Complex becomes noticeable (Araújo 1992a, Araújo et al. 1993 a, b, c, Fonseca et al. 1993, Sousa et al. 1993 in ERSHA 2001).

Chapter 5– Hydrologic and Hydrogeological setting

5.1 Hydrology

Most of the rivers that flow in Portugal, including Tagus and Guadiana, are born in Spain. The hydrographic basins of these rivers are thus shared by the two countries. The basin area of most of the rivers is two to three times bigger in Spain; about 78% of the area of the basins is in Spanish territory and the remainder 22% belongs to the Portuguese territory. Such evidences are determinant in the administration and planning of the hydric resources between the two countries. Guadiana's basin is about 66,960 km², of which 11,700 km² are within the Portuguese territory while Tagus's basin is 80,629 km² of which 24,860 km² belong to Portugal. The water table sampling on dug wells concentrated along the Aquifer System Estremoz-Cano extends to the surrounded Metamorphic and Igneous rocks of the OMZ, aiming at collecting data also from lower elevations.

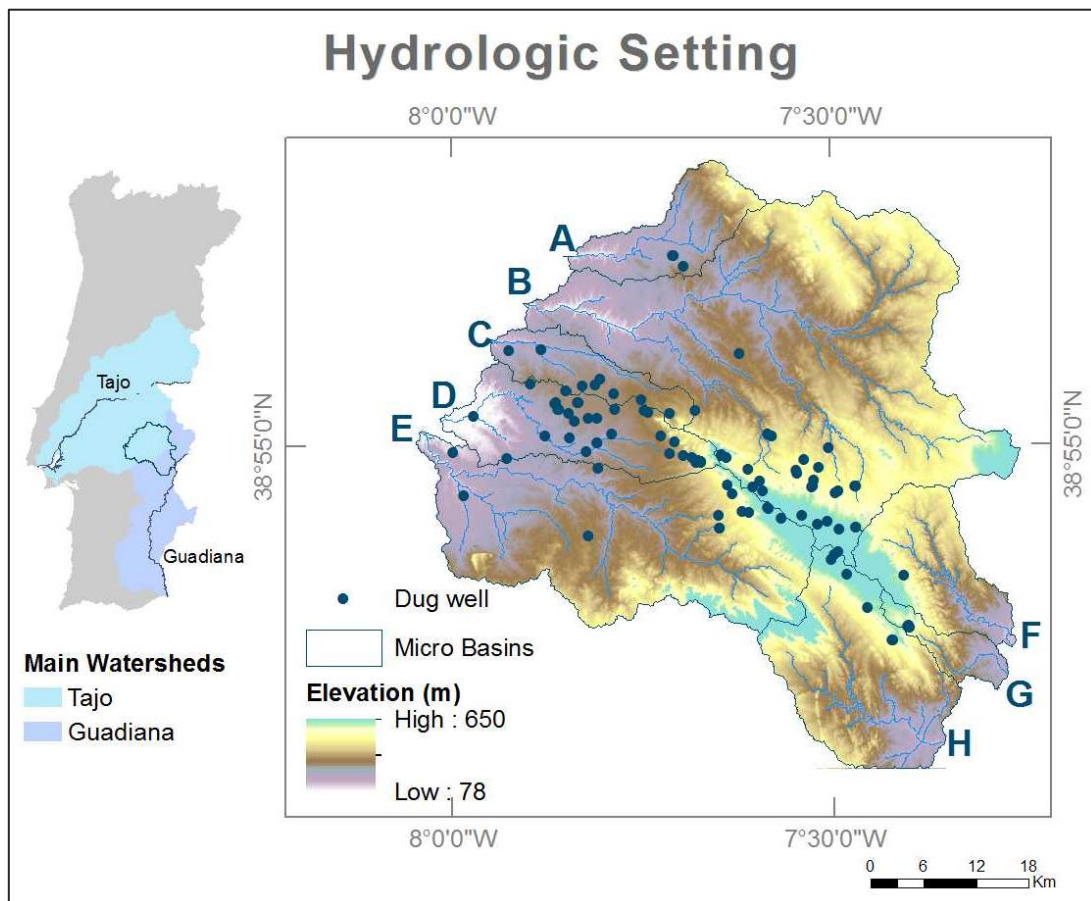


Figure 11: The main basins and micro-basins (A to H) of the study area. Main watersheds adapted from APA (Environment Atlas from the Portuguese Agency of the Environment).

The definition of the study area corresponds to the micro-basins draining to the sampled dug wells, resorting to the Watershed Tool of the Hydrology Tool Set in ArcGis® (see Chapter 6). At the scale of Portugal mainland, the micro-basins of the study area are part of the two major basins of the Guadiana and Tagus rivers. The three basins at the SE extreme of the study area, with a total area of roughly 577 km², collect water from the Guadiana basin, while the remaining micro-basins to the NW, with about 2,241 km², collect water from the Tagus's basin (Figure 11).

In general, the micro-basins of the study area are elongated except for watershed B; in addition to being bigger, it is also rounder and less elongated. The drainage pattern is essentially dendritic developed in consequence of the erosion of rocks with similar resistances. The flow is mostly intermittent and water flows only during the wet season when streams drain water both from underground and from rain. During the dry season, water table lowers bellow water bed and flow stops, occurring only in case of rain, during or immediately after rain events.

Directly proportional to the flow length, the drainage density (λ) expresses the drainage efficiency of a watershed apart from the streams flow persistence. The study area watersheds are poorly drained, all of them presenting values less than or equal to 0.3 km/km² (Table3).

$$\lambda = \frac{\Lambda}{A}$$

Λ - Total length of the watershed courses

A – Watershed area

Table 3: Drainage density of the micro basins within the study area.

	Watershed Area (A) km ²	Streams Length (Λ) km	Drainage density (Λ/A)
A	141.124	42.984	0.305
B	1137.200	304.886	0.268
C	106.502	30.701	0.288
D	226.360	60.767	0.268
E	630.274	167.131	0.265
F	185.719	53.695	0.289
G	55.438	16.413	0.296
H	335.381	97.763	0.291
Total	2817.999	774.341	0.275

5.2 Hydrogeological setting

The definition of the main aquifer systems in Portugal mainland was carried out in 1994, by INAG I.P. (currently APA) with the aim of facilitating the systematization of groundwater reserves, rendering easier to routinely screen, characterize and manage the main aquifer systems. It considers an aquifer or a combination of aquifers hydrogeological units, or confining units similar on their hydrogeological behavior. The four main hydrogeological units in Portugal mainland mostly coincide with the four main paleogeography zones in Portugal territory. In the Meso-Cenozoic basins constituted by detrital and carbonate rocks are located the most productive aquifers, while in the Hesperic Massif are located the less productive. Also known by Ancient Massif, the Hesperic Massif predominantly consists of crystalline hard rocks. The aquifers of the igneous, meta-sedimentary and metamorphic rocks of the Ancient Massif are less productive, except for the carbonated Paleozoic rocks, for instant in the anticline of Estremoz. In Portugal mainland four main hydrogeological units are distinguished:

- Ancient massif
- Ocidental Meso-Cenozoic edge
- Southern Meso-Cenozoic edge
- Tagus-Sado Tertiary basin

The definition of the aquifer systems recognize within the hydrogeological units of Portugal by INAG in 1994 was based on the definition of Aquifer System of Navarro et al. (1989). According to the author an aquifer system is a special domain limited in surface and depth where one or more aquifers are or not related, but still constituted a practical unity for research and exploration. The definition of aquifer considered by INAG on the systematization of groundwater of Portugal, is based on Almeida et al. (2000), he defined an aquifer as a geological unity capable to transfer water in economical rentable quantities.

Again and nearly coincident with the geostructural divisions of the ancient massif, three hydrogeological subunits and their sectors and sub-domains on the Ancient Massif are distinguished and individually characterized: CIZ (Center-Iberia Zone); OMZ (Ossa-Morena Zone); SPZ (Portuguese South Zone).

During a hydrogeological study taken between 1997 and 2000, ERHSA (Study of the groundwater resources of Alentejo), eleven aquifer systems were identified, individualized and characterized with the main objective of distinguish the sectors and systems with different productivities. The studied area locates in the OMZ, covering a significant part of the Metamorphic and igneous rocks of the OMZ the Aquifer System Estremoz-Cano, Alter do Chão-Monforte, a small part of the Igneous rocks of Nisa,

Portalegre and Santa Eulália Sector and of the aquifer system Elvas-Vila Boim, and almost all Pavia-Mora aquifer system (Figure 12). The description of the hydrogeological characteristics that here follows is based mostly in ERHSA 2001.

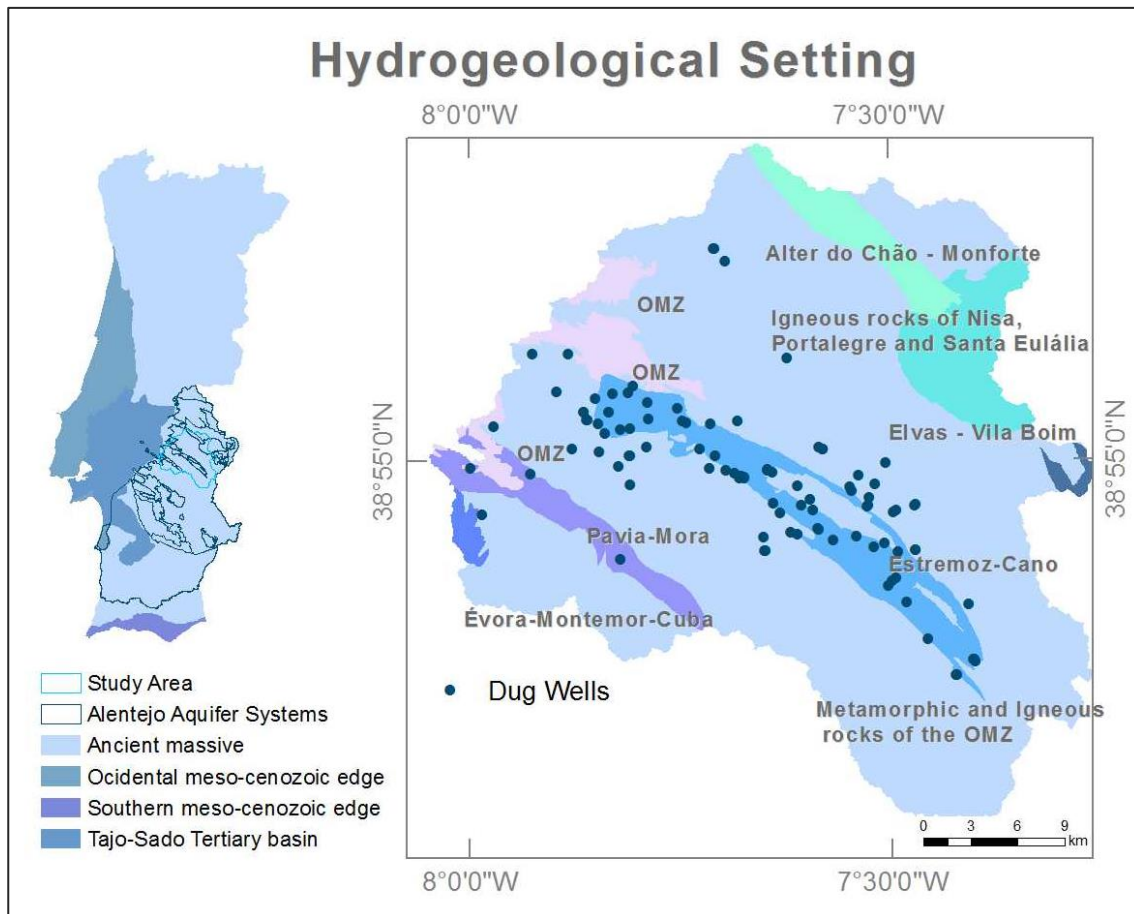


Figure 12: The four main hydrogeological units in Portugal mainland (Adapted from SNIRH 1995) and the Aquifer Systems within the study area (Adapted from ERHSA 2001) as well as the wells where the SWL was measured.

5.2.1 Hesperic massif – Low productivity Sector of the OMZ

The eruptive and meta-sedimentary rocks of the ancient massif are classified by hydrogeologists as hard crystalline and fractured rocks with low porosity, low permeability and reduced hydrogeological productivity. The water storage and circulation in hard rocks occurs mainly along cracks and fractures and is highly dependent on the kind of rock fracturing and the weathered thickness. Both permeability and porosity decrease with depth, where rock's weathering is also minor. Apart from the type of rocks, hard rocks productivity is basically influenced by the fracture density, interlink of the fractures, opening and filling of materials inside the fractures and its intrinsic permeability, and especially by the total weathered thickness (Chambel 2014, in publication). The more productive aquifers are associated to

formations with weathered thickness ranging between 10-20 m as a consequence of a higher secondary porosity and an easier interconnection between fractures. That is why most of the ancient rocks, subject to more orogenic processes, are the most productive hard rock aquifers in Alentejo (Chambel et al 2007). In the metamorphic and igneous rocks of the ancient massif, including the OMZ, the thickness of the weathered layers goes normally from 0 to 6 m. Further down the fractured system is very incipient and the fracture net is scarce at deepness of more than 30-40 m (Chambel et al. 2007). Basic rocks have generally the most extended weathered layers (Chambel et al. 2007), which is due to the higher level of weathering of its minerals compared with more acid rocks.

The OMZ differs from both SPZ and CIZ by the presence of calcareous and dolomitic formations, metamorphic limestones (marbles) and a large extension of basic to intermediate igneous rocks in addition to the acid igneous, metamorphic and meta-sedimentary rocks that generally characterize the ancient massif. The hydrogeological behaviour of the rocks on the OMZ slightly varies with the type of surface terrains, enough to recognize some trend behavior in what concerns the productivity of the aquifers and the waters chemistry. The aquifers productivity varies according many circumstances, but it's normally lower in shale terrains and acid igneous rocks, higher in basic and meta-volcanic rocks and shales with abundant quartz veins and finally can be very high in calcareous terrains (Almeida et al. 2000; Chambel et al. 2007).

Several studies reveal estimated values to the recharge in the aquifers of the ancient massif:

- Schist – 5% (Rodrigues and Roque, 1990 in Almeida et al. 2000)
- Basic eruptive rocks – 4% (Duque, 1997 and Duque and Almeida 1998 in Almeida et al. 2000)
- Acid eruptive rocks – 13% (Vieira da Silva and Palma, 1990 in Almeida et al. 2000)
- Meso-Cenozoic deposits – 10 to 20% (Almeida et al. 2000)

Even so, this must be seen as the characterization of specific areas and not as a global result for all the aquifers and low productivity sectors in Alentejo. In the ERHSA Project (ERHSA 2001), the average recharge percentages in relation to precipitation used for the rocks of the low productivity sectors of the OMZ was 5%, also based in previous works of Oliveira et al. (2006), based on the decomposition of flow curves in surface water courses in the region.

5.2.2 Estremoz-Cano Aquifer system

The aquifer system Estremoz-Cano corresponds to a NW-SE elongated structure that occupies an approximated area of 203 km², intercepting the parishes of Casa Branca, Cano and Sousel in the county of Sousel; Santa Vitória do Ameixial, Santo Estevão, Santa Maria, São Domingos de Ana Loura, Arcos and Glória in the county of Estremoz and further the parishes Rio de Moinhos and Matriz in the county of Borba; Conceição, Bencatel and Pardais in Vila Viçosa county, and lastly in the SE extreme, the parish of Nossa Senhora da Conceição in the county of Alandroal. The aquifer systems provides public water supply for all the five counties.

This system depends on carbonated formations where two sectors are distinguished: the Cano sector constituted by carbonated Quaternary rocks, and the Estremoz sector formed by Paleozoic marbles and meta-dolomitic formations (Cupeto 2003). Both sectors show a high heterogeneity and anisotropy in what concerns their permeability and productivity, typical of karst systems. The most productive water wells are located in the contact between the Paleozoic carbonated formations and the evolving formations of Estremoz anticline and in the Cano sector (ERHSA 2001). The existence of hydraulic connectivity is possible between both sectors based on the geological structure, the fracturing net, and the hydric behavior of both aquifers. In fact, the Cano Sector is a discharge area for the Estremoz Sector, and corresponds to an ancient lake receiving the carbonate waters of the Estremoz Sector. The actual sedimentary limestones in the Cano Sector correspond to the deposition of calcium bicarbonate from groundwater discharging in the basin along the last thousands of years.

With an annual average precipitation of 638.80 mm and an infiltration rate of 30%, the infiltration efficiency is quantified in 191.04 L/m² per year (ERHSA 2001). The groundwater stored in this system is explored not only for public supply but also for private consumers, industry and agriculture.

Cano Sector

In the NW extreme of the anticline is located the Cano sector associated to the quaternary calcareous rocks; this sector behaves as a phreatic and porous aquifer. The Cano sector is constituted by the endorheic basin of Cano. Although some areas are more productive than others, this sector has a homogeneous behavior (Cupeto 1991). In this sector, two aquifers can be identified: a superior one that refers to the Pleistocenic calcareous Cano, and an inferior one associated to the dolomitic and carbonated Paleozoic formations of Estremoz (Cupeto 1991). The permeability in the calcareous lake of Cano is approximately interstitial and the waters are mainly calcium-bicarbonate, sometimes calcium-magnesium-carbonate (Cupeto 2003).

Estremoz sector

This sector corresponds to a karst-fractured phreatic cracked aquifer, mainly associated to the dolomitic formations and the marble of the Estremoz anticline. This aquifer is limited internally and externally by low productive metamorphic rocks that mostly behave as impermeable formations when compared with the limestones. Water infiltration, circulation and rocks dissolution in karst environments mostly depend on secondary porosity and the fracturing net. Natural springs mostly occur along the contact between surrounding shales and karst pipelines where water flows. With a NE-SW dense fracturing net, the Estremoz anticline is highly compartmentalized but also impermeable in some areas due to the clayey fill along some of the fractures (ERHSA 2001).

The water circulation in the sector of Estremoz occurs both along fractures and karst structures; therefore the net circulation is divided into two sub-systems (Carvalhosa et al. 1987): the karst openings and the micro-fractures.

The Estremoz sector's hydrogeology splits in two other sectors: the SE sector, to the south of the city of Estremoz, where groundwater flow direction is transverse to the aquifer and can reach flow gradients up to 50‰; and the NW sector, where flows are towards NW and gradients do not exceed 13‰ (ERHSA 2001) (Figure 13).

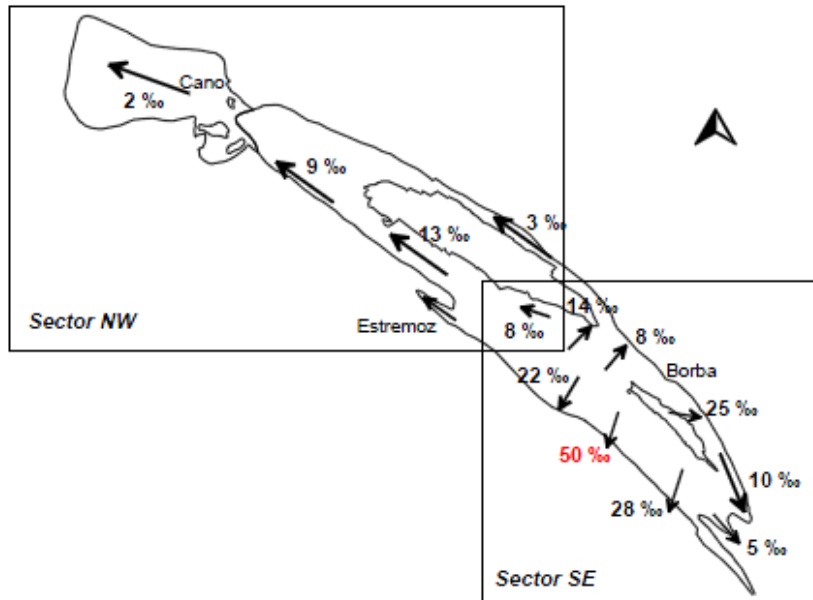


Figure 13: Water flow directions in the Aquifer System Estremoz-Cano; (Adapted from ERHSA 2001).

The justification for this high gradients can be found in the partitioning of the aquifer, namely in its S-W part, where large impermeable deep vertical dykes of sub-volcanic rocks cut the aquifer in the NW-SE direction, turning it difficult the groundwater movement in the NE-SW direction.

5.2.3 Elvas –Vila Boim Aquifer system

With a total area of 113.2 km², the study area covers a small part of the W extreme aquifer system in the Vila Fernando parish of Elvas County. The geological formations that store the water of this aquifer system are: the psammitic- coarse formation; the carbonated formation of Elvas; Vila Boim formations; and the Terrugem formation. The study area covers part of the carbonated formation of Elvas formed by dolomitic limestones and marbles (CD), the main lithological support of this system, where the water table is near the topographic surface. In the W sector, the recharge is provided by the precipitation (ERHSA 2001). With an infiltration rate of 25% and an average annual precipitation of 599 mm, in this system the efficient infiltration is quantified in 150 L/m² per year (ERHSA 2001). The public water supply is mostly assured by the water of the Caia artificial lake and only small locations still consume water from the Elvas-Boim Aquifer System.

The flow values inquired during ERHSA range from 1 to 6 L/s in most of the wells of the SW sector. In a general approach, the groundwater circulation and the flow direction tend to follow topography. In the study area the flow is towards NW (ERHSA 2001) (Figure 14).



Figure 14: Water flow directions in the Aquifer System of Elvas-Vila Boim; A – Area covered by the study area (Adapted from ERHSA 2001).

5.2.4 Aquifer system Alter do Chão-Monforte

With a total area of 69 km², the aquifer system outcrop area is an elongated ellipse along the NW-SE direction that intercepts Alter do Chão, Cabeço de Vide, Viamonte and Monforte parishes from the counties of Alter do Chão, Fronteira and Monforte, respectively.

The aquifer system of Alter do Chão-Monforte is organized in two connected aquifers. The midland aquifer with an area of about 30 km² is associated to the basic and ultrabasic rocks of Alter do Chão and Cabeço de Vide Massif, while the peripheral aquifer, with about 39 km², is within the calcareous, basic and ultrabasic formations. Both aquifers are phreatic, being the midland aquifer fractured and the peripheral aquifer a karst-fractured aquifer. The recharge is provided by rainfall with an annual average precipitation of 631 mm, of which 13% infiltrates, corresponding to an efficient infiltration of 82.03 L/m² (ERHSA 2001). This aquifer is very important and it is the main water supply resource for public and private use of the counties where it is located, whether to domestic consume, agriculture or industry.

The flow direction in the aquifer system at the regional scale is essentially towards SW and the natural discharge occurs in springs, typically along the contact between both aquifers (ERHSA 2001).

5.2.5 Igneous rocks of Nisa, Portalegre and Santa Eulália

With an outcropping area of about 1450 km², this low productive sector occurs in two separated areas: the first one occurs in a significant area of the counties of Nisa, Castelo de Vide, Marvão, Crato, Portalegre and Alter do Chão, while the second outcrops in the counties of Monforte, Arronches and Elvas. The study area intercepts the south aquifer sector in the Monforte parish, where it occupies nearly the whole parish area.

This sector is a fractured, very heterogeneous and anisotropic, with low hydrogeological potential where the flow is very low. With an annual mean precipitation of 724 mm and 5% of mean infiltration capacity, the efficient infiltration corresponds to 36 L/m² (ERHSA 2001).

The water wells are essentially used for agriculture and cattle rising, and only a small percentage of wells (15%) is used for public supply in the small villages.

5.2.6 Aquifer system Pavia-Mora

With about 267 km², elongated and NW-SE oriented, this system crosses the Pavia, Vimieiro and Santa Maria (Évoramonte) parishes, respectively in the counties of Mora, Arraiolos and Estremoz.

This aquifer is within the metamorphic rocks of the OMZ and the two micas granite of Mora, Evoramonte and Seda, which occupy almost all the aquifer system. The water circulation in this aquifer is typical of fissured aquifers, and water mainly percolates along porous and fractures in the weathered zone and deeply along fractures. This aquifer is essentially phreatic and its moderate productivity is due to a dense fracturing network and to the presence of weathered horizons. The annual average precipitation is 605 mm, of which 10% infiltrates (ERHSA 2001) corresponding to an efficient infiltration of 60.50 L/m². The heterogeneity of this aquifer reflects on the values of the measured flow in wells, which range from 0 to 28 L /m². Most of the groundwater in this aquifer is abstracted for private domestic use, agriculture and cattle in small farms.

The study carried out during the ERHSA Project (2001) allowed defining the infiltration in Alentejo aquifers, based on previous works using different methodologies, reflecting the recharge and the productivity thereof. In what concerns to the aquifers within the study area, infiltration is higher in the aquifers Estremoz-Cano and Elvas-Vila Boim and lower in the metamorphic and igneous rocks of the OMZ (Table 4).

Table 4: Efficient infiltration in the aquifer systems of the study area.

	Anual Mean Precipitation (mm/ano)	Infiltration (%)	Efficient Infiltration (L/m ²)
Aquifer System Alter do Chão-Monforte	631	13	82.03
Igneous rocks of Nisa , Portalegre and Santa Eulália	724.3	5	36,22
Aquifer System Elvas-Vila Boim	598.8	25	149.7
Aquifer System Estremoz-Cano	636.8	30	191.04
Aquifer System Pavia-Mora	605	10	60.5
Metamorphic and igneous rocks of the OMZ	627	5	31.35

Chapter 6 – Exploratory Models for water table occurrence prediction

6.1 Theoretical framework

The earth surface is a continuous field of an infinite number of points, each representing an infinite number of different natural characteristics. Raster surfaces consist of continuous data organized in a matrix of equal size cells, where each stores data that represents a real-world phenomenon such as elevation, the basis of the present work.

Since it is impossible to measure real elevation for each of the infinite points that constitute the earth topographic surface, elevation surface models apply an algorithm to a set of sampled real elevation data information in order to interpolate it into a digital elevation model (DEM) close to reality. The spatial analysis of the topographic surface draining water to the sampled aquifer systems started with a DEM at different resolutions to acquire and infer on extra information about the surface metrics, shape and processes, namely its curvature, hydrologic information and its influence on infiltration processes. In fact a varied amount of spatial phenomena are proved to be statistically self-similar over different scales (Goodchild and Mark 1987). To identify and distinguish possible local structural phenomena and better understand the influence of topography in the water flow and infiltration processes, all the raster analysis were held in four different resolutions corresponding to four different cell sizes:

- 25 | 50 | 100 | 200 (meters)

When defining the raster cell size, one must take into account that on the one hand cells must be small enough to capture the surface detail but on the other hand to be large enough so that computer and data storage can be efficient. In what concerns to elevation data this is typically a homogeneous variable in a certain area so that cell size can be larger without the loss of accuracy.

The more homogeneous an area is for a given variable, such as topography and land use, the larger the cell size can be without affecting accuracy. During the raster analysis output rasters were created with the same resolution than the input data.

During the inquiry of a relation between the topographic surface and the water table new four indexes were created and tested, two local and focal indexes and two structural indexes:

Local Indexes:

- Normalized Mean Curvature– Local Curvature
NMC
- Convexity Index– Local Convexity
Convex

Structural Indexes:

- Structural Convexity Indexes
StructConvex_1
StructConvex_2

All four indexes started from a common dataset:

- Altimetry – Elevation points and contour lines (equidistance of 10 meters) from The Topographic Military Maps 1: 25000.

SWL sampling was done randomly and with the support of the Topographic Military Maps 1: 25000 where wells are identified (Figure 15). The location of the wells was then recorded in a GPS Garmin.



Figure 15: Example of a dug well where SWL was measured resorting to a piezometric probe as illustrated in the image.

All features were projected in the same Coordinate System:

Projection: Lisboa_Hayford_Gauss_IgeoE

Geographic Coordinate System: GCS_Datum_Lisboa_Hayford

Datum: D_Datum_Lisboa_Hayford

6.2 Definition of the Study Area

The main aquifer systems intended to study in the present work, were the aquifer system Estremoz-Cano and the surrounding Metamorphic and Igneous Rocks hydrogeological Sector of the OMZ, covering data from two distinct aquifer's type. The first one is karsty type and the second one fractured type. Given the wells dispersion, their heterogeneous and random spatial distribution in the terrain and the difficulty to access or even find many of the wells identified in the Topographic Military Maps, the sample of the SWL was conditioned by the accessibility thereto. In the Aquifer System Estremoz-Cano this was easier to achieve once this is a more productive aquifer and the well's density is higher, increasing near the main villages. Once the wells were properly represented and geographically projected in ArcGis[®], the digital elevation model (DEM) was constructed with the altimetry of the corresponding topographic military maps. By overlapping and analyzing the hydrographic network obtained with the Flow Accumulation Tool, the pour-points were then featured. Resorting to the Watershed Tool of the Hydrology Toolset in the Spatial Analyst the micro basins were then defined corresponding to the study area of the present thesis.

Following is a resume and a scheme of the several steps executed up to the study area definition:

1. Topo to Raster Tool

Input feature data: Alti (Type: Contour) and Alti_pts (Type: Point_elevation)

Cell Size: 25 | 50 | 100 | 200

Output: DEM_25 | 50 | 100 | 200

2. Fill Tool

Input surface raster: DEM_25 | 50 | 100 | 200

Cell Size: 25 | 50 | 100 | 200

Output: Fill_25 | 50 | 100 | 200

3. Flow Direction Tool

Input surface raster: Fill_25 | 50 | 100 | 200

Cell Size: 25 | 50 | 100 | 200

4. Flow Accumulation Tool

Input flow direction raster: FL_direc25|50|100|200

Output: FI_Acc25|50|100|200

5. Watershed Tool

Input flow direction raster: FL_direc25 | 50 | 100 | 200

Input raster or feature pour point data: pour_point

Output: watershed_25|50|100|200

Spatial Analysis

The ArcGIS Spatial Analyst extension is the key to model and analyze spatial surfaces, supplying a varied set of tools to perform raster-based spatial analysis. Among others, Spatial Analyst allows to explore rasters, perform statistical analysis, interpolate data values, create Map Algebra expressions, integrate raster data with traditional vector data sources, combine datasets, derive new information from existing data and perform complex raster operations. The set of raster analysis that can be performed additionally include other terrain analysis, surface interpolation, hydrological analysis and statistical analysis.

Topo to Raster

Interpolation predicts the surface characteristics for any geographic data point missing spatial information, based on a limited number of sample data and on the assumption that spatially distributed objects are spatially correlated. Spatial interpolation has as principle the “first law of geography” of Waldo R. Tobler in 1930, also known as Tobler’s Law of Spatial Autocorrelation, which can be paraphrased as follows: “all places are related but nearby places are more closely related than distant places.”

Created from the ANUDEM program by Michel Hutchinson in 1988/89, Topo to Raster interpolates a digital elevation model (DEM) from point, line or polygon elevation data specifically calculated for the creation of a correct hydrological surface. The created surface ensures a correct representation of ridges and streams from the input contour data and thereafter a connected drainage structure representing a natural drainage surface. For Contour Input Data, Topo to Raster first generates a generalized morphology of the surface based on the contour curvature, and then the algorithm implements the contour elevation z-values.

For the creation of the DEM of the study area (Figure 16) the input features containing the elevation data (Alti and Alti_pts) cover the total extent of the Military Topographic Maps 1: 25 000 enumerated below:

- 368 – 372; 381 – 385; 395 – 399; 409 – 413; 423 – 427; 437 – 441; 448 – 452

Topo to raster interpolation conditions defined for the DEM:

Input: Alti (Type: Contour)
 Alti_pts (Type: Point_elevation)
Drainage enforcement: ENFORCE

Primary type of input data: Contour
Raster resolution
Cell Size: 25|50|100|200
Output: DEM_25|50|100|200

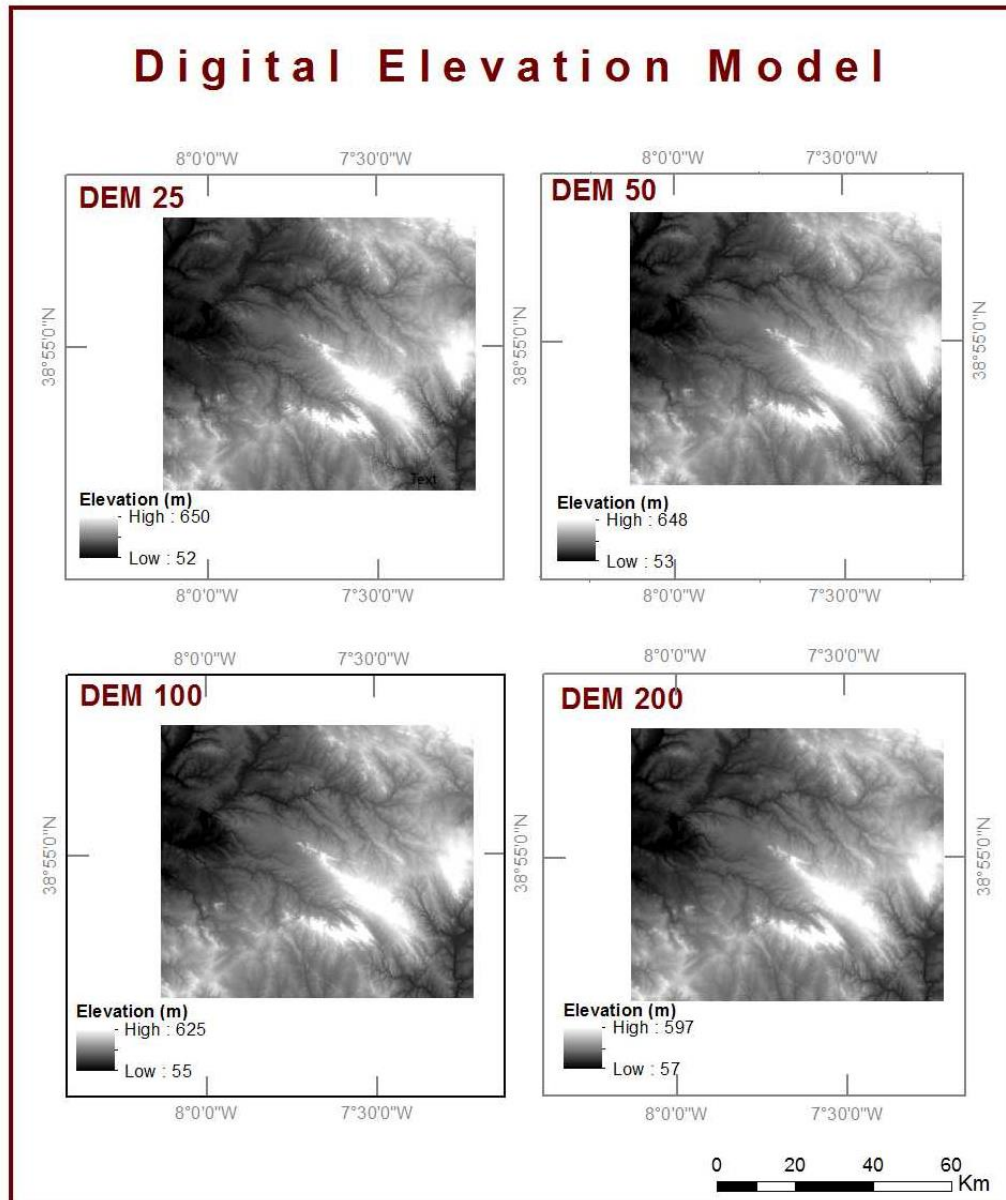


Figure 16: Digital elevation model of the study area for different raster resolutions.

Fill Tool

The creation of a DEM without any false sinks implies that sinks are raised to the lowest elevation value on the border of the depression (Jenson and Domingue 1988). Except for the natural depressions associated to karst or glacial geomorphology, the presence of sinks in DEMs are normally due to errors in data or to sampling effects and the rounding of the elevation values to the nearest integer value. In order to ensure a correct representation of the drainage system and consequently the delineation of basins and streams originated during the DEM computing process sinks must be filled. Previous research has almost universally recognized that depressions, that is, areas surrounded by higher elevation values, in the DEM data are the nemesis of determining hydrologic

flow directions because depressions must be filled before the flow can continue (Jenson and Domingue 1988).

As the selfsame name describes, the Fill tool fills the sinks in the DEM by an iterative process during which the fill tool identifies sinks and fills them by increasing the elevation value of the sink cells to the lower elevation value of the adjacent cells. Sinks will be filled to the z-limit; this is the maximum depth that will be filled to level the sinks to the lowest adjacent neighbor cell (Figure 17).

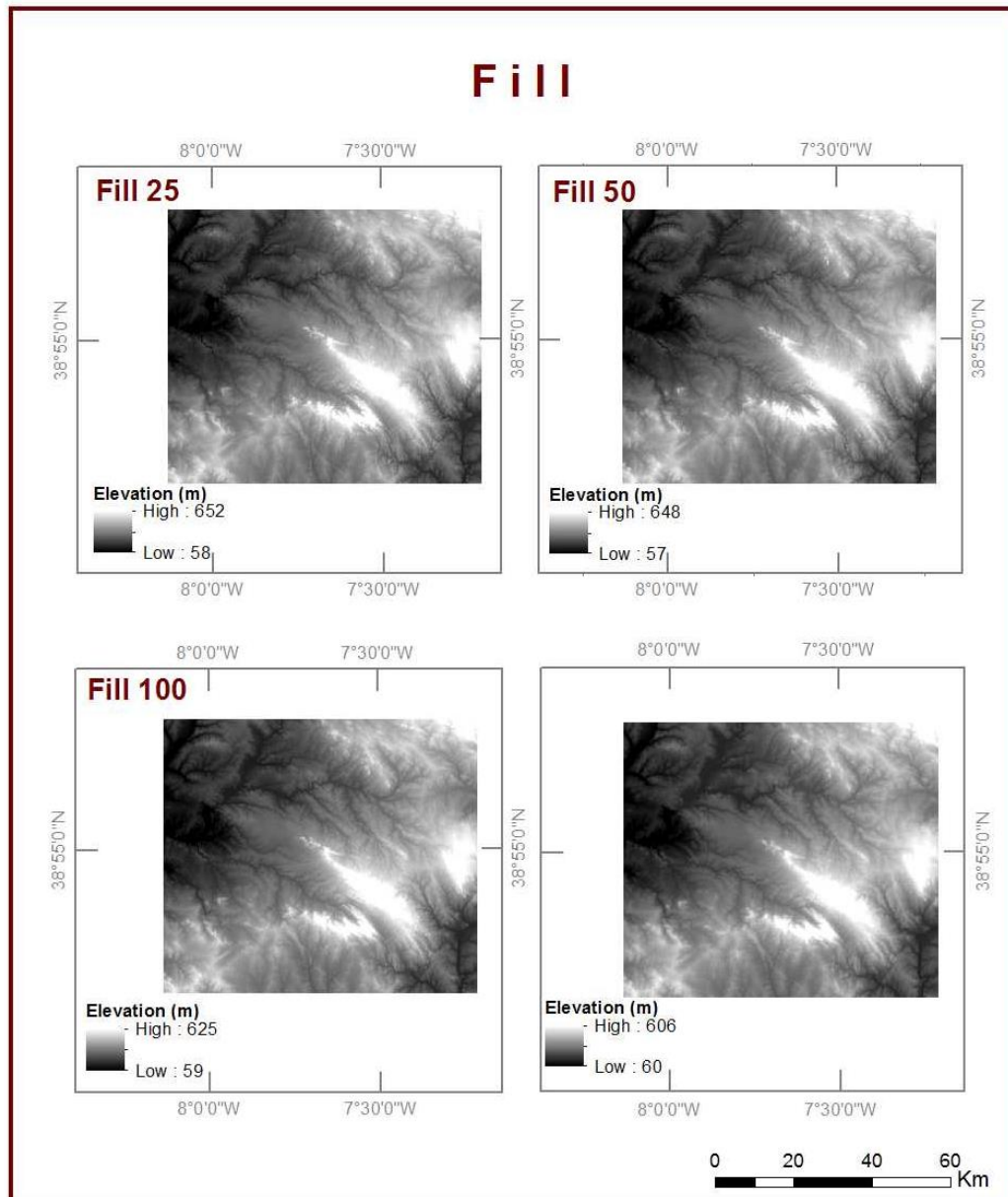


Figure 17: Digital elevation Model after filling the sinks by using the Fill Tool of the Hydrology Toolset.

Flow Direction

Since we are modeling water movement at the surface, two essential questions must be answered: Where does the water come from and to where is it flowing?

When modeling water movement at the surface in a raster there are eight possible valid output directions to where water can flow. Knowing that water always flows towards the steepest descendent direction, water drop of each cell relative to its eight adjacent cells is calculated based on the change in the elevation value and the horizontal distance between the cell's centers.

$$\text{Water Drop} = \frac{\text{Change in } z \text{ value}}{\text{Horizontal Distance}} * 100$$

For adjacent orthogonal cells, the horizontal distance corresponds to the distance between cell centers, which is equal to the cell size, while for diagonal adjacent cell the horizontal distance is the product between the cell size and the square root of 2 (cell size*√2).

A code is defined to each of the eight directions toward which water may flow (Figure18). This approach is referred as an eight-direction (D8) flow model and follows an approach presented in Jenson and Domingue (1988). Once the steepest downslope direction is established, the output cell is attributed with the value that codes that direction.

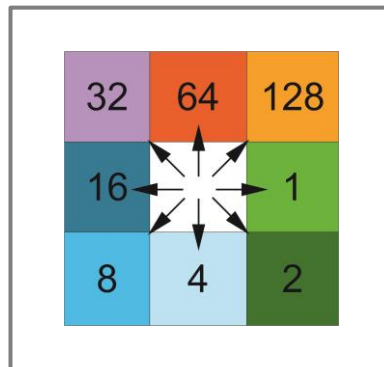


Figure 18: Color and number coding of the direction flow scheme use in Flow Direction.

Consequently the Flow Direction is the crucial tool for modeling hydrologic characteristics of a surface and water flow, once it outputs a raster showing the direction from where water will flow out for each cell of the DEM (Figure 19).

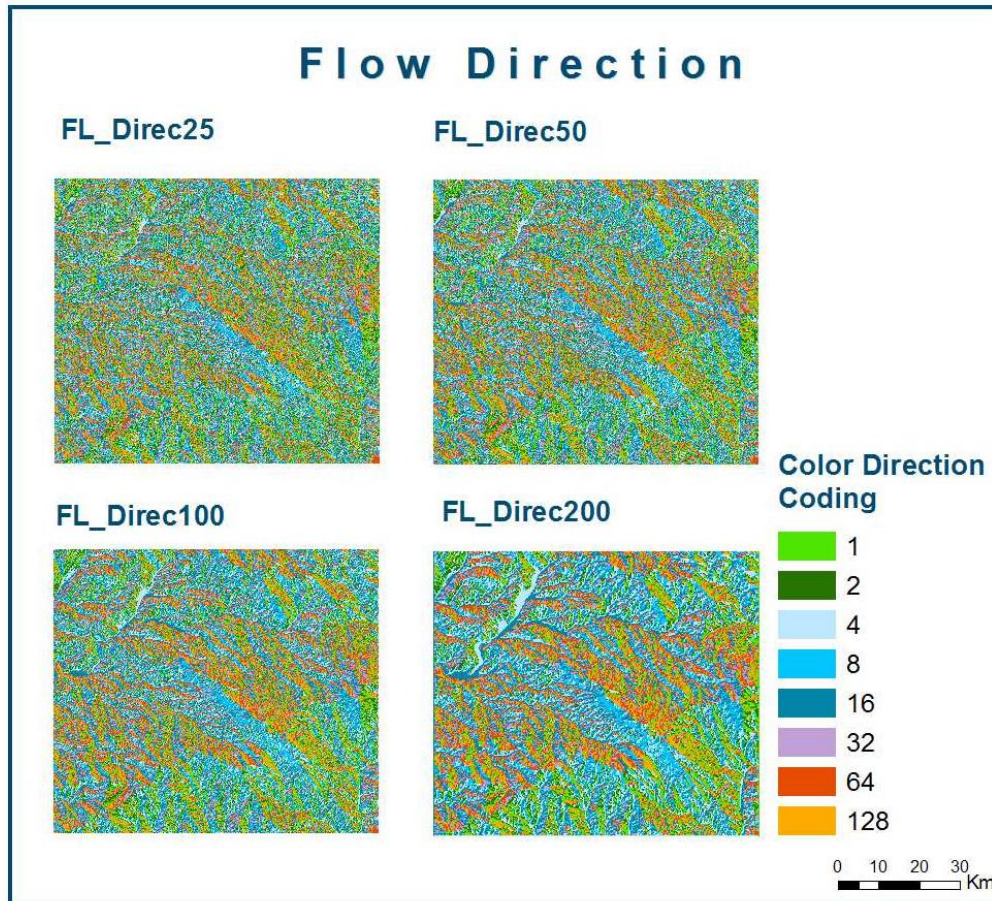


Figure 19: Flow direction within the study area for different raster resolutions.

Flow Accumulation

The flow accumulation tool creates an output raster in which to each downslope cell is assigned the number of accumulated cells flowing into that cell (Figure 20). In this way, each cell value in the output raster corresponds to the number of cells flowing into each cell. The direction of flow is given by the input flow direction raster.

While cells with the higher flow accumulation values define areas of concentrated flow and may be used to identify stream channels, cells with no flow accumulation correspond to topographic highs that can display ridges.

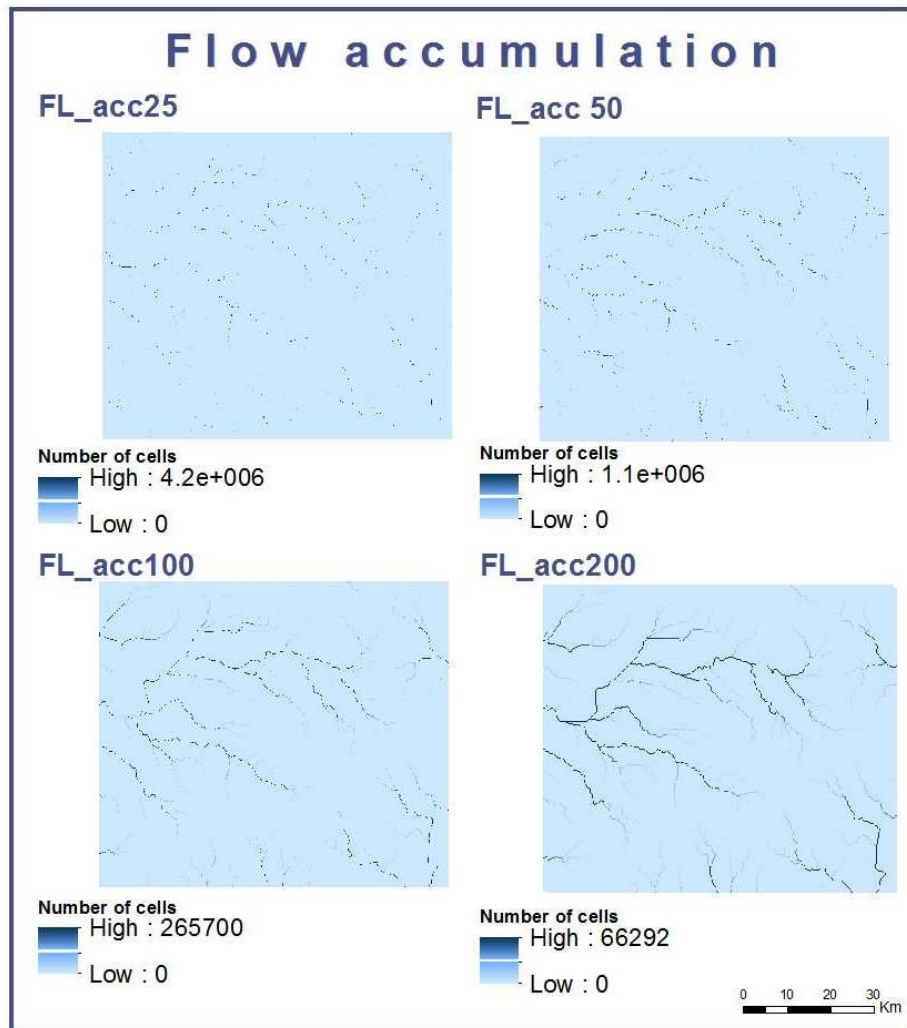


Figure 20: Flow accumulation within the study area for different raster resolutions.

Watershed

The delineation of a drainage basin with the Watershed Tool results in the computing of a flow direction raster after the identification of the pour points. The watershed tool delineates the upslope area that drains water to the given pour points or outlets. The Watershed Tool allows not only the definition of the main watersheds but also the delineation of the sub-basins.

Since surface water flow is only a subset of the Hydrologic cycle, and knowing that part of the water that reaches the surface percolates until it reaches the water table, the area on which the present work focuses was defined by the delineation of the water catchment area (the sub-basins) that drains water in the area where SWL was measured. The SWL sampling was done along the total Aquifer Estremoz-Cano, extending to the Igneous and Metamorphic Rocks of the OMZ hydrogeological Sector.

The definition of the pour points that define the sub-basins in the study area came through the creation of a feature class named “pour_points” and thereof identification and edition in the stream network defined by the cells with the higher flow accumulation values in the flow accumulation raster “FL_acc200”. The delimitation of the micro basins, resorting to the watershed tool was defined for the maximum resolution considered (cell size 25 m) (Figure 21).

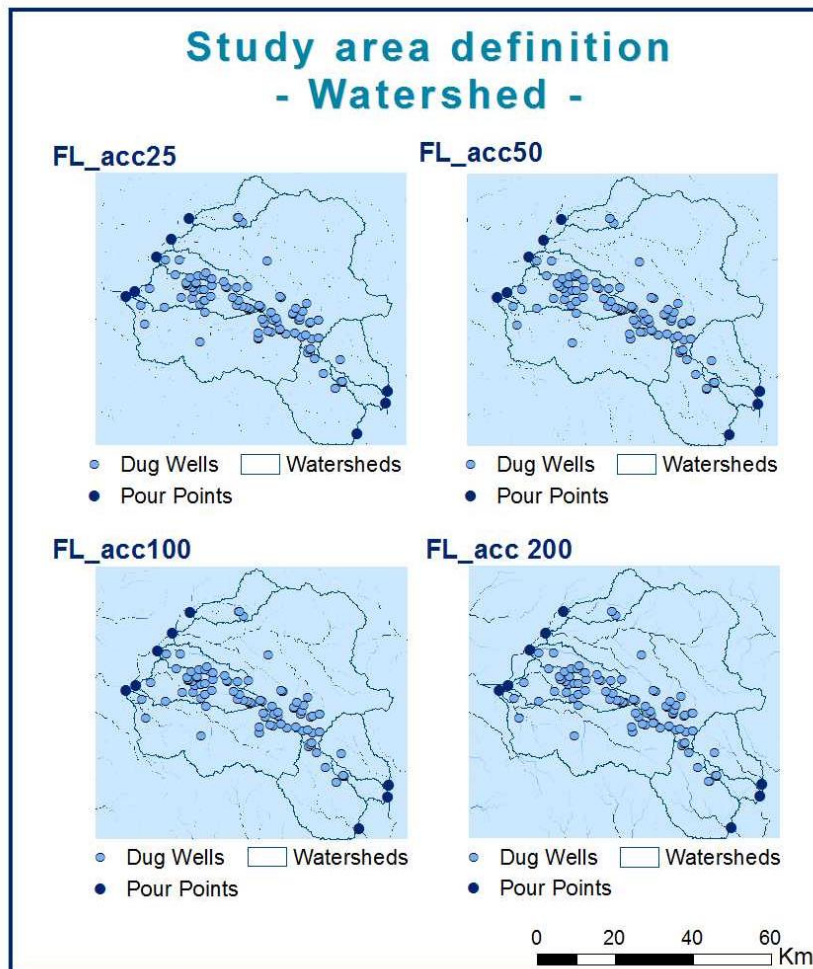


Figure 21: Definition of the study area by resorting to the Watershed Tool of the Hydrology Toolset.

Once the study area was delineated all the new output rasters were generated by extracting the cells within the area of the defined mask, in the case the watersheds.

6.3 Statistical Analysis Introduction

In order to predict a certain phenomenon based on observed data, the mechanism responsible by the observed phenomena is object of several theories (Murteira et al 2002). While a theory induces the creation of mathematical formulations from where a model raises, the model itself demonstrates, and explains the theory.



The present work aims at creating a model that predicts water table level in groundwater reservoirs after the topographic metrics, explicitly curvature, based on the assumption that the phreatic line tends to mark and go along with the topographic line.

Theory: Phreatic line tends to follow the topographic line

Theory's Object: Static Water Level (SWL) variation along with the surface curvature

Observed data: SWL measured in the field and elevation data.

Water tends to infiltrate in the relief tops where the bedrock is more exposed and fractured, which promotes water infiltration. Water table is not a direct consequence of the surface curvature; however, the curvature influences water infiltration and under convex surfaces the phreatic level tends to come up to the surface delineating the topography. Hence, the relation between the dependent variable (SWL) and the independent variables considered for the models presented in this work shows a functional dependence, where the dependent variable magnitude is a function of the magnitude of the independent variables but the opposite is not applicable (Maroco, 2003).

Currently the term "Regression Analysis" defines a set of statistical techniques used to model and predict the relation between one or more dependent variables from a set of independent variables, also known as predictors (Maroco 2003). Hereafter is the scheme of the steps taken to infer on the model that best explains SWL (Figure 22).

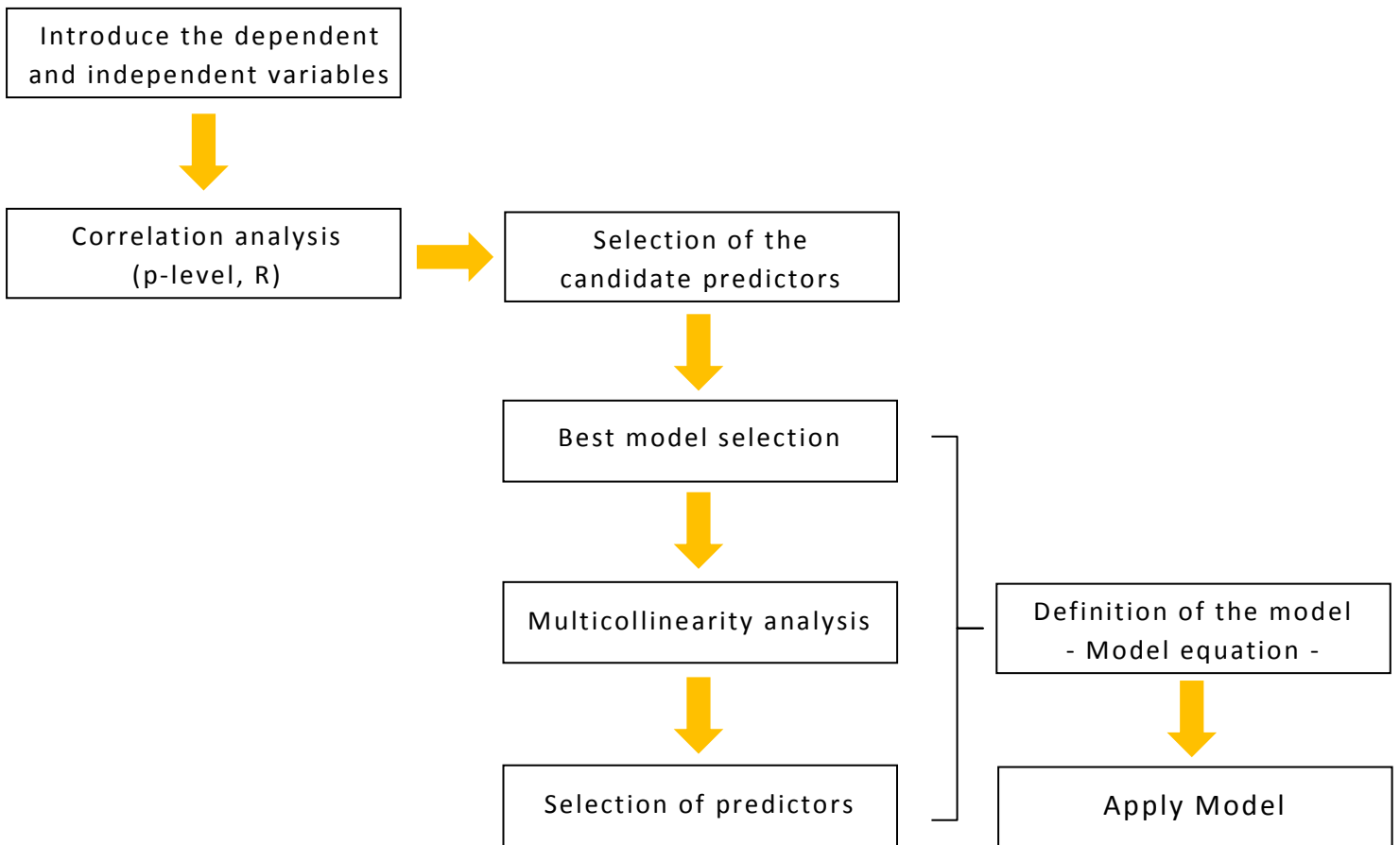


Figure 22: Flowchart of the statistical analysis and the best model definition

6.3.1 Inferring and validating the best model

During the exploratory phases of the relation between SWL and the surface curvature, several indices were calculated on the demand for the independent variables that best explain SWL. There is not a perfect method to select the best predictors for the best model. The determination coefficient (R^2) is a good index to evaluate the model's quality and adjustment; however, over-adjusted models with more independent variables than the accurately necessary present low estimation capacity when applied to a reality different from the one used to estimate the model (Maroco 2003).

Different parameters support the analysis and forecast the viability of a linear association that explains the behavior of the dependent variables according to the independent variables.

P - Level (p) – Significance level

P-level describes the significance level of correlations and represents an estimated degree of certainty from which the result may be assumed as true and representative of the population. The STATISTICA assumes by default that correlations are significant for $p\text{-level} < 0.05$; however, p -values lower than 0.01 and 0.1 are also frequently used. Therefore, p -level is a decreasing index of the reliability of a correlation result for which the higher the Statistical significance the less reliable is the relation between the variables in the sample.

R – Correlation coefficient

The Pearson correlation coefficient (R) infers on the magnitude and the direction of a linear association between two variables and determines the extent to which values of the two variables are linearly related to each other. The value of R varies between -1 and 1, in which the closer to the extreme the values are, the higher the linear association is, and therefore the correlation of the linear regression. Negative values of R ($-1 \leq R \leq 0$) indicate a negative linear association where the increase of a variable corresponds to the decrease of the second variable, whereas positive values indicate a positive linear association where the increase of a variable corresponds to the increase of the second variable.

$ R < 0.2$	Very weak
$0.2 \leq R < 0.4$	Weak
$0.4 \leq R < 0.7$	Moderate
$0.7 \leq R < 0.9$	High
$0.9 \leq R \leq 1$	Very high

R^2 – Determination coefficient

The determination coefficient (R^2) is calculated from R and varies between 0 and 1 despite mostly being presented and interpreted as a percentage value. The R^2 reflects the predictive capability of a model and measures the total variability proportion explained by a linear regression. In other words, R^2 measures the total variability of the dependent variable (Y) assigned to the dependence of Y to the independent variables (X_i) (Maroco 2003). For $R^2 = 0$ the model proposed does not fit to the data, whereas when $R^2 = 1$ the adjustment of the model to the data is perfect.

Multicollinearity

If in everything else different explanations for the same phenomena are identical, the simplest is the best. Known as Occam's razor, the principle of parsimony from William of Ocklam is enunciated as "*entia non sunt multiplicanda praeter necessitate*" (entities

must not be multiplied beyond necessity). This principle reflects multicollinearity problems that might arise when a strong correlation exists between the independent variables. Therefore, multicollinearity is a condition translated by a strong association and correlation between the independent variables. For a multiple regression model, when independent variables are far correlated, the model can turn out to be confusing and meaningless. Theoretically and under optimal conditions, independent variables are not correlated; yet in practice most cases present multivariate correlation matrices, showing some correlation between several of the independent variables. The origin of multicollinearity for independent variables may be in a common dependency with a variable not considered in the model data. Multicollinearity does not vary the determination quality (R^2) of a regression except when independent variables are perfectly linearly correlated ($R = 1$).

Nevertheless, it is essential to follow a multicollinearity diagnostics during the selection of the best independent variables and the model validation, so that the model objectives and the correlation coefficient may be fulfilled with total confidence (Maroco 2003). The multicollinearity diagnostics is normally performed in a bivariate correlation matrix, although it limits the diagnosis to independent variable pairs. When more than two independent variables are collinear, the bivariate correlation matrix procedure is not applicable. Multicollinearity problems arise for high bivariate correlations when $|R| > 0.75$ (Maroco 2003). In order to avoid multicollinearity problems, in the models that hereafter are presented, where considered at most two independent variables the less multicollinear possible.

6.3.1.1 Models verified

A linear association between the SWL (dependent variable) and the topographic surface metrics (independent variables) was assumed has a premise in the present work. A linear regression explains and predicts the behavior of the dependent variable in function of one or more independent variables. For the present work the first intention was to find the best predictors that would explain SWL in a multiple linear regression. However, the statistical analysis displayed a weak linear correlation and as the work was developing it was empirically proved that the best model is a Piecewise Linear regression.

Multiple Linear Regression

The multiple linear regression is a statistical model that explains the behavior of the dependent variable, quantitatively expressed by Y and two or more independent variables, quantitatively expressed by X_i ($i=1, \dots, p$).

The analytic expression representing a multiple linear regression is:

$$Y_j = \beta_0 + \beta_1 X_{1j} + \beta_2 X_{2j} + \dots + \beta_p X_{pj} + \varepsilon_i \quad (j=1, \dots, n)$$

β_0 – Intercepts

β_i – Regression coefficients ($i=1, \dots, p$)

ε_j – Error term (reflects the natural variation in Y)

Piecewise Linear Regression

The Piecewise Linear Regression is a common nonlinear regression model, though it estimates two separated linear regression equations. The point where the two lines separate is called the breakpoint (b_0) and the equation of this model is the result of the sum of both linear regression equations of the two lines. The equation of the first line estimates the y values that are less or equal to the breakpoint while the equation of the second line estimates the y values that are greater than the breakpoint.

The analytic expression representing a Piecewise Linear Regression is:

$$Y_j = (\beta_0 + \beta_1 X_{1j} + \beta_2 X_{2j} + \dots + \beta_p X_{pj}) * (y \leq b_0) + (\beta_0 + \beta_1 X_{1j} + \beta_2 X_{2j} + \dots + \beta_p X_{pj}) * (y > b_0)$$

β_0 – Intercepts

β_i – Regression coefficients ($i=1, \dots, p$)

ε_j – Error term (reflects the natural variation in Y)

6.4 Exploratory Models for water table occurrence prediction

6.4.1 Normalized Mean Curvature Index (NMC)

The new curvature index, Normalized Mean Curvature (*NMC*), was calculated with the main objective of smoothing the curvature calculated by ArcGis® in order to decrease the image noise and homogenize the surface, so as to be more authentic and closer to reality. Starting from the ESRI Curvature, *NMC* was created considering an average curvature within a defined neighborhood and normalizing the average curvature values to range from 0 to 1, facilitating the posterior statistical analysis. The following flowchart illustrates the several steps in the calculation of *NMC* at different cell sizes (Figure 23).

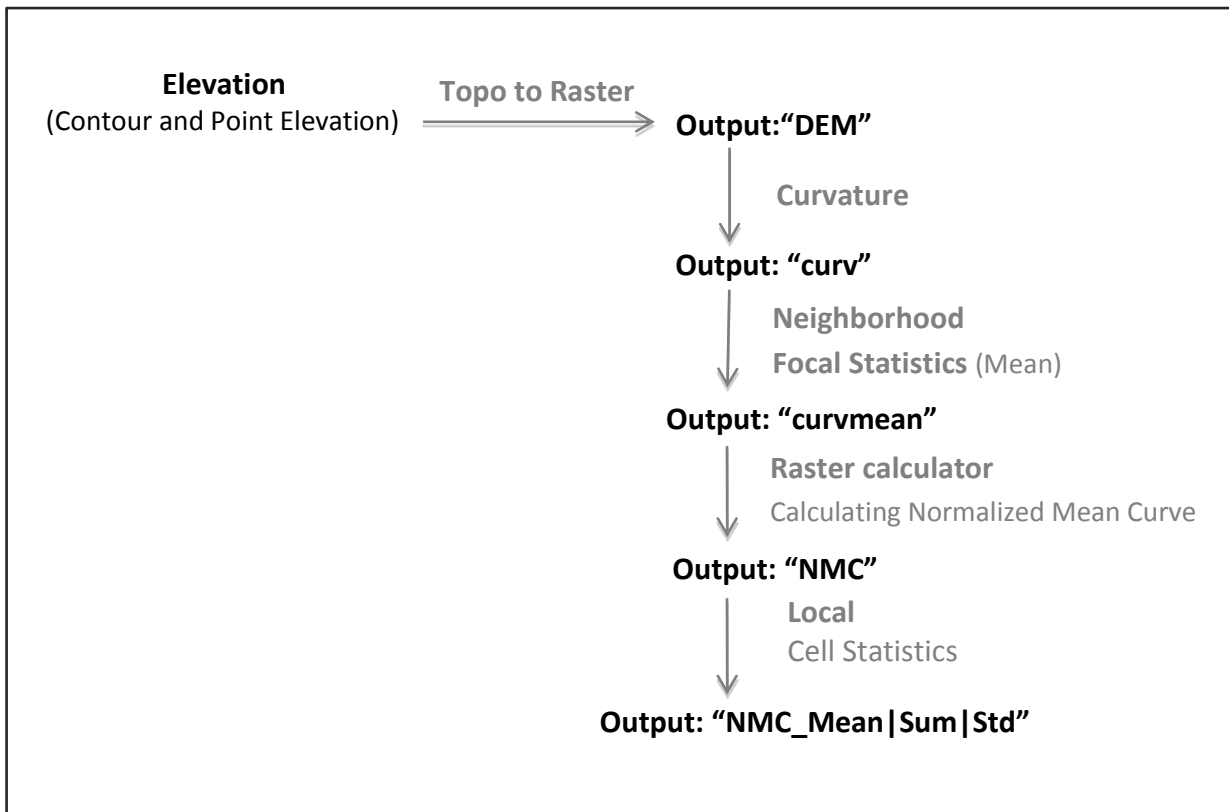


Figure 23: Flowchart illustrating the computation of NMC

During the calculation of *NMC* in each step four different output rasters were computed, one for each resolution according to the cell sizes considered. Above follows a resume of the conditions held in each step followed by a more detailed description of each tool used.

1. Curvature Tool

Input: DEM_25 | 50 | 100 | 200

Cell Size: 25 | 50 | 100 | 200

Raster analysis → **Mask:** Study area

Output: curv_25 | 50 | 100 | 200

2. Neighborhood Tool - Focal Statistics

Neighborhood settings:

Input: curv_25|50|100|200

Circle with a 3 cells radius

Statistic type: Mean

Cell Size: 25 | 50 | 100 | 200

Mask: Study area

Output: curvmean_25 | 50 | 100 | 200

3. Raster calculator

$$\text{Map algebra expression: } NMC = \frac{\text{curvmean} + \text{Low value}}{\text{Low value} + \text{High value}}$$

Output: NMC_25 | 50 | 100 | 200

Table 5: Higher and lower mean curvature calculated for each curvature raster at different resolutions.

	High	Low	Sum
curvmean_25	1.80876	0.881641	2.690401
curvmean_50	0.687087	0.368999	1.056086
curvmean_100	0.224895	0.181005	0.40590
curvmean_200	0.104655	0.059352	0.164007

4. Local tool – Cell Statistics

Input: NMC_25 | 50 | 100 | 200

Output: NMC_Sum | Mean | Std

6.4.1.1 Curvature Tool from ArcGis®

The analysis of the surface curvature was first held resorting to the Curvature Tool available in the Spatial Analyst extension of ArcGis® 10 (Figure 24) which calculates the second derivative of the input surface, in this case the DEM of the study area. The curvature tool calculates the second derivative, that is, the tilt of the slope, on a cell-by-cell basis. The result is an output raster where the curvature of the surface for each cell is the fit through that cell and the eight surrounding neighboring cells (Figure 25). The output curvature surface combines both the profile curvature and the plan curvature. While the profile curvature corresponds to the curvature along the maximum direction slope, the plan curvature is the surface curvature perpendicular to the direction of the maximum slope. Cells with positive values in the curvature raster have a surface upwardly convex

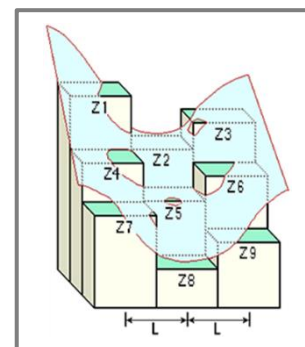


Figure 24: ArcGis® surface curvature scheme
(Source: ArcGis® 10 Help).

whereas negative values indicate cells upwardly concave. Flat surfaces with no curvature have null values.

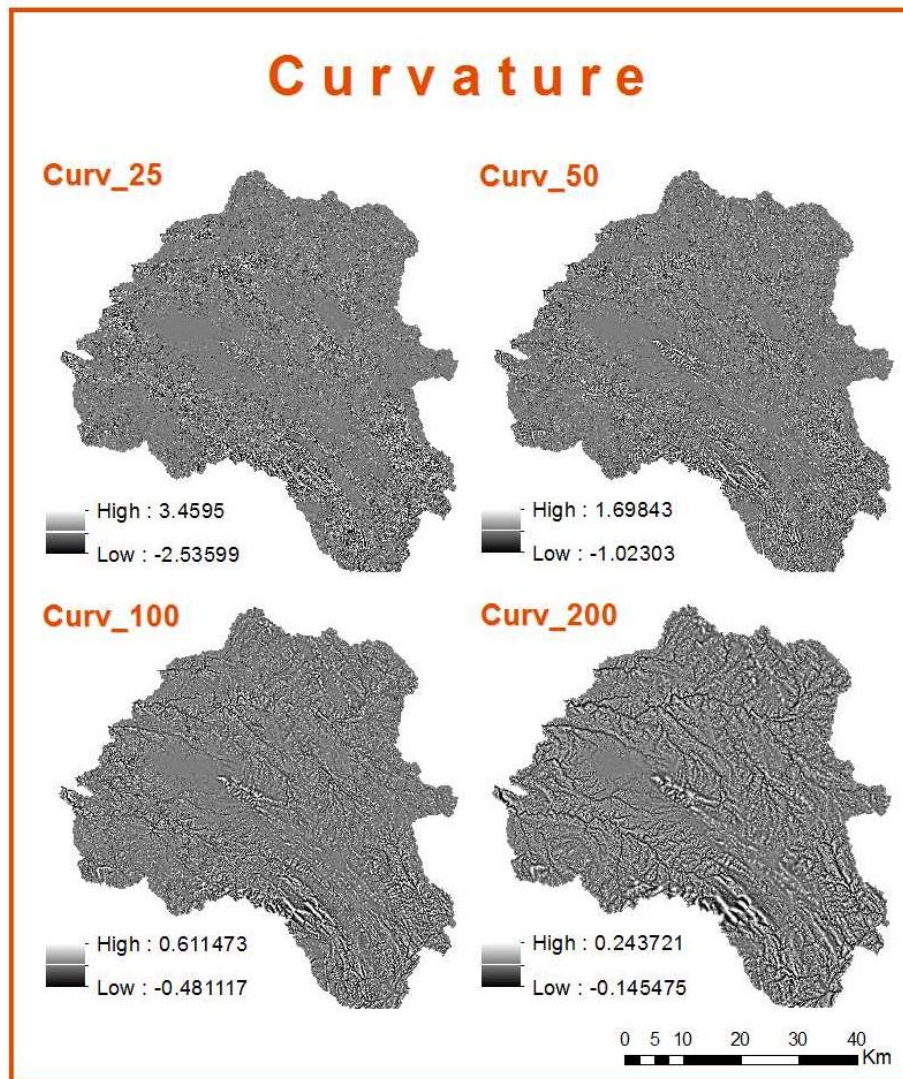


Figure 25: Curvature within the study area calculated with the Curvature Tool of the Spatial Analyst Extension of ArcGIS 10[®].

6.4.1.2 Neighborhood Tool - Focal Statistics

The Neighborhood Tool of the Spatial Analyst toolset creates an output raster where each cell value is calculated based on the values of the surrounding cells in a specified neighborhood. From the available Neighborhood tools, Focal Statistics performs a neighborhood operation in which for each cell a statistical parameter is calculated (e.g. minimum, maximum, average, range, sum, etc.) with the cell values of the specified neighborhood. The output computed is a raster where each cell value is the result of the statistical function performed with the neighborhood input cell values (Figure 26). When

neighborhoods overlap the cells in one neighborhood they may also be included in the neighborhood of another processing cell. There are four types of neighborhoods that can be defined during the focal statistics performance: annulus, circle, rectangular or edge.

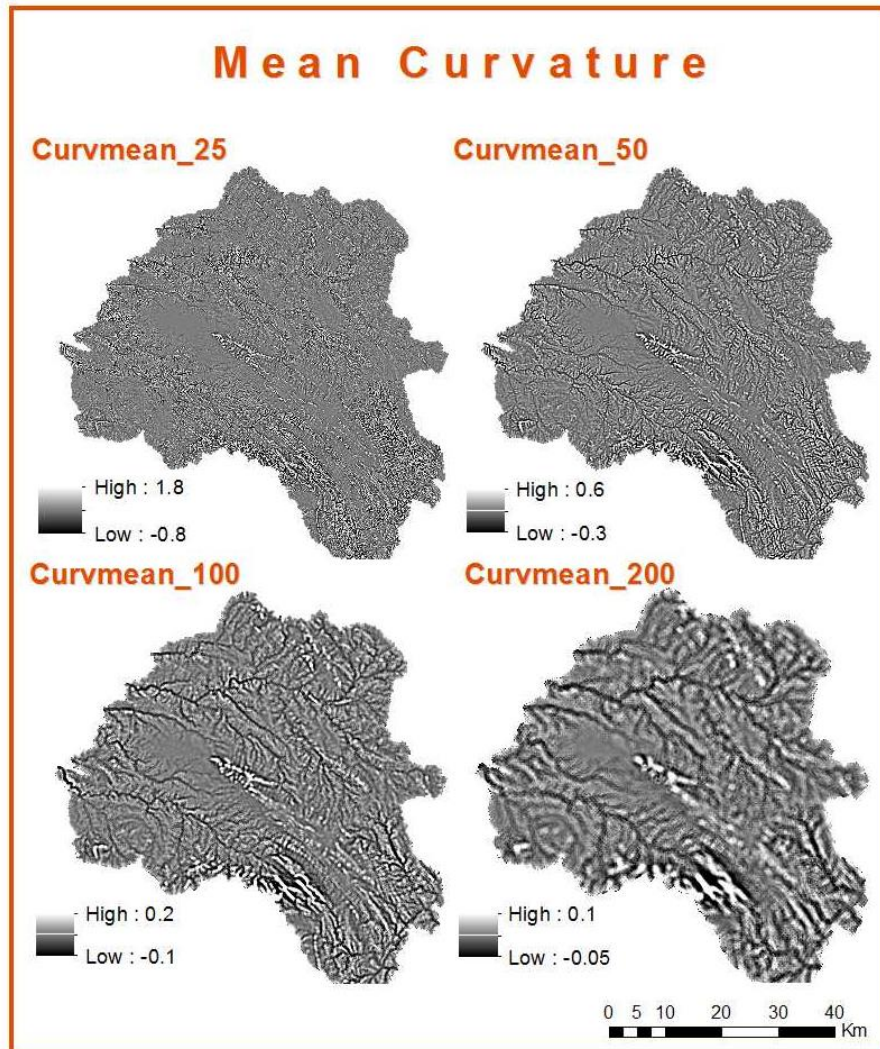


Figure 26: Mean Curvature within the study area calculated after the Curvature Raster with the Neighbor Tool of the Spatial Analyst Extension of ArcGis 10[®].

The calculation of the mean curvature was performed within a circle neighborhood with a radius of 3 cells (Figure 26). For a circle neighborhood, the values of all cells falling inside the radius of the circle will be considered in the calculation of the chosen statistical parameter (Figure 27).

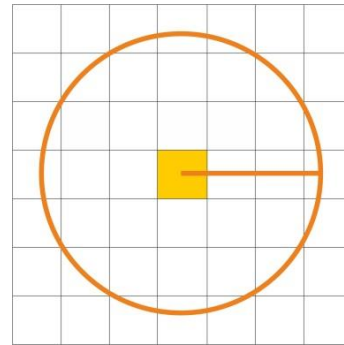


Figure 27: Scheme of the circle neighborhood applied with the neighborhood tool

6.4.1.3 The Normalized Mean Curvature Index

This is a local index evaluating and characterizing the terrain's curvature in a specific area according to the cell size defined and hence the raster resolution. This way the index evaluates the curvature within an area of 625 m² bounded by cells with 25 m sizes; 2,500 m² for cells with 50 m sizes, 10,000 m² for cells with 100 m sizes and 40,000 m² for a raster whose cells are 200 m sizes (Figure 28).

For the curvature calculated by ArcGis[®] positive values correspond to cells where the surface is upwardly convex whereas negative values correspond to cells where the surface is upwardly concave. Therefore flat surfaces curvature is zero.

In the present thesis the ArcGis[®] mean curvature was normalized ranging between 0 and 1 and consequently a new curvature index was defined: the normalized mean curvature (NMC) that was calculated based in the follow formula:

$$NMC = \frac{\text{curvmean} + \textit{Low value}}{\textit{Low value} + \textit{High value}}$$

By normalizing the curvature values the interval's values corresponding to upwardly convex surfaces and upwardly concave surfaces also change as well as the values of cells corresponding to a flat surface. Table 6 summarizes the values for which the surface is upwardly convex, flat or upwardly concave for each resolution considered.

Table 6: Values for which the surface is upwardly convex, flat or upwardly concave in the NMC Index.

Cell Size	Curvature Values		
	Upwardly Convex	Flat Surface	Upwardly Concave
25	[0 - 0.327699[0.327699]0.327699 - 1]
50	[0 - 0.349402[0.349402]0.349402 - 1]
100	[0 - 0.445936[0.445936]0.445936 - 1]
200	[0 - 0.361887[0.361887]0.361887 - 1]

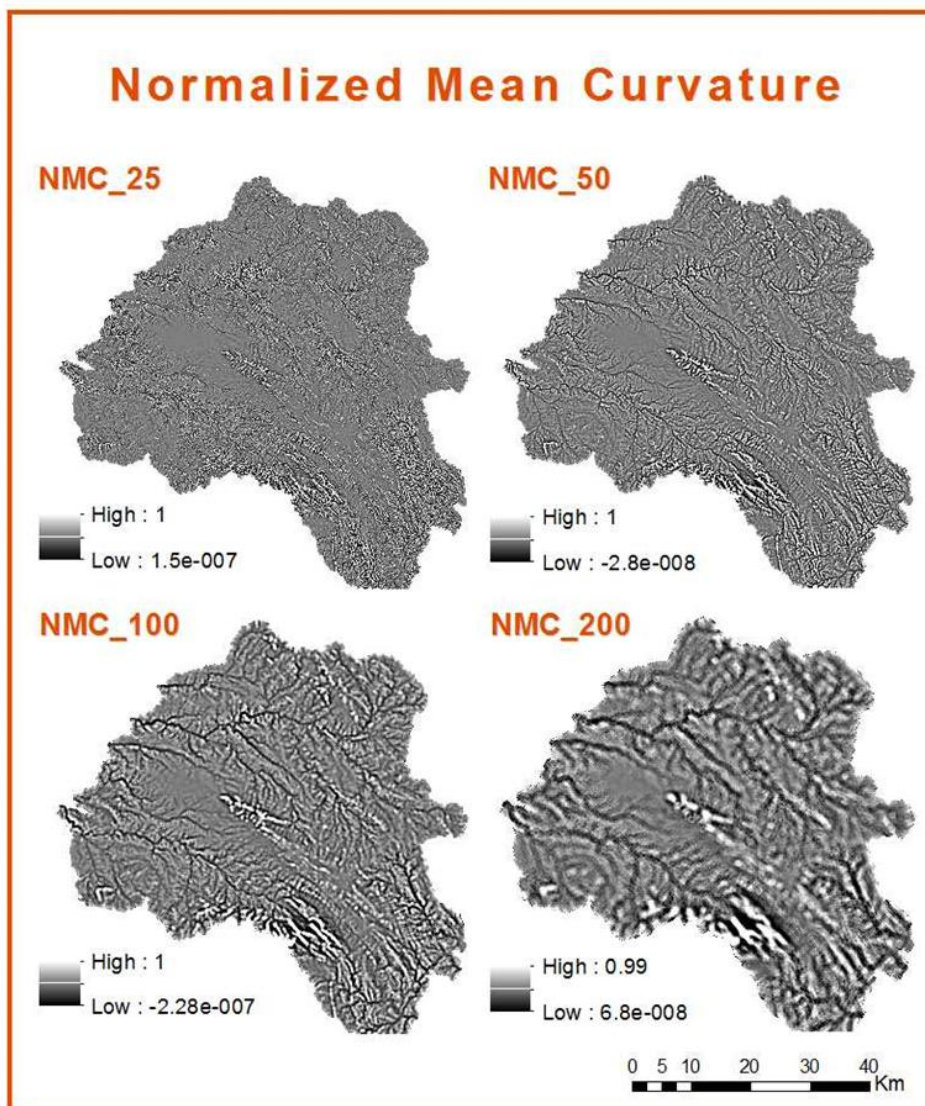


Figure 28: NMC Index calculated after the curvature from ArcGis 10[®] for different resolutions.

6.4.1.4 Local tool – Cell Statistics

The Local tool allows the combination of the information for multiple input rasters with the same exact location. The value of each cell of the output raster is the result of a combination, a calculated statistic or evaluated criteria of the values for each cell in the different input rasters

For the statistical analysis of the NMC index, the statistics of the NMC at the four different resolutions defined was also considered as an explanatory variable to explain SWL (Figure 28). Thus, the Cell Statistic Tool was used to calculate the Sum, the Mean and the Standard Deviation (Std) of each cell considering the four rasters calculated for the NMC with a cell size of 25, 50, 100 and 200 meters (Figure 29).

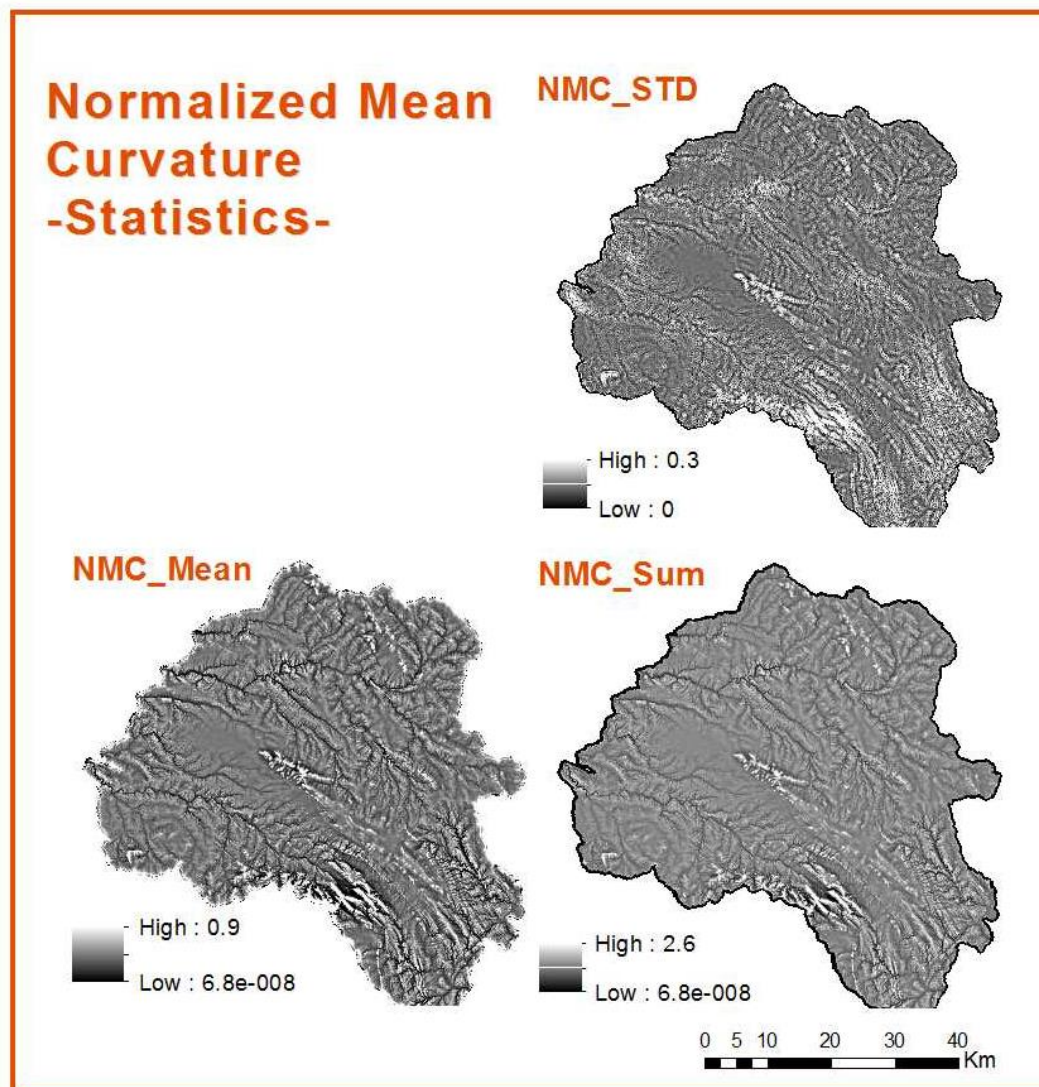


Figure 29: Cells Statistics of NMC Index calculated with the Local Tool of the Spatial Analyst Extension of ArcGis 10[®].

6.4.1.5 Statistical Analysis

Table 7 shows the correlation analysis, with the calculation of the significance level and the correlation coefficient by Statistica7 between the dependent variable and the independent variables computed during the determination of the Normalized Mean Curvature.

Dependent variable – SWL_m

Independent variables – curv; curv_mean; NMC; NMC_Sum | Mean | STD
(For different cell sizes: 25 | 50 | 100 | 200)

Table 7: Correlation Analysis for all the independent variables calculated in the computing of NMC.

Independent Variables	SWL_m	
	p-level	R
curv_25	0.292364	0.106879
curv_50	0.014294	0.245548
curv_100	0.000393	0.349388
curv_200	0.033846	0.213505
curvmean_25	0.000198	0.365598
curvmean_50	0.000058	0.392678
curvmean_100	0.571641	0.057532
curvmean_200	0.333737	0.098160
NMC_25	0.000198	0.365599
NMC_50	0.000058	0.392680
NMC_100	0.571638	0.057532
NMC_200	0.333725	0.098162
NMC_Sum	0.045919	0.201118
NMC_Std	0.866539	0.017106
NMC_Mean	0.045917	0.201120
DEM_25	0.000001	0.471222
DEM_50	0.000001	0.469727
DEM_100	0.000001	0.470095
DEM_200	0.000001	0.463158

The selection of the variables to include in the model is based on the correlation values and regarding that correlations are significant for p-level lower than 0.1. Once in the present analysis all the variables have a p-level lower than 0.1, in order to narrow the selection and increase the significance of the variables to include in the model to set, only the independent variables with p-level <0.001 will be considered as candidates for the model (highlighted in the table 8).

Table 8 summarizes the correlation and determination coefficients between SWL and each one of the independent variables, previously selected, for both multiple regressions: piecewise and linear.

Table 8: Correlation and determination coefficient among the dependent variable (SWL) and the independent variables selected for a Piecewise Linear regression and a Multiple Linear Regression in the calculus of NMC.

Candidate Independent Variables	SWL			
	Piecewise Linear Regression		Multiple Linear Regression	
	R	R ²	R	R ²
curv_100	0.82523	68.10%	0.34141	11.66%
curvmean_25	0.83201	69.22%	0.35589	12.67%
curvmean_50	0.83682	70.03%	0.38366	14.72%
NMC_25	0.82688	68.37%	0.21758	4.73%
NMC_50	0.83091	69.04%	0.25065	6.28%
DEM_25	0.83883	70.36%	0.471222	22.21%
DEM_50	0.83837	70.29%	0.469727	22.06%
DEM_100	0.83841	70.29%	0.470095	22.10%
DEM_200	0.83729	70.11%	0.463158	21.45%

The model that best explains SWL is a Piecewise Linear Regression for which the predictive capability is higher than 68% for all the candidate independent variables. Once they are all highly correlated ($0.7 \leq R < 0.9$) to the SWL but also likely to be correlated among them the selection of the independent variables to consider in the model presupposes a multicollinearity analysis (Table 9).

Table 9: Bivariate correlations matrix for the independent variables considered in the calculation of NMC.

	curv_100	NMC_25	NMC_50	curvmean25	curvmean_50	DEM_25	DEM_50	DEM_100	DEM_200
curv_100	1.00	0.62	0.61	0.62	0.61	0.12	0.12	0.12	0.11
NMC_25	0.62	1.00	0.65	1.00	0.65	0.02	0.02	0.01	0.00
NMC_50	0.61	0.65	1.00	0.65	1.00	-0.06	-0.06	-0.06	-0.08
curvmean_25	0.62	1.00	0.65	1.00	0.65	0.02	0.02	0.01	0.00
curvmean_50	0.61	0.65	1.00	0.65	1.00	-0.06	-0.06	-0.06	-0.08
DEM_25	0.12	0.02	-0.06	0.02	-0.06	1.00	1.00	1.00	1.00
DEM_50	0.12	0.02	-0.06	0.02	-0.06	1.00	1.00	1.00	1.00
DEM_100	0.12	0.01	-0.06	0.01	-0.06	1.00	1.00	1.00	1.00
DEM_200	0.11	0.00	-0.08	0.00	-0.08	1.00	1.00	1.00	1.00

Highlighted are the values whose independent variables are less multicollinear. Aiming to achieve the best model several pairs of independent variables were tested in a Piecewise Linear Regression. Table 10 presents the ones that best explain SWL.

Table 10: Proposal of the 3 models that best explain SWL based on the independent variables considered in the computation of NMC.

Model	Independent Variables	Piecewise Linear Regression		Multiple Regression	
		R	R ²	R	R ²
1	NMC_25 DEM_50	0.86261	74.41%	0.59085	34.91%
2	curvmean25 DEM_25	0.86260	74.41%	0.59088	34.91%
3	NMC_50 DEM_25	0.86120	74.16%	0.63285	40.05%

MODEL 1

The statistical analysis presented above permitted to define that the model that better explains water table occurrence is a Piecewise Linear Regression with the independent variables NMC_25 and DEM (Table 11).

$$\text{SWL (m)} = (-3.51435 + 19.38942 * \text{NMC}_{25} + 0.000329 * \text{DEM}_{50}) * (\text{SWL} \leq 4.724848) + (-13.3468 + 50.94833 * \text{NMC}_{25} + 0.011958 * \text{DEM}_{50}) * (\text{SWL} > 4.724848)$$

Table 11: Results for Model 1- Piecewise Linear Regression for the independent variables NMC_25 and DEM_50.

N = 99	Model is: Piecewise linear regression with breakpoint						
	Dependent variable: SWL_m Loss: Least squares Final loss:184.60806439 R= .86261 Variance explained: 74.410%						
	Const.B0	NMC_25	DEM_50	Const.B0	NMC_25	DEM_50	Breakpt.
Estimate	-3.51435	19.38942	0.000329	-13.3468	50.94833	0.011958	4.724848

6.4.2 Convexity Index (*Convex*)

Similar to the curvature calculated by ArcGis®, the new index now being proposed is a focal index, reflecting a local convexity, this is the terrain's convexity within each cell of the computed raster. Such as in the preceding model this new index was calculated for four different resolution, therefore evaluating the terrain's convexity within an area of 625 m² for cells with 25 m size; 2500 m² for cells with 50 m, 10000 m² for cells with 100 m and 40 000 m² for a raster whose cells are 200 m size. The following flowchart illustrates the several steps in the calculation of *Convex* (Figure 30).

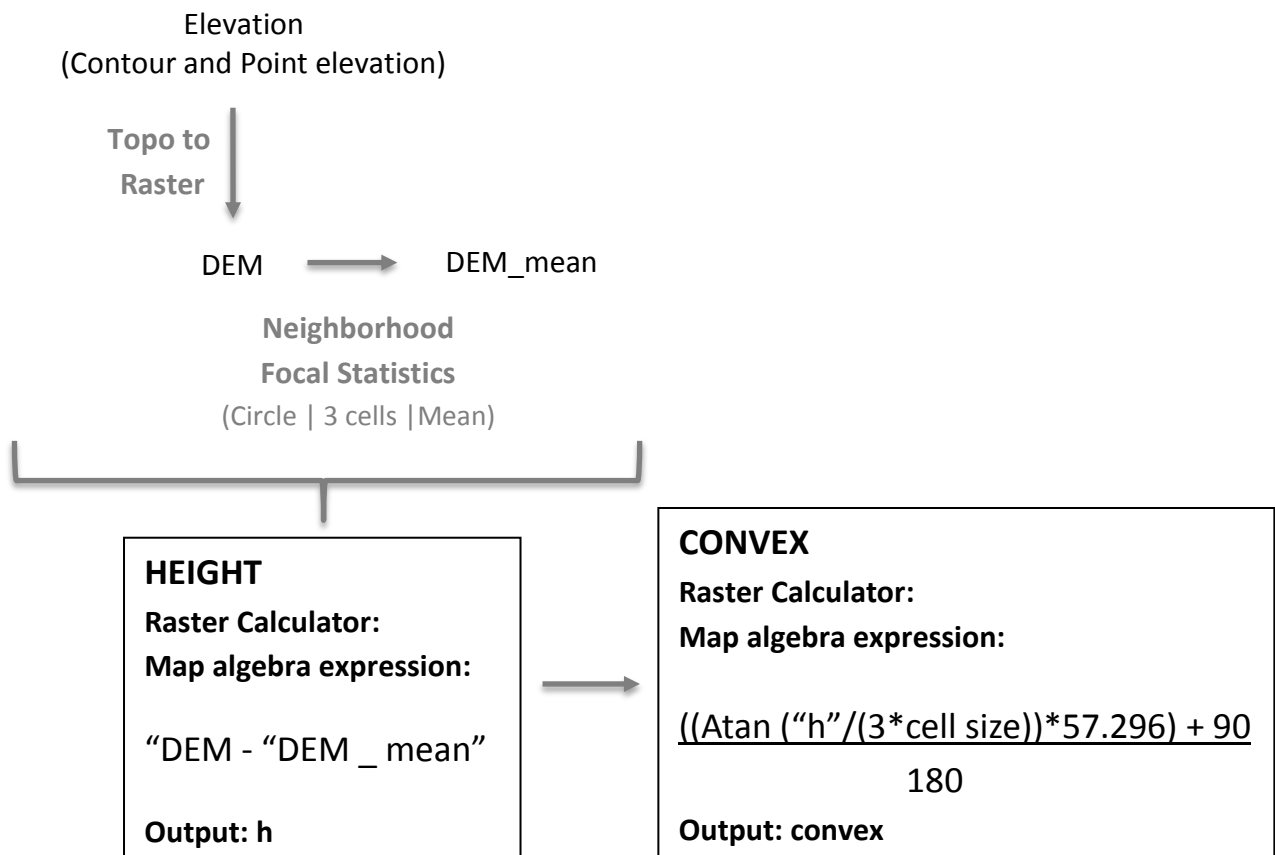


Figure 30: Flowchart with the scheme of the calculation of *Convex*.

Bellow follows a resume of the conditions hold in each step followed by a more detailed description of each of the steps taken.

1. Neighborhood Tool – Focal Statistics

Neighborhood settings:

Input: DEM_25|50|100|200

Circle with a 3 cells radius

Statistic type: Mean

Cell Size: 25 | 50 | 100 | 200

Mask: Study area

Output: DEM_mean25 | 50 | 100 | 200

2. Raster calculator

$$h = DEM - DEM_mean$$

Output: h_25 | 50 | 100 | 200

3. Raster calculator

$$Convex = \frac{(Atan (h/d) * 57.29578) + 90}{180}$$

Output: convex_25 | 50 | 100 | 200

6.4.2.1 Convex calculation

Convex is a local index evaluating the surface's curvature by applying the follow equation:

$$Convex = \frac{(Atan (h/d) * 57.29578) + 90}{180}$$

Where:

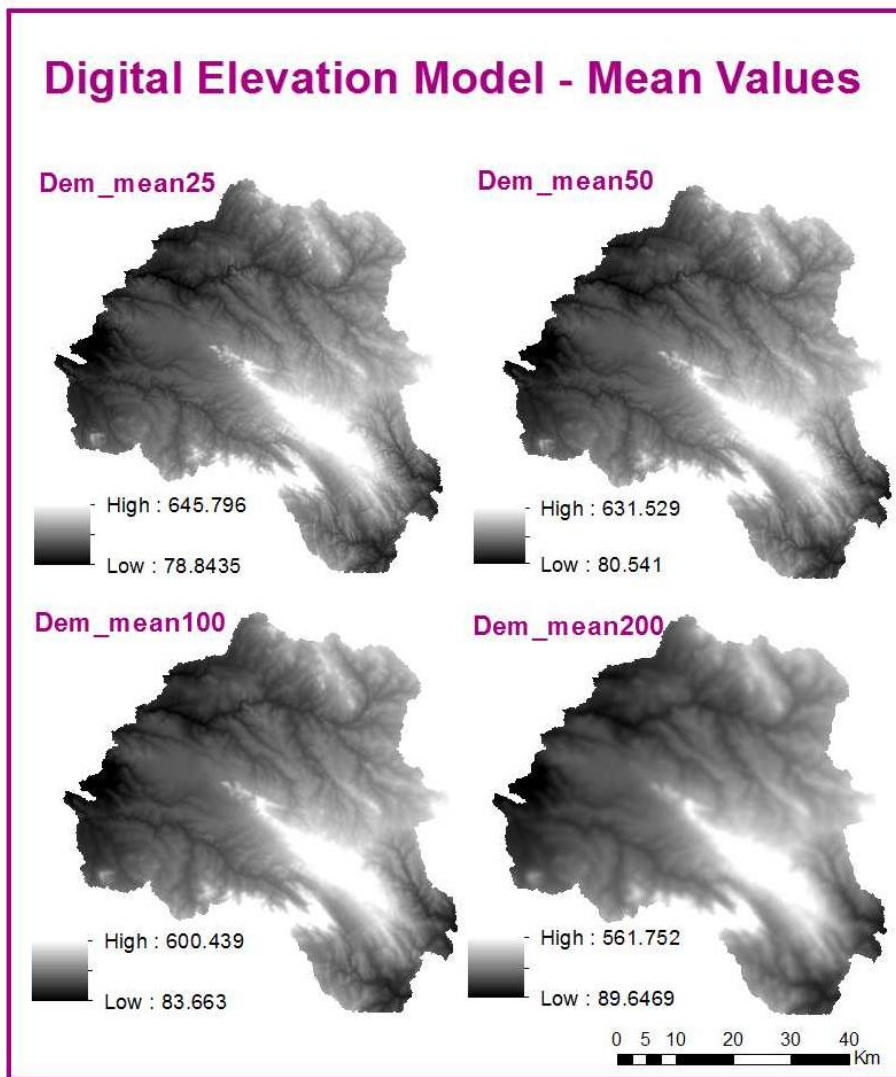


Figure 31: Mean Digital Elevation Model; mean elevation for a tree cells circle neighborhood.

The height (Figure 32) considered in the calculus of *Convex* is the result of the difference between the elevations of the DEM computed with topo-to-raster interpolation method and the focal mean elevation of the DEM around a 3 cell circle neighborhood (Figure 31).

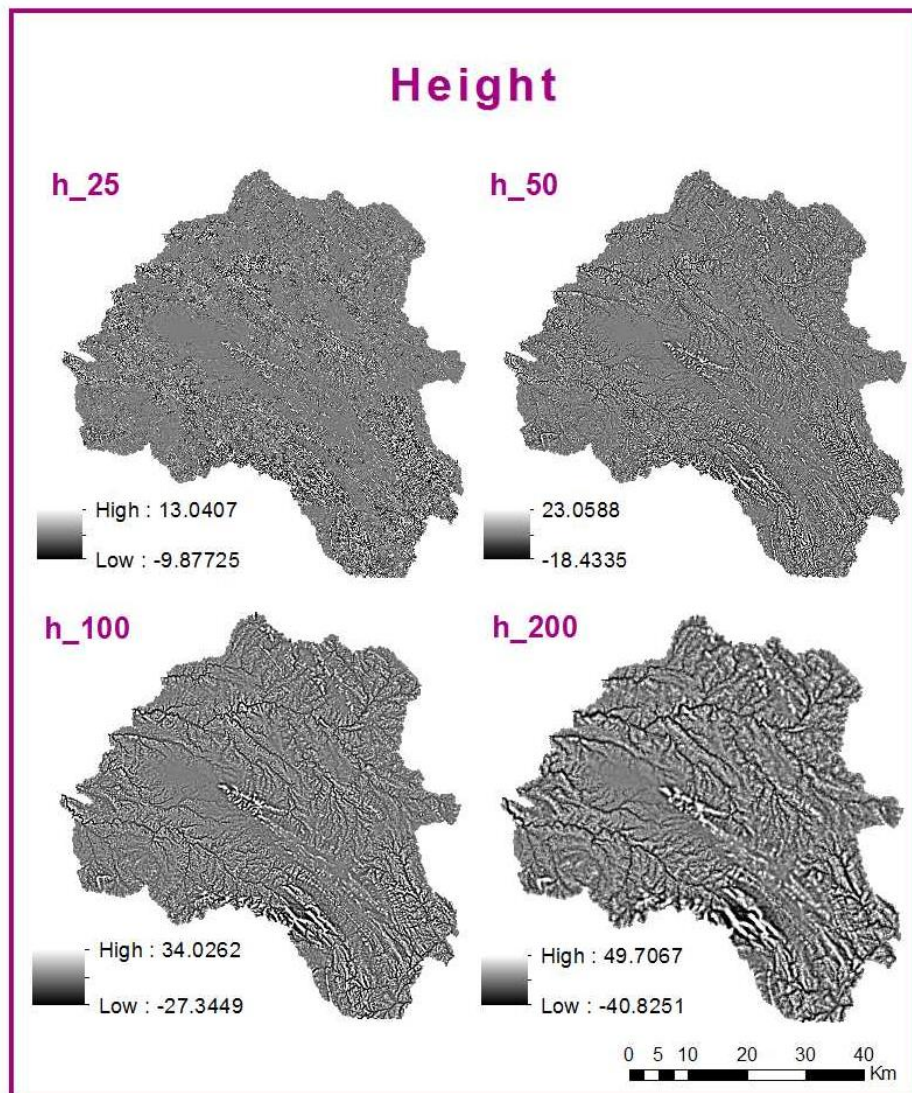


Figure 32: Height calculated from the difference between the elevation and the mean elevation; variable considered in the calculation of *convex*.

Horizontal distance (d)

The calculus of the convexity is done fitting a horizontal distance of 3 cells. For the cell sizes considered in the calculus of the convexity at different resolutions the horizontal distance equals (Table 12):

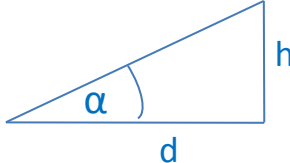
$$d = 3 \times \text{Cell Size}$$

Table 12: Horizontal distance applied in the calculus of *convex*, depending on the cell size for each of the resolution considered.

Raster Resolution (Cell Size)	d
25	75
50	150
100	300
200	600

Inverse Tangent (Atan)

The inverse tangent calculated in ArcGis® corresponds to the arc α measured in radians whose tangent (Tan) is y :

$$\left\{ \begin{array}{l} \mathbf{Tan}(\alpha) = y \\ \alpha = \mathbf{Atan}(y) \end{array} \right.$$


$$y = \frac{\mathbf{height}(h)}{\mathbf{horizontal\ distance}(d)}$$

Conversion factor (57.29578)

As the output values of the Atan function computed in ArcGis® are in radians, in order to convert them to degrees for interpreting the terrain gradient the values are multiplied by the conversion factor of radians to degrees ($180 / \pi$) which approximately equals 57.2958.

Convexity normalization

The output values of the function Atan converted to degrees range from -90° to 90° , which in absolute values correspond to a total range of 180° . To normalize the convexity values, in order for them to range from 0 to 1, Atan was summed 90° and the result was divided by 180° .

6.4.2.2 Statistical Analysis

The statistical analysis of the variables obtained during the computing of the focal convexity index, *convex*, started from the calculus of the significance level and the correlation coefficient by Statistica7, between the SWL and the independent variables (Table 13):

Dependent variable – SWL_m

Independent variables: h; convex; DEM; DEM_mean

(For different resolutions, cell size: 25 | 50 | 100 | 200)

Table 13: Correlation Analysis for all the independent variables calculated for the computing of NMC.

Independent Variables	SWL	
	p-level	R
DEM_25	0.000001	0.47122
DEM_mean25	0.000001	0.45927
h_25	0.015253	0.24327
convex_25	0.015245	0.24329
DEM_50	0.000001	0.46973
DEM_mean50	0.000001	0.46478
h_50	0.000124	0.37619
DEM_100	0.000001	0.47009
DEM_mean100	0.000002	0.46724
h_100	0.000111	0.37879
convex_100	0.000111	0.37877
DEM_200	0.000001	0.46315
DEM_mean200	0.000002	0.45315
h_200	0.225356	0.12295
convex_200	0.225375	0.122945

Likewise in the statistical analysis of the independent variables calculated for the computing of NMC the variables are highly significant showing a p-level in most cases lower than 0.1. In order to narrow the selection and increase the significance of the variables to consider for the model to be set, there will only be considered the variables with p-level <0.001, highlighted in the table 14

Table 14 summarizes the correlations between SWL and each one of the candidate independent variables, separately for both multiple regressions: piecewise and linear.

Table 14: Correlation and determination coefficients for each independent variable calculated during the calculus of *Convex* for both models Piecewise and multiple linear regressions.

Candidate Independent Variables	SWL			
	Picewise Linear Regression		Multiple Linear Regression	
	R	R ²	R	R ²
DEM_25	0.83883	70.36%	0.471222	22.21%
DEM_mean25	0.83864	70.33%	0.470073	22.10%
DEM_50	0.83837	70.29%	0.469727	22.06%
DEM_mean50	0.83788	70.20%	0.464787	21.60%
h_50	0.83512	69.74%	0.37619	14.15%
convex_50	0.83512	69.74%	0.37619	14.15%
DEM_100	0.83841	70.29%	0.470095	22.10%
DEM_mean100	0.83766	70.17%	0.459287	21.09%
h_100	0.83067	69.00%	0.37879	14.35%
convex_100	0.83066	69.00%	0.37877	14.35%
DEM_200	0.83729	70.11%	0.463158	21.45%
DEM_mean200	0.83662	69.99%	0.453155	20.53%

The model that best explains SWL is a Piecewise Linear Regression for which the predictive capability is higher than 68% for all the candidate independent variables. Once they are all highly correlated ($0.7 \leq R < 0.9$) to the SWL but also likely to be correlated among them the selection of the independent variables to consider in the model presupposes a multicollinearity analysis (Table15).

The model that best explains SWL is again a Piecewise Linear Regression model, for which predictive capability is greater than 69% for all the independent variables, which are highly correlated with SWL ($0.7 \leq R < 0.9$). Previously to the model definition the multicollinearity analysis for the candidate independent variables are presented in Table16.

Table 15: Bivariate correlations matrix for the independent variables for the calculus of *Convex*.

	DEM_25	DEM_50	DEM_100	DEM_200	h_50	h_100	convex_50	convex_100
DEM_25	1	0.9999	0.9998	0.9991	-0.0072	-0.0013	-0.0072	-0.0013
DEM_50	0.9999	1	0.9997	0.9993	-0.0065	-0.0032	-0.0065	-0.0032
DEM_100	0.9998	0.9997	1	0.9992	-0.0119	0.0024	-0.0119	0.0024
DEM_200	0.9991	0.9993	0.9992	1	-0.0272	-0.0197	-0.0272	-0.0197
h_50	-0.0072	-0.0065	-0.0119	-0.0272	1	0.7357	1	0.7357
h_100	-0.0013	-0.0032	0.0024	-0.0197	0.7357	1	0.7357	1
convex_50	-0.0072	-0.0065	-0.0119	-0.0272	1	0.7357	1	0.7357
convex_100	-0.0013	-0.0032	0.0024	-0.0197	0.7357	1	0.7357	1

Highlighted in the table above are the values whose independent variables are less multicollinear. Aiming to achieve the best model several pairs of independent variables were tested for a Piecewise Linear Regression. In Table 16 the best pair of independent variables that empirically explain SWL ensuring a low multicollinearity between the pair of independent variables are presented.

Table 16: Proposal of the 3 models that best explain SWL based on the independent variables considered in the computation of *Convex*.

Model	Independent Variables	Piecewise Linear Regression		Multiple Regression	
		R	R ²	R	R ²
1	convex_50 DEM_25	0.86475	74.78%	0.60518	36.62%
2	convex_50 DEM_50	0.86444	74.73%	0.60371	36.45%
3	convex_100 DEM_100	0.85654	73.37%	0.60299	36.61%

MODEL 2

After the statistical analysis presented above, the conclusion is that the model that best explains water table occurrence is a Piecewise Linear Regression with the independent variables convex_50 and DEM_25 (Table 17).

$$\text{SWL (m)} = (-104.016 + 213.6101 * \text{convex_50} + 0.000887 * \text{DEM_25}) * (\text{SWL} \leq 4.724848) + (-160.947 + 328.8578 * \text{convex_50} + 0.011501 * \text{DEM_25}) * (\text{SWL} > 4.724848)$$

Table 17: Results for Model 2- Piecewise Linear Regression for the independent variables convex_50 and DEM_25.

	Model is: Piecewise linear regression with breakpoint						
	Dependent variable: SWL__m_ Loss: Least squares						
	Final loss: 181.95050516 R= .86475 Variance explained: 74.779%						
	Const.B0	convex_50	DEM_25	Const.B0	convex_50	DEM_25	Breakpt.
Estimate	-104.016	213.6101	0.000887	-160.947	328.8578	0.011501	4.724848

6.4.3 Structural Index

The surface analysis that are here after described leans towards the prediction of groundwater occurrence explained by a structural convexity variable (*StructConvex1*) that reflects the general convexity of the surface. During the calculus of this new variable, different variables were tested in the statistical analysis, all of which started from the topography and the water flow behavior at the surface. There for the trial variables tested in order to explain SWL were computed resorting to the Hydrology tools namely the Flow Length, the key tool for the definition of a structural index. Bellow follows a resume of the several steps taken during the definition of a Structural Convexity Index, resulting on several independent variables that were then considered in the statistical analysis, and a flowchart with the scheme of the computing of *StructConvex1* (Figure 34).

6.4.3.1 Structural Convexity Index 1 (*StructConvex1*)

1. Flow Length

Input flow direction raster: FL_direc25 | 50 | 100 | 200

Cell Size: 25 | 50 | 100 | 200

Direction of measurement: DOWNSTREAM

Output: FL_length25 | 50 | 100 | 200

2. Flow Length – Transport Convexity

Input flow direction raster:

Cell Size: 25 | 50 | 100 | 200

Direction of measurement: DOWNSTREAM

Input weight raster: convex_25|50|100|200

Output: transp_convex25 | 50 | 100 | 200

3. Raster Calculator:

“transp_convex 25|50|100|200”

“FL_length25|50|100|200”

Output: t_convex_mean25|50|100|200

Raster Calculator: $(\text{Ln}(1 + \text{“t_convex_mean25|50|100|200”})) * \text{“DEM_25|50|100|200”}$

Output: StructConvex1_25|50|100|200

STRUCTURAL CONVEXITY INDEX (*StructConvex_1*)

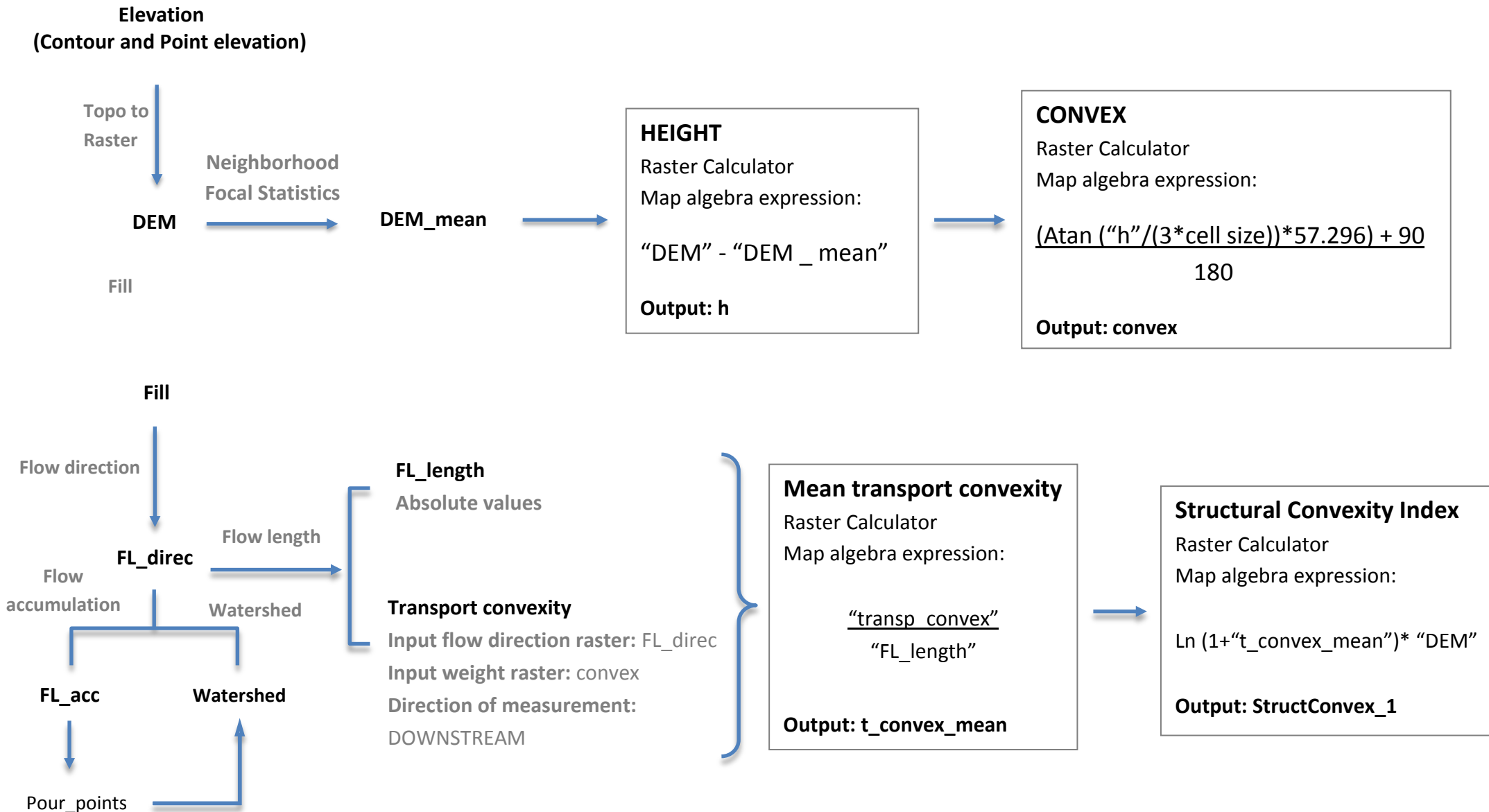


Figure 34: Flowchart illustrating all the steps in the computing of StructConvex_1

Flow Length Tool

The Flow length tool application allows the calculation of the longest flow path in a watershed. It calculates the distance along the flow path measured in the flow direction raster, resulting on an output raster where the length of the flow path is the distance from each cell to the watershed pour points.

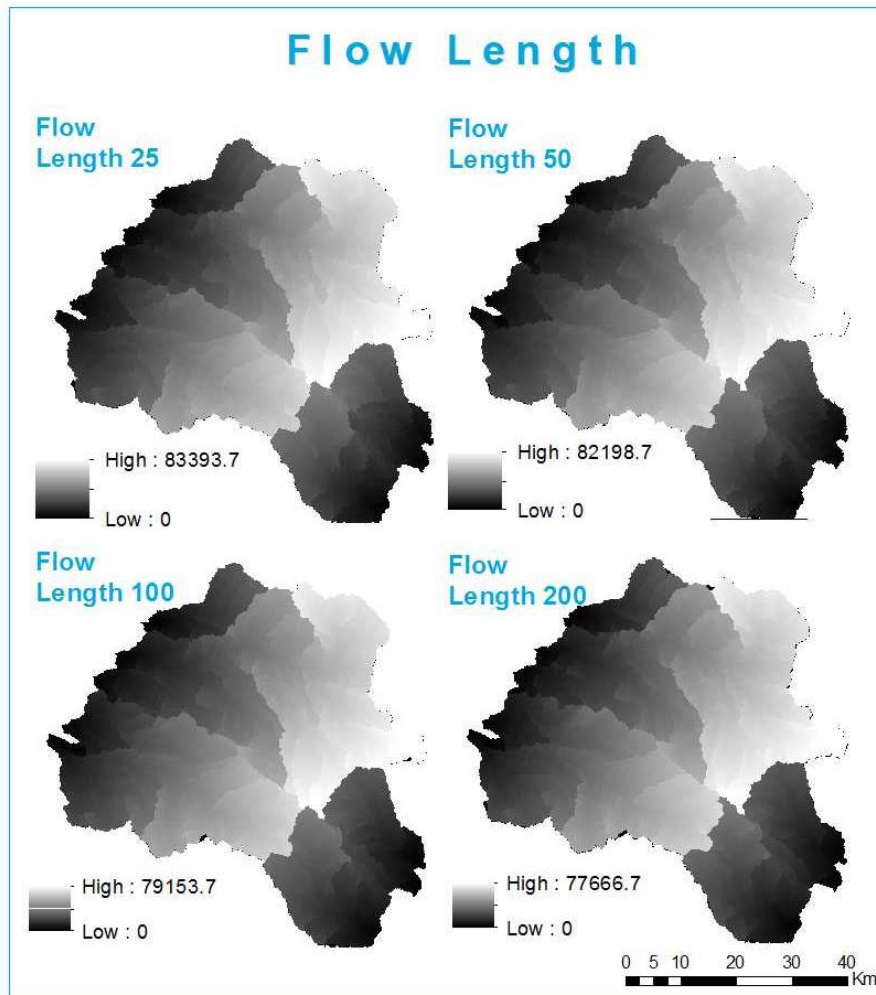


Figure 35: Flow Length within the study area, showing the downstream distance along a flow path for each cell to the pour points of each water flows.

In the computation of *StructConvex1*, two different rasters were calculated using the Flow Length tool. The first one (*Fl_length*) (Figure 35) computed the absolute flow path length while the second (*transp_convex*) (Figure 36) calculated the flow length along the topographic surface considering as an input weight raster the local convexity calculated previously with *Convex*. The flow path length can either be measured upstream or downstream within the watershed. In the calculation of a transport convexity ("*transp_convex*"), the flow length was measured downstream, that is, the calculation of the flow length was determined in the downslope direction and the distance of the flow path measured from each cell to the micro basins pour-points. In the calculation of the

transported convexity, the convexity index raster was added as an Input Weight raster whereby to each cell the *convex* was applied as a weight in the calculation of the transport convexity.

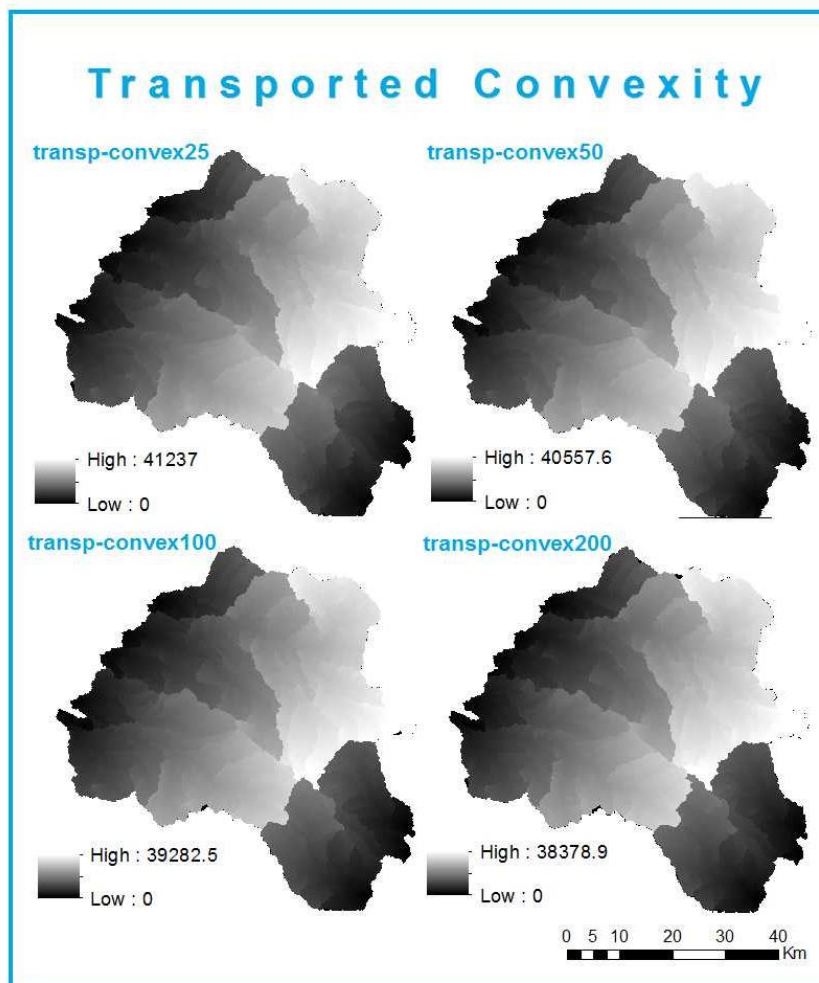


Figure 36: Transported Convexity computed with the Flow length Tool considering as an input weight the *Convex* calculated before.

The transported convexity was then divided by the absolute length obtaining a mean transported convexity (Figure 37).

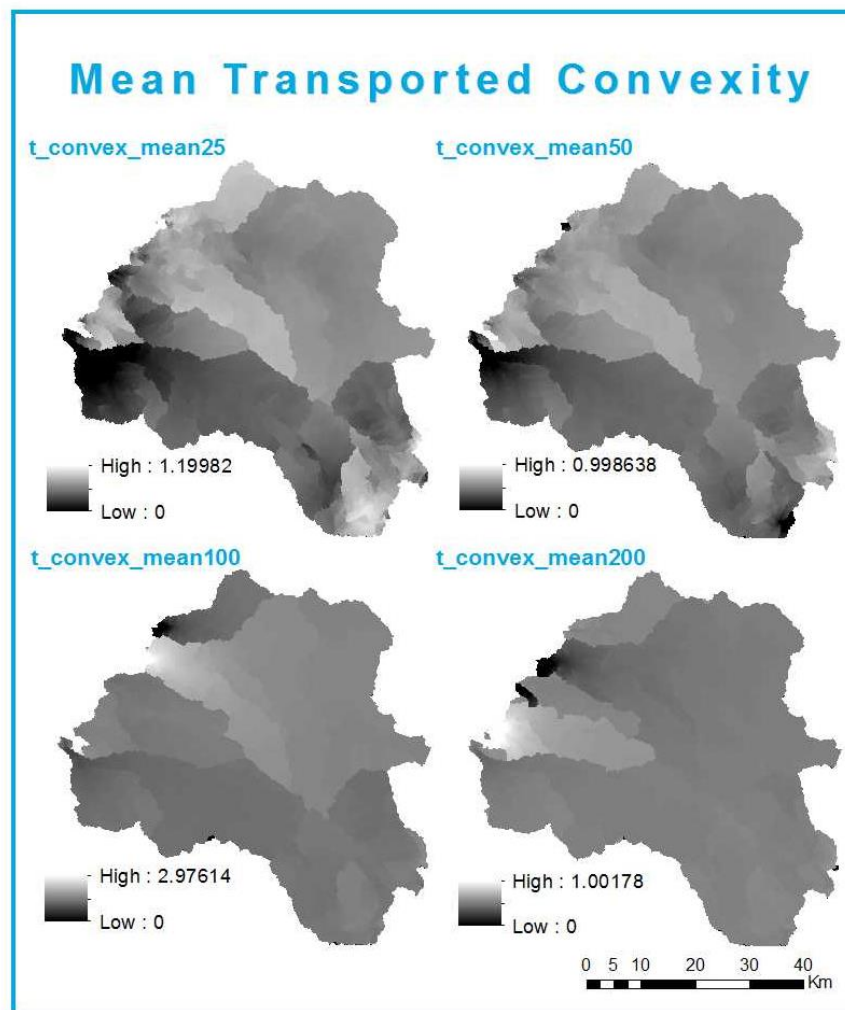


Figure 37: Mean Transported Convexity calculated by dividing the Transported Convexity by the Flow Length for the watersheds in the study area.

Lastly a new raster was created by calculating the natural logarithm of the mean transported convexity and multiplying it by the elevation given by the DEM (Figure 38). Hence a new variable was defined aiming to explain SWL – *StructConvex1*.

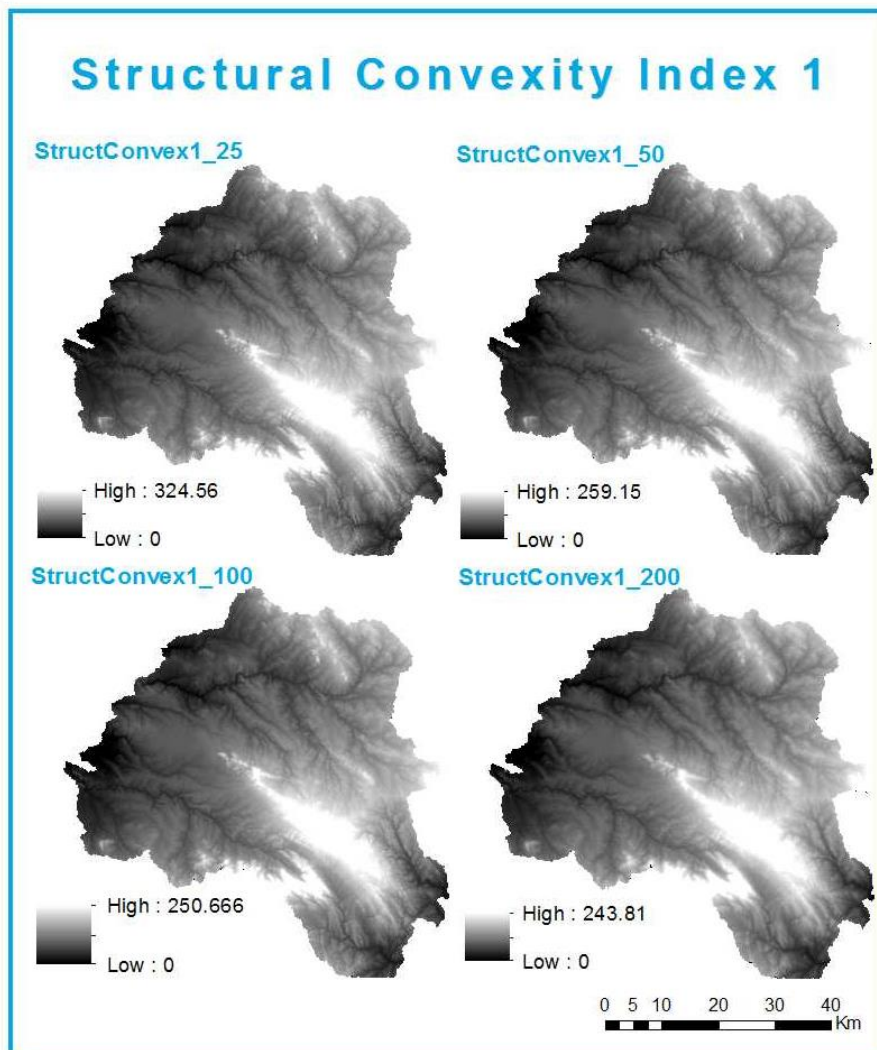


Figure 38: Structural Convexity Index (*StructConvex1*) for the study area

6.4.3.1.1 Statistical Analysis

Table 18 summarizes the significance level and the correlation coefficient between the SWL and each one of the independent variables separately.

Dependent variable: SWL_m

Independent variables: t_convex_mean; transp_convex; StructConvex1; DEM; DEM_mean; Convex (For all different resolution, cell size: 25 | 50 | 100 | 200)

Table 18: Correlation Analysis for all the independent variables calculated during the computing of *StructConvex1*.

Independent Variables	SWL	
	p-level	R
convex_25	0.015245	0.24329
t_convex_mean25	0.428938	0.0803917
transp_convex25	0.005814	0.2753189
StructConvex_25	0.000001	0.4701644
DEM_mean25	0.000001	0.45928722
DEM_25	0.000001	0.4712220
convex_50	0.000124	0.37619
t_convex_mean50	0.763454	0.03062827
transp_convex50	0.006577	0.27142209
StructConvex_50	0.000001	0.46909032
DEM_mean50	0.000001	0.46478775
DEM_50	0.000001	0.46972775
convex_100	0.000111	0.37877
t_convex_mean100	0.333925	0.09812220
transp_convex100	0.007563	0.26694413
StructConvex1_100	0.000001	0.46724500
DEM_mean100	0.000002	0.45928722
DEM_100	0.000001	0.47009508
convex_200	0.225375	0.122945
t_convex_mean200	0.173108	0.13801151
transp_convex200	0.009477	0.25955321
StructConvex_200	0.000001	0.46377474
DEM_mean200	0.000002	0.45315507
DEM_200	0.000001	0.46315848

All independent variables considered for explaining SWL are highly significant: they all show a p-level lower than 0.1 and in most case lower than 0.01. Similarly to the previous analysis, highlighted are the variables with p-level lower than 0.01, the independent variables candidate to be considered for the definition of model 3.

Table 19: Correlation and determination coefficients for each independent variable calculated for the determination of *StructConvex1* for both models Piecewise and multiple linear regressions.

Candidate Independent Variables	SWL_m			
	Picewise Linear Regression		Multiple Linear Regression	
	R	R ²	R	R ²
transp_convex25	0.83407	69.57%	0.275318	7.28%
StructConvex1_25	0.83866	70.34%	0.470164	22.11%
DEM_25	0.83883	70.36%	0.471222	22.21%
DEM_mean25	0.83864	70.33%	0.470073	22.10%
convex_50	0.83512	69.74%	0.37619	14.15%
transp_convex50	0.83364	69.50%	0.271422	7.37%
StructConvex1_50	0.83827	70.27%	0.469090	22.00%
DEM_50	0.83837	70.29%	0.469727	22.06%
DEM_mean50	0.83788	70.20%	0.464787	21.60%
convex_100	0.83066	69.00%	0.37877	14.35%
transp_convex100	0.83273	69.34%	0.266944	7.13%
StructConvex1_100	0.83833	70.28%	0.467245	21.83%
DEM_100	0.83841	70.29%	0.470095	22.10%
DEM_mean100	0.83766	70.17%	0.459287	21.09%
transp_convex200	0.83091	69.04%	0.259553	6.74%
StructConvex1_200	0.8372	70.10%	0.463774	21.49%
DEM_200	0.83729	70.11%	0.463158	21.45%
DEM_mean200	0.83662	69.99%	0.453155	20.53%

Again the model that best explains SWL is a Piecewise Linear Regression for which all the candidate independent variables are highly correlated to SWL and whose predictive capability varies between 69% and 71% for all the candidate independent variables (Table 19) . As in the previous analysis follows the multicollinearity analysis to outwit multicollinearity problems that may occur (Table 20 to 23).

Table 20 to 23: Bivariate correlation matrixes for the candidate independent variables calculated for the determination of *StructConvex1*.

	DEM_25	DEM_mean25	transp_convex25	StructConvex1_25
DEM_25	1	1	0.7152	1
transp_convex25	0.7152	0.7149	1	0.716
StructConvex25	1	0.9999	0.716	1
DEM_mean25	1	1	0.7149	0.9999

	DEM_50	DEM_mean50	convex_50	transp_convex50	StructConvex1_50
DEM_50	1	0.9999	-0.0065	0.7149	1
DEM_mean50	0.9999	1	-0.0194	0.7146	0.9999
convex_50	-0.0065	-0.0194	1	0.0109	-0.0075
transp_convex50	0.7149	0.7146	0.0109	1	0.7147
StructConvex50	1	0.9999	-0.0075	0.7147	1

	convex_100	DEM_100	DEM_mean100	StructConvex_100	transp_convex100
convex_100	1	0.0024	-0.0257	-0.001	-0.0042
DEM_100	0.0024	1	0.9996	0.9999	0.7078
DEM_mean100	-0.0257	0.9996	1	0.9996	0.7077
StructConv	-0.001	0.9999	0.9996	1	0.7103
transp_con	-0.0042	0.7078	0.7077	0.7103	1

	DEM_200	DEM_mean200	transp_convex200	StructConvex200
StructConvex1_200	0.9998	0.9986	0.6953	1
DEM_200	1	0.9988	0.6963	0.9998
transp_convex200	0.6963	0.7004	1	0.6953
DEM_mean200	0.9988	1	0.7004	0.9986

From the analysis of the correlation coefficients, the significance level and the determination coefficient for a Piecewise Linear Regression and a Multiple Linear Regression and considering the multicollinearity between the variables, the model that best explains SWL is a Piecewise Linear regression with the sets of the independent variables shown in Table 24.

Table 24: Proposal of the two models that best explain SWL based on the independent variables considered in the computation of *StructConvex1*.

Model	Independent Variables	Piecewise Linear Regression		Multiple Regression	
		R	R ²	R	R ²
2	Convex_100 StructConvex1_100	0.85645	73.35%	0.601768	36.21%
3	Convex_50 StructConvex1_50	0.86442	74.72%	0.603517	36.42%

Table 25: Results for Model 3- Piecewise Linear Regression for the independent variables convex_50 and StructConvex1_50.

N=99	Model is: Piecewise linear regression with breakpoint						
	Dependent variable: SWL__m_ Loss: Least squares Final loss: 182.36205982 R= 0.86442 Variance explained: 74.721%						
	Const.B0	convex_50	StructConvex1_50	Const.B0	convex_50	StructConvex1_50	Breakpt.
Estimate	-103.971	213.5222	0.002198	-161.377	329.7590	0.028502	4.724848

MODEL 3

After the statistical analysis presented above, the conclusion is that the model that best explains water table occurrence is a Piecewise Linear Regression with the independent variables StructConvex1_50 and convex_50 (Table 25).

$$\text{SWL} = (-103.971 + 213.5222 * \text{convex_50} + 0.002198 * \text{StructConvex1_50}) * (y \leq 4.724848) + (-161.377 + 329.7590 * \text{convex_50} + 0.028502 * \text{StructConvex1_50}) * (y > 4.724848)$$

6.4.3.2 Structural Convexity Index 2 (*StructConvex2*)

From the statistical analysis of the independent variables calculated and computed for the definition of *StructConvex1* it was found that the transported convexity is more significant and correlated to the SWL than the mean transported convexity. Therefore a second structural convexity index was calculated - *StructConvex2* (Figure 40), resulting from the natural logarithm of the transported convexity, as described below and outline in the flowchart on Figure 39.

1. Flow Length

Input flow direction raster:
Cell Size: 25 | 50 | 100 | 200

Direction of measurement:
DOWNSTREAM

Output: FL_length25 | 50 | 100 | 200

convex_25|50|100|200

Output:transp_convex25 |50 |100 | 200

3. Raster Calculator:

Ln ("transp_convex25 | 50 | 100 | 200")

2. Flow Length

Input flow direction raster:
Cell Size: 25 | 50 | 100 | 200

Direction of measurement:
DOWNSTREAM

Input weight raster:

Output: StructConvex2_25|50|100|200

STRUCTURAL CONVEXITY INDEX (*StructConvex_2*)

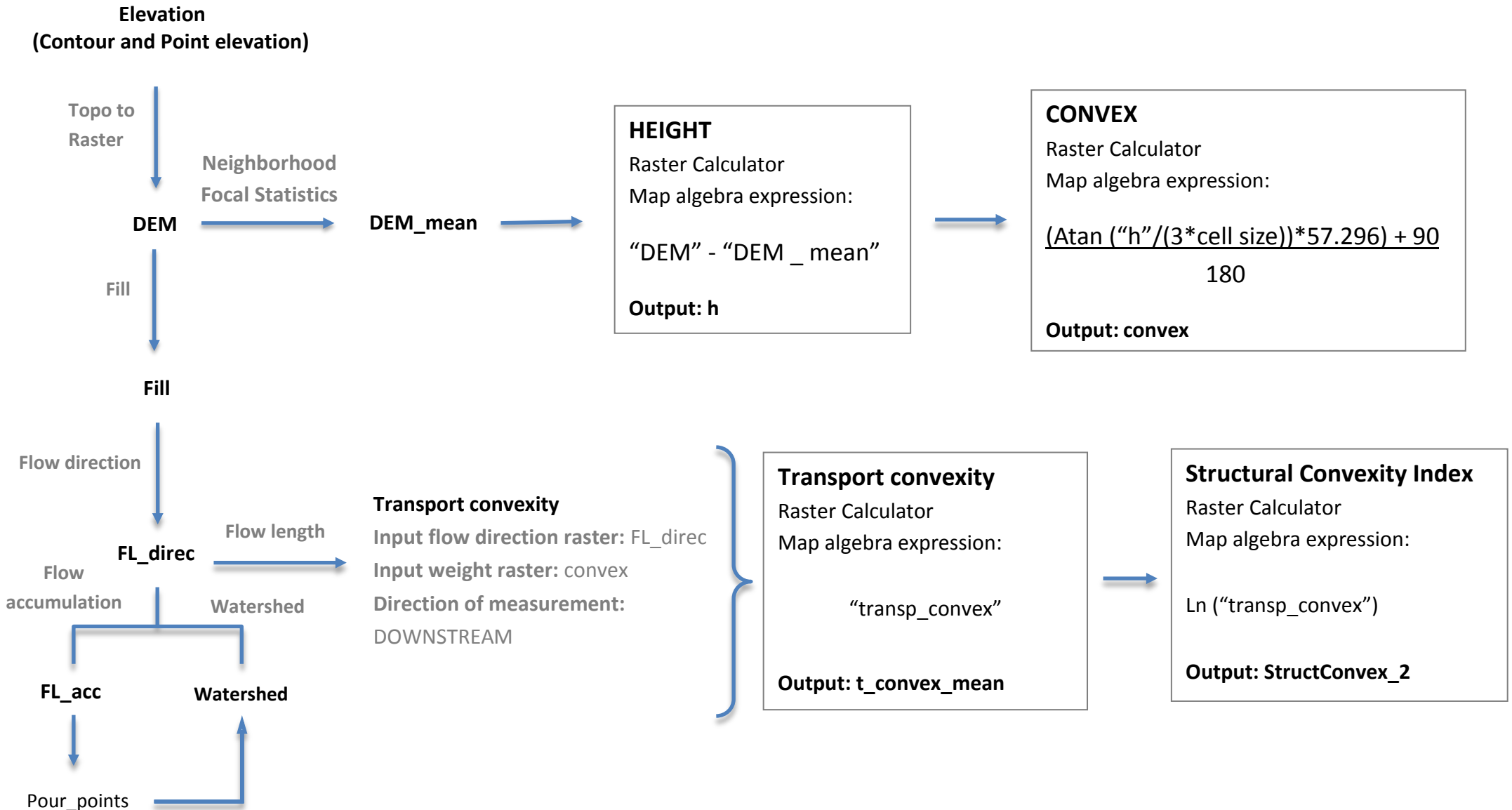


Figure 39: Flowchart illustrating all the steps in the computing of StructConvex_2

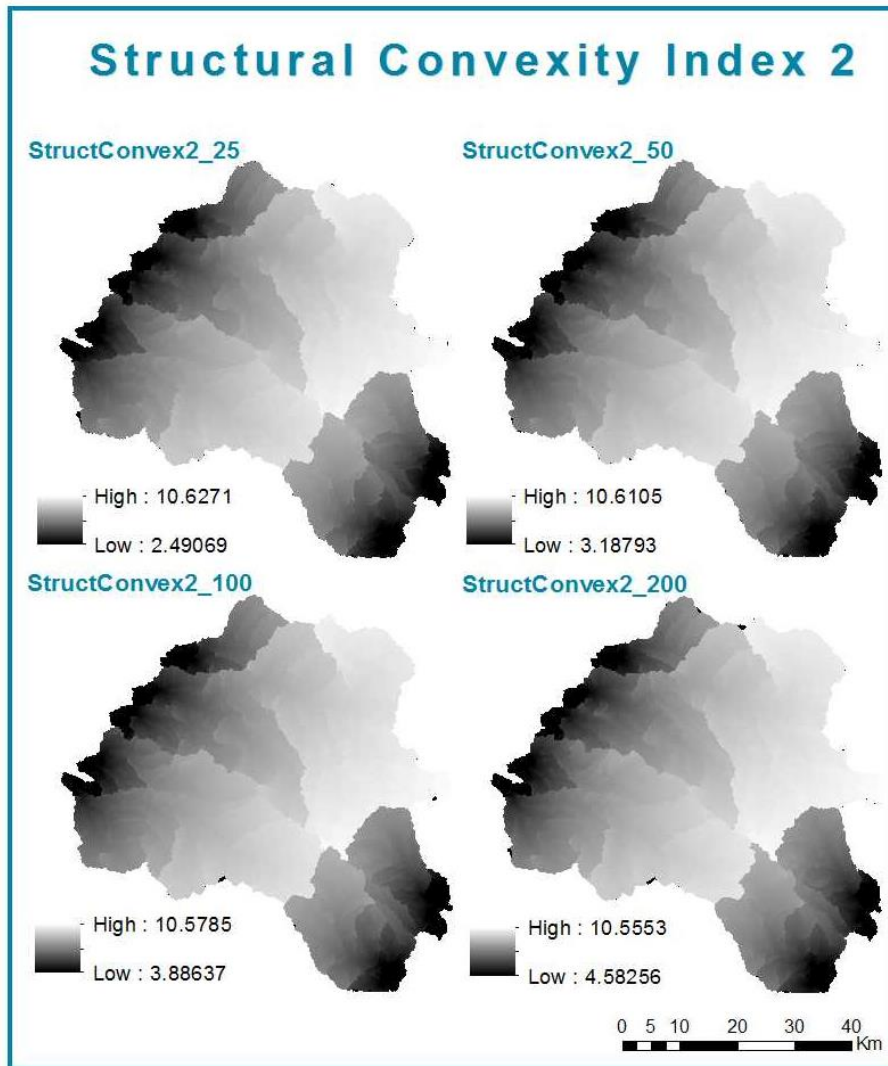


Figure 40: Structural Convexity Index (*StructConvex2*) for the study area.

6.4.3.2.1 Statistical Analysis

The statistical analysis started with the calculus of both p-level and R between the SWL and the independent variables calculated during the computing of the second structural index, *StructConvex2*:

Dependent variable – SWL_m

Independent variables: convex; DEM; transp_convex; *StructConvex2*;

(For different resolutions, cell size: 25 | 50 | 100 | 200)

Table 26 summarizes the correlations between SWL and each one of the independent variables separately.

Table 26: Correlation Analysis for all the independent variables calculated during the computing of *StructConvex2*.

Independent Variables	SWL	
	p-level	R
transport_convex25	0.005814	0.275318
StructConvex2_25	0.007388	0.267699
Convex_25	0.015245	0.243290
DEM_25	0.000001	0.471222
transport_convex50	0.006577	0.2714220
StructConvex2_50	0.008599	0.2627642
Convex_50	0.000124	0.3761900
DEM_50	0.000001	0.4697277
transport_convex100	0.007563	0.2669441
StructConvex2_100	0.009134	0.2607750
Convex_100	0.000111	0.3787700
DEM_100	0.000001	0.47009508
transport_convex200	0.009477	0.259553
StructConvex2_200	0.014665	0.244651
Convex_200	0.225375	0.122945
DEM_200	0.000001	0.463158

The selection of the variables to include in the model is based on the correlation values and considering that correlations are significant for p-level lower than 0.1. Once all the independent variables are very significant, the ones with a p-level > 0.01 are the ones considered as candidates to explain SWL. Table 27 summarizes the comparison between the correlation coefficient and the determination coefficient for the candidate independent variables in a Multiple Linear Regression and a Piecewise Linear Regression.

Table 27: Correlation and determination coefficients for each independent variable calculated for the determination of *StructConvex2* for both models Piecewise and multiple linear regressions.

Candidate Independent Variables	SWL			
	Picewise Linear Regression		Multiple Linear Regression	
	R	R ²	R	R ²
transport_convex25	0.83407	69.57%	0.2753189	7.28%
StructConvex2_25	0.83548	69.80%	0.26769978	7.16%
Convex_25	0.82386	67.87%	0.24328671	5.91%
DEM_25	0.83883	70.36%	0.4712220	22.21%
transport_convex50	0.83364	69.50%	0.27142209	7.37%
StructConvex2_50	0.83510	69.74%	0.26276422	6.90%
Convex_50	0.83512	69.74%	0.37619	14.15%
DEM_50	0.83837	70.29%	0.46972775	22.06%
transport_convex100	0.83273	69.34%	0.26694413	7.13%
StructConvex2_100	0.83443	69.62%	0.26077514	6.80%
Convex_100	0.83066	69.00%	0.378770	14.35%
DEM_100	0.83841	70.29%	0.47009508	22.10%
transport_convex200	0.83091	69.04%	0.25955321	6.74%
StructConvex2_200	0.83187	69.20%	0.24465186	5.98%
DEM_200	0.83729	70.11%	0.46315848	21.45%

As expected the model that best explains SWL is a Piecewise Linear Regression for which all the candidate independent variables are highly correlated to SWL and whose predictive capability varies between 69% and 71% for all the candidate independent variables. As in the previous analysis the multicollinearity analysis to outwit multicollinearity problems that may occur are represented in Tables 28 to 31.

Table 28 to 31: Bivariate correlations matrix for the candidate independent variables calculated for the determination of *StructConvex2*.

	convex_25	DEM_25	transp_convex_25	Struct_Convex_3_25
convex_25	1	0.0859	0.1122	0.0604
DEM_25	0.0859	1	0.7152	0.7119
transp_convex_25	0.1122	0.7152	1	0.9331
Struct_Convex_3_25	0.0604	0.7119	0.9331	1

	convex_50	DEM_50	transp_convex_50	StructConvex_3_50
convex_50	1	-0.0065	0.0109	0.0097
DEM_50	-0.0065	1	0.7149	0.7131
transp_convex_50	0.0109	0.7149	1	0.9311
StructConvex_3_50	0.0097	0.7131	0.9311	1

	convex_100	DEM_100	transp_convex_100	StructConvex_3_100
convex_100	1	0.0024	-0.0042	-0.0362
DEM_100	0.0024	1	0.7078	0.6945
transp_convex_100	-0.0042	0.7078	1	0.9164
StructConvex_3_100	-0.0362	0.6945	0.9164	1

	DEM_200	transp_convex200	StructConvex_3_200
DEM_200	1	0.6963	0.6711
transp_convex200	0.6963	1	0.8961
StructConvex_3_200	0.6711	0.8961	1

The model that best explains SWL is the Piecewise Linear regression model for which the predictive capability is greater than 69% for all the independent variables.

From the analysis of the correlation coefficients, the significance level and the determination coefficient both for a Piecewise Linear Regression and a Multiple Linear Regression and considering the multicollinearity between the variables, it was concluded that the model that best explains SWL is a Piecewise Linear regression with the sets of the independent variables represented in Table 32.

Table 32: Proposal of the 3 models that best explain SWL based on the independent variables considered in the computation of *StructConvex2*.

Model	Independent Variables	Piecewise Linear Regression		Multiple Regression	
		R	R²	R	R²
2	Struct_Convex2_50 Convex_50	0.85402	72.93%	0.45679289	20.87%
3	Struct_Convex2_100 Convex_100	0.85134	72.48%	0.46787476	21.89%

MODEL 4

After the statistical analysis presented above, the conclusion is that the model that best explains water table occurrence is a Piecewise Linear Regression with the independent variables StructConvex21_50 and convex_50 (Table33).

$$\text{SWL (m)} = (-107.779 + 217.7657 * \text{convex_50} + 0.201075 * \text{StructConvex2_50}) * (\text{SWL} \leq 4.724848) + (-122.849 + 237.2412 * \text{convex_50} + 1.172006 * \text{StructConvex2_50}) * (\text{SWL} > 4.724848)$$

Table 33: Results for Model 4- Piecewise Linear Regression for the independent variables convex_50 and StructConvex2_5.

Model is: Piecewise linear regression with breakpoint							
Dependent variable: SWL_m Loss: Least squares							
Final loss:195.24610806 R= .85402 Variance explained: 72.936%							
	Const.B0	convex_50	StructConvex2_50	Const.B0	convex_50	StructConvex2_50	Breakpt.
Estimate	-107.779	217.7657	0.201075	-122.849	237.2412	1.172006	4.724848

Chapter 7 - Conclusion

For the statistical analysis, the Piecewise Linear Regression is undoubtedly the model that best explains SWL, presented for all the independent variables analyzed, considering high correlation values ($0.7 \leq |R| < 0.9$) and determination coefficients above 68%. From the comparative analysis of the best models inquired (Table 34) it follows that the model that best explain SWL is Model 2 defined by a Piecewise Linear Regression with the following independent variables: *Convex* for a resolution defined by cells 50 m sides and the *DEM* with cell sizes of 25 m.

Table 34: Best models inquired all through the statistical analysis.

Model	Independent Variables	Piecewise Linear Regression		Multiple Regression	
		R	R ²	R	R ²
2	convex_50 DEM_25	0.86475	74.78%	0.60518	36.62%
3	Convex_50 StructConvex1_50	0.86442	74.72%	0.603517	36.42%
1	NMC_25 DEM_50	0.86261	74.41%	0.59085	34.91%
4	Struct_Convex2_50 Convex_50	0.85402	72.93%	0.45679289	20.87%

A predicted value for Static Water Level can thus be calculated in Map Algebra by applying Model 2 described by the follow equation(Figure 41):

$$\text{SWL} = -104.016 + (213.6101 * \text{"convex_50"}) + (0.000887 * \text{"Dem_25"}) + (-160.947) + (328.8578 * \text{"convex_50"}) + (0.011501 * \text{"Dem_25"})$$

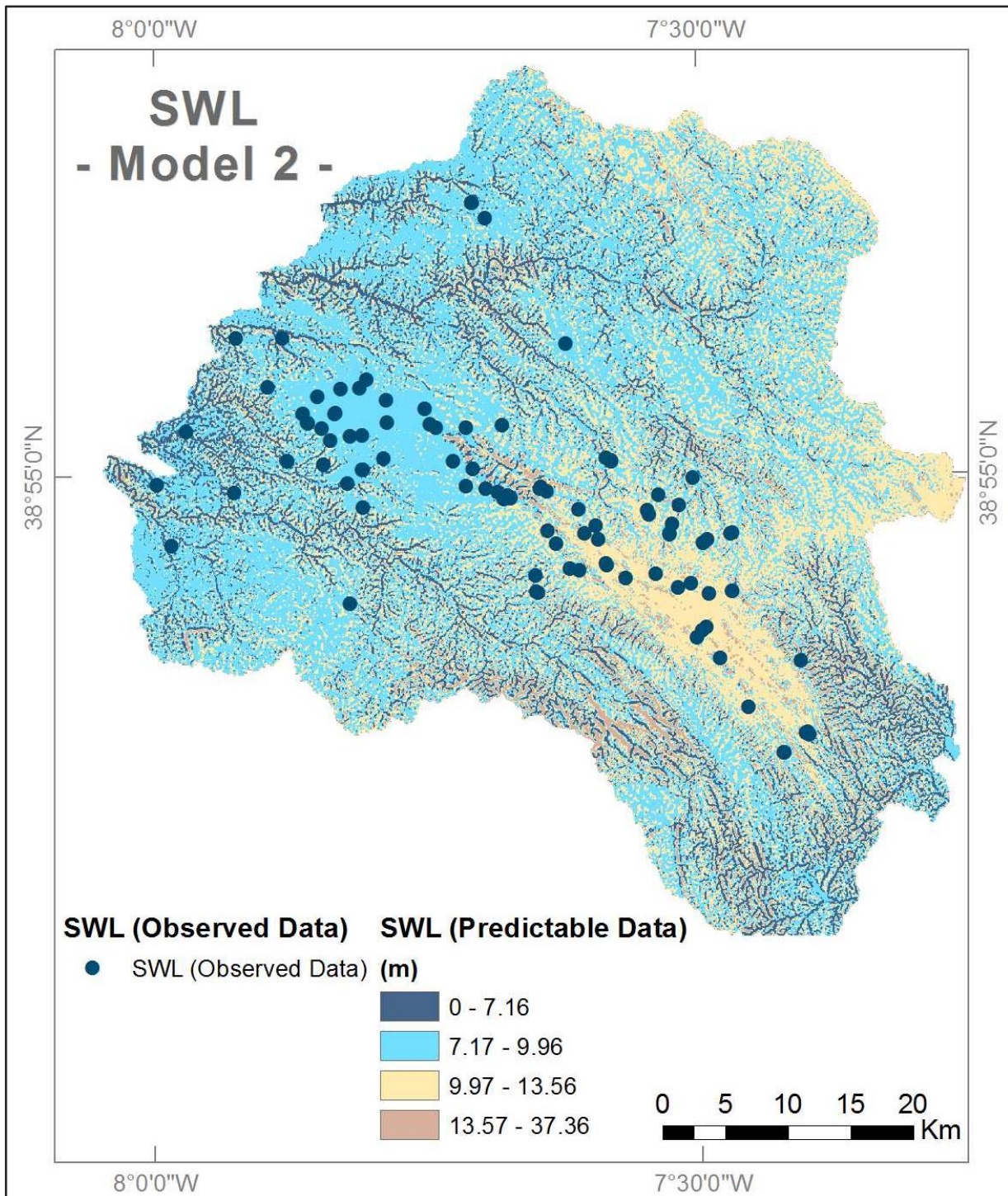


Figure 41: SWL calculated with Model 2.

The model clearly relates groundwater occurrence with topography and its metrics which, as a matter of fact, would be predictable. Topography reflects itself the differences between the different lithologies taking place in the terrain as a result of the different behavior of geological formations to the weathering processes. Despite the tendency of water flow direction to be the same both at surface and underground the form of the surface doesn't reflect the inner hydrogeological characteristic of the aquifer systems, for that it must be taken into account the distinct hydrogeological

behavior of water in different aquifers such as the Aquifer System Estremoz-Cano and the metamorphic and Igneous Rocks of the OMZ.

Applying Model 2 to both systems separately the difference between both becomes clear with different results for the correlation coefficient and the determination index (Tables 35 and 36).

Tables 35 and 36: Estimation results for Model 2 for both aquifer systems where SWL was measured (A4- Estremoz Cano Aquifer System; OMZ – Igneous and metamorphic rocks of OMZ).

N=35	Model is: Piecewise linear regression with breakpoint (Wells_A4)						
	Dependent variable: SWL_m_Loss: Least squares Final loss:78.016476144 R= .84352 Variance explained: 71.152%						
	Const.B0	Dem_25	convex_50	Const.B0	Dem_25	convex_50	Breakpt.
Estimate	-168.400	0.006071	342.0009	-72.7484	0.017179	149.5848	6.038857

N=60	Model is: Piecewise linear regression with breakpoint (Wells_OMZ)						
	Dependent variable: SWL_m_Loss: Least squares Final loss:72.925580184 R= .89015 Variance explained: 79.237%						
	Const.B0	Dem_25	convex_50	Const.B0	Dem_25	convex_50	Breakpt.
Estimate	-85.9925	-0.00015	177.4973	-246.529	0.00345	504.5989	3.994167

The model works extremely well for the fractured aquifer of the OMZ with nearly very high correlation coefficient and a predictive capacity of 80%. In what concerns the karsty aquifer of Estremoz-Cano both correlation and determination coefficients are slightly lowers, which represents the heterogeneity of spatial water distribution inherent to this type of aquifers. In fact, it is well known that in the karst systems the groundwater level is not so dependent of the topographic surface of the terrains, due to the much higher flow velocity in these hydrogeological systems, which permits the quick outflow of most part of infiltrated groundwater, with a higher tendency for the leveling of the phreatic level.

It is important to stress that despite the excellent results obtained, the models presented in the actual work result from a first and yet premature analysis tested for a specific topographic and hydrogeological case study. Yet, the potential of the model here presented is enormous with a high applicability in the near future, with the advantage of being tested for any geographic area were SWL values, for a certain hydrologic year, are known. Therefore, it matters to apply it in different hydrogeological and topographic areas.

It is also worth mentioning that with Map Algebra of Arcgis® the result of SWL obtained with Model 2 can be projected in a raster from where different maps can derive, such as an infiltration map and a map with the representation of the discharge zones of water table at the surface.

Bibliography

- Araújo, A., Piçarra Almeida, J., Borrego, J., Pedro, J., Oliveira, T., (2006). As regiões central e sul da Zona de Ossa-Morena. Em: *Geologia de Portugal no contexto da Ibéria* (Dias, R., Araújo, A., Terrinha, P. e Kullberg, J. Editores). Univ. Évora, Évora, 35-61.
- Araújo, A. (1995). Estrutura de uma geotransversal entre Brinches e Mourão (Zona de Ossa-Morena): implicações na evolução geodinâmica da margem sudoeste do Terreno Autóctone Ibérico. Tese de Doutoramento, Dep. Geociências da Univ. de Évora, 200 p.
- Boswinkel J. A., Information Note, (2000). International Groundwater Resource Assessment Centre (IGRAC), Netherlands Institute of Applied Geoscience, Netherlands.
- Carvalhosa, A., Gonçalves, F., Oliveira, V. (1987) – Carta Geológica de Portugal na escala 1:50 000 e Notícia Explicativa da folha 36 – D Redondo. Serviços Geológicos de Portugal.
- Chambel, A. Duque, J., Nascimento, J., (2007). Regional study of hard rocks aquifers in Alentejo, South Portugal: methodology and results. IAH-SP Series, Jirí Krásný & John M. Sharp Eds, Taylor & Francis, 2007, 73-93.
- Chambel, A. (2014, in publication). Outcrop groundwater prospecting, drilling and well construction in hard rocks in semi-arid regions. *Fractured Rock Hydrogeology*. Sharp, J. Ed., Taylor and Francis, 61-78.
- Custodio, E. & Llamas, M. (1983) – *Hidrología Subterránea*. Ediciones Omega, S. A., Barcelona, Vol. 1 e 2, 2350 pp.
- Cupeto, C. A. (1991). Contribuição para o conhecimento hidrogeológico do maciço de Estremoz (Cano-Sousel). Dissertação apresentada à Universidade de Lisboa para obtenção de grau de Mestre em Geologia Aplicada e do Ambiente, Lisboa, 180 p.
- Cupeto, C. A. (2003). A água como factor de gestão, planeamento e desenvolvimento integrado Sistema Aquífero Estremoz-Cano (A4) Zona dos Mármore. Dissertação apresentada à Universidade de Lisboa, para obtenção de grau de Doutor, Lisboa, 274 p.
- Driscoll, F. G. (1986) - *Groundwater and Wells*, 2nd ed., Johnson Division, St. Paul, Minnesota, 1089 pp.
- ERHSA, (2001). Estudo dos recursos hídricos subterrâneos do Alentejo – Relatório Técnico. Universidade de Évora, Instituto da Água, Instituto Geológico e Mineiro, Direcção Regional do Ambiente do Alentejo.

- Feio, M. A. (1993). O Relevo do Alto Alentejo (traços essenciais). *Finisterra*, XXVIII, 55-56, pp. 149-199.
- Hutchinson, M. F., and T. I. Dowling. (1991). A continental hydrological assessment of a new grid-based digital elevation model of Australia. *Hydrological Processes* 5: 45–58.
- Lencastre, A. and Franco, F. M. (1984). *Lições de Hidrologia*. Universidade Nova de Lisboa, Faculdade de Ciências e Tecnologia, Lisboa.
- Lopes, L. (2003). *Contribuição para o conhecimento tectono-estratigráfico do Nordeste Alentejano. Transversal Terena-Elvas*. Tese de doutoramento, Universidade de Évora, 568 p. Lopes, L. and Martins, R. (2008). *Anticlinal de Estremoz: Geologia e Tecnologia de Exploração de Mármore*s. Universidade de Évora, Évora.
- Maroco, João (2003). *Análise Estatística com utilização do SPSS*. 2nd Edition, Sílabo Editions, Lisbon, 508 p.
- Murteira, B., Ribeiro, C.S., Silva, A.J., Pimenta, C. (2002). “Introdução à Estatística”. Instituto Superior de Economia e Gestão, Universidade Técnica de Lisboa. McGraw Hill Editor, Lisboa, 647 p.
- Oliveira, M. M. (2006). The estimation of groundwater recharge of fractured rocks in Portugal using surface flow measurements. Proceedings of the “2nd Workshop of the Iberian Regional Working Group on Hard Rock Hydrogeology”, Portuguese Chapter of the International Association of Hydrogeologists (AIH-GP), 221-233.
- Ribeiro, A., Pereira, E., Silva, J. B., Dias, R., Araújo, A., Marques, F., Merino, H., Fonseca, P., (1990). *Caledonian events in the Iberian Variscan Fold Belt: Geodynamic significance and implications for European Variscides*. International Conference on Paleozoic Orogens in Central Europe, Gottingen-Giessen. Abstracts. International Geological Correlation Program 233.
- Santos, F. L. (1999). *Movimento e Qualidade de Água na Zona Vadosa: conceitos, métodos e técnicas de controlo*. Publicações Universidade de Évora, 1999. Série Ciências da Natureza e do Ambiente nº 2, 180 p.
- Sarmiento, G.N., Piçarra, J.M., Oliveira, J.T. (2000). *Conodontes do Silúrico (Superior?) - Devónico nos “Mármore de Estremoz”, Sector de Estremoz-Barrancos (Zona de Ossa Morena, Portugal)*. Implicações estratigráficas e estruturais a nível regional. I Congresso Ibérico de Paleontologia/VIII International Meeting of IGCP 421, Évora, Resumos 284-285.

Electronic references:

- Almeida, C., Mendonça, J. J. L., Jesus, M.R., Jesus, Gomes, A. J. (2000). *Sistemas Aquíferos de Portugal Continental*. Centro de Geologia e Instituto da água. Lisboa.

URL:

http://snirh.pt/snirh/download/aquiferos_PortugalCont/Introducao_Macico_Antigo.pdf and http://snirh.pt/snirh/download/aquiferos_PortugalCont/Ficha_A4.pdf

- Instituto Geográfico Português (2010). Carta de uso e ocupação do solo de Portugal continental para 2007. Memória descritiva. IGeo. Lisboa. URL: http://www.igeo.pt/nivel/memoria_descritiva_cos2007.pdf
- ICA (2011). Departamento de Producción de la Agencia Estatal de Meteorología de Espanha e Departamento de Meteorologia e Clima, Instituto de Meteorologia de Portugal (2011). Atlas Climático Ibérico, *Iberian Climate Atlas*. URL: http://www.ipma.pt/resources.www/docs_pontuais/ocorrencias/2011/atlas_clima_iberico.pdf
- Goodchild, M. F., and D. M. Mark. (1987). The fractal nature of geographic phenomena. *Annals of Association of American Geographers*. 77 (2): 265–278. URL: <http://www.geog.ucsb.edu/~good/Goodchild-CV.html>
- Jenson, S. K., and J. O. Domingue. (1988). "Extracting Topographic Structure from Digital Elevation Data for Geographic Information System Analysis." *Photogrammetric Engineering and Remote Sensing* 54 (11): 1593–1600. URL: <http://citeseerx.ist.psu.edu/viewdoc/summary?doi=10.1.1.138.6487>
- Nicolau, R. (2002). *Modelação e Mapeamento da Distribuição Espacial da Precipitação – Uma Aplicação a Portugal Continental*. Faculdade de Ciências e Tecnologia da Universidade Nova de Lisboa. Dissertação apresentada para obtenção do Grau de Doutor. 356 p. URL: http://www.igeo.pt/teses/rita%20nicolau/Indice_Geral.pdf
- WFD (2000). Directive 2000/60/EC of the European Parliament and of the council of 23 October 2000 establishing a framework for Community action in the field of water policy. *Official Journal of the European Communities*. URL: <http://eur-lex.europa.eu/LexUriServ/LexUriServ.do?uri=OJ:L:2000:327:0001:0072:EN:PDF>

Internet pages with relevant information:

- <http://snirh.pt/>

- <http://www.pordata.pt>

- <http://insaar.inag.pt>

- <https://www.ipma.pt/pt/>

- <http://www.dgadr.pt/ar/cartografia/notaexplisolo.htm>

- <http://www.dgadr.mamaot.pt/nota-explicativa>

- http://agricultura.isa.utl.pt/agribase_temp/solos/default.asp

- <http://www.fao.org/Wairdocs/ILRI/x5546E/x5546e04.htm#TopOfPage>

- <http://help.arcgis.com/en/arcgisdesktop/10.0/help/>

- <http://ga.water.usgs.gov/>

- <http://www.unep.org>

- <http://help.arcgis.com/en/arcgisdesktop/10.0/help>

- <http://www.neng.usu.edu/cee/faculty/dtarb/TarbotonBakerFinal.pdf>

- http://www.igeo.pt/e-IGEO/egeo_downloads.htm